Stability of Discontinuous Elastic Rods with Applications to Nanotube Junctions

David Thomas Lane

University College London

Centre for Nonlinear Dynamics,

Department of Civil, Environmental & Geomatic Engineering,
Gower Street,
London,
WC1E 6BT

January 29, 2012

'I, David Thomas Lane, confirm that the work presented in this thesis is my own and has not been previously submitted to this or any other institution for any degree, diploma or other qualification. Where information has been derived from other sources, I confirm that this has been indicated in the thesis.'

David Thomas Lane
January 29, 2012

Abstract

Buckling and post-buckling stability of elastic rods with discontinuities in bending stiffness and curvature, as well as rods lying on an interactive surface is investigated using the theory of conjugate points. Second order matching conditions at points of discontinuity are formulated, which allow the classic Jacobi condition to be extended to incorporate calculus of variations problems with discontinuous integrands.

Static equilibrium equations for intrinsically straight, inextensible and unshearable discontinuous rods are formulated. Conjugate points are found by numerically solving the Jacobi equation as an initial value problem. For the case of a rod interacting with a surface, an external force potential is added to the energy functional, causing the Jacobi operator to be an integrodifferential operator.

Morse index theory is used to find expressions for critical buckling values of load parameters with respect to parameters measuring jumps in bending stiffness, or parameters measuring the strength of the rod-surface interaction. Bifurcation diagrams of buckled rod solutions are presented, with the Morse stability index calculated for each solution branch. These are found to be consistent with the theory of stability exchange at folds for distinguished diagrams. The presence of a jump in bending stiffness is shown, in some cases, to cause an extra stable solution branch. Numerical continuation of folds in two parameters is used to find the parameter space for which these stable branches exist. The rod equilibrium equations are solved numerically using parameter continuation for a boundary value problem. Clamped boundary conditions are considered, as well as pinned boundary conditions, which require a more robust adaptation of the classic Jacobi condition.

The theory is applied to the modelling of carbon nanotube intramolecular junctions, in which the bonding of two or more carbon nanotubes causes a jump in the diameter, chirality or cross-section shape of the resulting tube, as well as a possible kink (jump in the centreline curvature) in the tube. The effects of van der Waals forces between a nanotube undergoing compression, and a substrate are modelled.

Table of Contents

List of Figures

List of Tables

Chapter 1

Introduction

In this thesis, we use the Cosserat theory of rods to model the deformation of carbon nanotubes with a finite number of jumps in the continuity of the bending stiffness and/or curvature. The buckling and post-buckling behaviour of such physical systems are studied, and stability analysis is performed. These points of discontinuity may represent nanotube junctions, in which the electronic properties along the nanotube change due to a change in the tube's chirality [1], diameter, or cross-section shape. A potential application of these junctions would be as transistors in nano-scale devices [5], [8], [45]. Since carbon nanotubes were first discovered by Lijima in 1991 [22], a large amount of research has been performed on the electronic properties of carbon nanotubes and nanotube junctions, e.g. [5], [8], [45], but there has been relatively little research on the mechanical behaviour of nanotubes or nanotube junctions when subjected to an external compressive force or end rotation. We justify using rod theory to model nanotubes by assuming the tubes to have a high aspect ratio (length to diameter ratio), and model the centreline of the tube as a rod, with any properties of the tube's surface being accounted for by the bending and torsional stiffnesses. Buehler *et al.* show in [4] that for appropriately large aspect ratios, the buckling behaviour of a carbon nanotube is reminiscent of the Euler buckling of a rod with clamped boundary conditions. As well as the effect of discontinuities along a nanotube, we also look at how van der Waals forces between the

---

[1]Nanotubes are created by rolling up a hexagonal lattice of carbon (graphite). Rolling the lattice at different angles creates a visible twist or spiral in the nanotube's molecular structure, though the overall shape remains cylindrical. This twist is called chirality.

tube and the surface it lies on, affects the spatial stability of the nanotube.

To study the stability of rod solutions, our main technique will be the calculus of variations. In the classical theory of variational calculus, an extremal with a discontinuous derivative, i.e. a piecewise smooth (or broken) extremal requires the well known Weierstrass-Erdmann corner conditions to be satisfied at a point of discontinuity [12]. For certain nanotube models in this thesis, we require extremals that are not only piecewise smooth but also piecewise continuous. Osmolovskii *et al.* [33], [34], [35] look into finding second order conditions (extensions to the classic Jacobi condition) for broken extremals of functionals with continuous integrands. Bliss and Mason [2], and Graves [14] studied the variational principles of systems with discontinuous integrands, which increases the number of variational problems that can be solved. Stability analysis of discontinuous systems requires second order conditions at points of discontinuity. In this case, we find the second order condition at a point of discontinuity $s = c$, to be

$$\left(W_{\mathbf{q}'\mathbf{q}'}\mathbf{h}' + W_{\mathbf{q}'\mathbf{q}}\mathbf{h}\right)(c-0) = \left(W_{\mathbf{q}'\mathbf{q}'}\mathbf{h}' + W_{\mathbf{q}'\mathbf{q}}\mathbf{h}\right)(c+0), \quad c \in (a,b), \qquad (1.1)$$

where $\mathbf{h} : [a,b] \to \mathbb{R}^p$ is a variation of the extremal $\mathbf{q} : [a,b] \to \mathbb{R}^p$, and $W(\mathbf{q}, \mathbf{q}')$ is the strain energy density function of the elastic rod. We describe an extremal as being stable if the second variation of the energy functional $E[\mathbf{q}]$ is non-negative for all allowed weak variations. This definition can be extended by defining the index as an integer I, which is equal to the maximal dimension of the subspace of variations for which the second variation $\delta^2 E[\mathbf{h}]$ is negative. The index value $I = 0$, therefore, corresponds to a stable extremal. The classic Jacobi condition states that an extremal is a local minimum (stable) if there are no points in $(a, b]$ that are *conjugate* to the point a. Morse [32] extended this theory by equating the index I to the number of points in (a, b) conjugate to a. Using the condition (1.1), we extend the definition of a conjugate point to find the index of an extremal of a functional with a discontinuous integrand.

We also consider variational problems with isoperimetric constraints. These enter the problem as a result of boundary conditions that fix both end positions of the rod. The constrained variational problem is a classical one. To find critical points of an

energy functional subject to isoperimetric constraints, extra terms are added to the functional using the Lagrange multiplier rule. Bolza [3] extended the definition of conjugate points to account for isoperimetric problems, and showed that the absence of these constrained conjugate points is equivalent to a stable extremal. Rogers [36] uses an alternative method to derive a constrained conjugate point. By writing the unconstrained Jacobi equation as an eigenvalue problem, and taking a suitable orthogonal projection, the constrained index (the number of constrained conjugate points) is shown to be equal to the number of negative eigenvalues of this projected eigenvalue problem. Bliss and Mason [2], and Graves [14] extended the Jacobi condition to variational problems of functionals with discontinuous integrands by adding suitable second order conditions, while Cole [7] extended the definition of the index to include such problems. However, none of these works consider isoperimetric constraints. For our problem, we find that given the condition (1.1), the orthogonal projection of the unconstrained Jacobi operator (used by Rogers [36]) still has the required properties to allow us to equate the number of negative eigenvalues to the constrained index for the isoperimetric discontinuous problem.

We consider rods that are inextensible and unshearable, and with a strain energy density function W, which is quadratic in the strains of the rod. Here, we study static deformations of an elastic rod, therefore W is a function of space, but not time. If the second variation is positive for all admissible variations, this corresponds to *spatial stability* of the rod equilibrium.

We use index theory to find buckling loads of rods. A rod buckles from a trivial straight solution to a buckled solution at a branch point. At such points there is a change in stability, therefore points where the index changes along the trivial branch correspond to buckling points of the straight rod with respect to an applied load. If we find an expression for a critical buckling value of a loading parameter λ, we can plot critical values of λ against a second parameter. Here, we plot critical values of λ against parameters measuring the jump in the bending stiffness, and parameters measuring the strength of the rod-surface interaction.

Post-buckling equilibria of the rod are computed numerically using parameter continuation[2] software AUTO97 [11]. Bifurcation diagrams are produced that label each solution branch with an index value. We find that the index values change at folds (limit points) in the solution branches. For *distinguished* bifurcation diagrams, the stability index computed by counting the conjugate points, agrees with the theory of stability exchange at folds, studied by Maddocks [26], and generalised further by Rogers [36] to cases where the bifurcation parameter enters the problem as a boundary condition. We solve the rod equilibrium equations as a boundary value problem with either clamped (the direction of the rod is fixed) or pinned (the end has zero moment) boundary conditions. Boundary conditions that fix the centreline position of the rod at both ends correspond to isoperimetric constraints in the variational problem. Numerically, we treat a discontinuity in the rod by simply solving the system of rod equations on each side of the discontinuity, and applying the appropriate matching conditions. Given the rod solutions obtained by solving the boundary value problem, we find it computationally more efficient to find the conjugate points by solving the Jacobi equation as an initial value problem, using the initial data obtained from the rod solutions.

This thesis is structured as follows, chapter 2 gives an overview of the variational principles that are required throughout the thesis. We find the necessary conditions for an extremal to be a weak local minimum in both the unconstrained and constrained calculus of variations problems. The problem is extended to the case of a functional with a discontinuous integrand, and we find the second order conditions necessary for the extended Jacobi condition. A new definition of conjugate points is defined, which allows us to find the Morse stability index of an extremal with discontinuities. We briefly discuss the variational problem with Neumann boundary conditions, and how the theory of conjugate points is affected when the boundary conditions are no longer the standard Dirichlet conditions, which are assumed in all standard textbooks on the calculus of

---

[2]Parameter continuation consists of finding an approximation to solutions of a differential or algebraic equation, as a parameter is varied. AUTO performs numerical parameter continuation using the pseudo arclength continuation method to compute solution curves with respect to a bifurcation parameter and find branch points along these curves. For more information on this method see [11],[21].

variations.

In chapter 3 we discuss the theory of elastic rods, which will be used in the subsequent chapters. We introduce Euler parameters, which relate the orientation of the rod cross-section to the fixed frame. Different sets of boundary conditions are discussed in terms of Euler parameters. Parametrising the three-dimensional space of the rod orientation with four Euler parameters avoids any singularities that can occur when using the more traditional method of Euler angles. However, this parametrisation can lead to the strengthend Legendre condition not holding. To fix this problem, we follow Manning [31] and others, and use a suitable orthogonal projection of the variations of the Euler parameters.

In chapter 4 we perform stability analysis on an intrinsically straight elastic rod with discontinuous bending stiffness. Critical buckling values of end force are calculated with respect to certain bending stiffness parameters. Stability index is calculated for buckled rod solutions with clamped boundary conditions. We look at a specific class of clamped rods with discontinuous bending stiffness, where each section of the rod has an elliptical cross section with the same circumference, but different eccentricity. The intention is to model a carbon nanotube junction in which part of the nanotube has been axially compressed in order to change the tube's electrical properties. We study the bifurcation diagrams of the rod solutions. We look at the case of *hard loading*, which specifies the end displacement, as well as *dead loading*, in which an end force is specified, and study the effects of both end force and end twisting moment.

In chapter 5 we discuss how the conjugate point theory changes when Neumann boundary conditions are used, and calculate the stability index for solutions of rods with pinned ends. In the Dirichlet case, it is shown that the number of conjugate points is equal to the number of negative eigenvalues of the Jacobi operator at the boundary b. However this is no longer true in the Neumann case, and further information about the zero valued eigenvalues must be found in order to find the index.

In chapter 6 we study a planar model of rods with a kink (a single discontinuity in the curvature). Equilibrium equations are formulated by solving the Euler-Lagrange

equations, and stability analysis is performed on the rod equilibria.

In Chapter 7 we study the effect of the presence of a surface with an interactive force potential. Equilibrium equations for the rod are formulated, now with an extra potential term added to the energy functional, where the new term represents the interactive force between the rod and the surface. The Jacobi operator is now found to be an integrodifferential operator, as opposed to the standard second order differential operator.

Finally, chapter 8 gives a discussion and summery of our results.

Chapter 2

Variational Principles

Jacobi's strengthend condition states that a critical point of a functional E is stable (a weak local minimum) if it has no conjugate points (see e.g. [12] or [37]). Morse [32] extended the idea of stability to show that the number of conjugate points is equal to the maximal dimension of the subspace of admissible weak variations for which the second variation $\delta^2 E$ is negative. This integer I, is called the index. If $I = 0$, then the second variation $\delta^2 E \geq 0$ for all admissible variations, and therefore the critical point is stable.

Jacobi's strengthend condition can be extended to the isoperimetric problem by defining an isoperimetric conjugate point [3]. Manning, Rogers, and Maddocks [31] extend the isoperimetric conjugate point theory by writing the Jacobi equation as an eigenvalue problem and showing that the index is equal to the number of negative eigenvalues. Extension of the index theory from the case of a functional with a continuous integrand to a functional with a discontinuous integrand is possible with the introduction of certain matching conditions at any jumps in continuity.

In this chapter we will study the constrained calculus of variations problem, and then show how by including these matching conditions, the stability index can be defined for a functional with discontinuous integrands.

2.1 Continuous Integrand

We shall briefly look at the calculus of variations problem of minimising a functional with a continuous integrand. We wish to minimise the following functional, subject to

m isoperimetric constraints.

$$\int_a^b W(\mathbf{q}, \mathbf{q}') \, \mathrm{d}s, \quad \mathbf{q}(s) \in \mathbb{R}^p, \tag{2.1}$$

$$\mathbf{q}(a) = \mathbf{f}_a, \quad \mathbf{q}(b) = \mathbf{f}_b, \tag{2.2}$$

$$\int_a^b g_k(\mathbf{q}) \, \mathrm{d}s = 0, \quad k = 1, \ldots, m. \tag{2.3}$$

Here, and throughout this thesis, the prime symbol ($'$) will denote differentiation with respect to the independent variable s. In order to find critical points that minimise the functional (2.1) subject to constraints (2.3), we seek critical points of a new functional

$$E[\mathbf{q}] = \int_a^b \left(W(\mathbf{q}, \mathbf{q}') + \boldsymbol{\lambda} \cdot \boldsymbol{g}(\mathbf{q}) \right) \, \mathrm{d}s, \tag{2.4}$$

where $\boldsymbol{\lambda} := (\lambda_1 \cdots \lambda_m)^T$ are Lagrange multipliers, and $\boldsymbol{g} := (g_1 \cdots g_m)^T$. Critical points are solutions of the Euler-Lagrange equations

$$\mathcal{L}_{\mathbf{q}} - \frac{\mathrm{d}}{\mathrm{d}s} \mathcal{L}_{\mathbf{q}'} = \mathbf{0},$$

where $\mathcal{L} := W + \boldsymbol{\lambda} \cdot \boldsymbol{g}$.

We are interested in weak variations of $\mathbf{q}$, which we shall define by letting $\mathbf{q}(s) = \mathbf{q}^{(0)}(s) + \epsilon \mathbf{h}(s)$, where $\mathbf{q}^{(0)}(s)$ is a critical point. Then $\mathbf{q} \to \mathbf{q}^{(0)}$ and $\mathbf{q}' \to \mathbf{q}^{(0)'}$ as $\epsilon \to 0$. We call $\mathbf{h}$ the variation of $\mathbf{q}$. The second variation of (2.4) is found by taking the second order term of $E[\mathbf{q}^{(0)} + \epsilon \mathbf{h}]$:

$$\delta^2 E[\mathbf{h}] = \frac{1}{2} \int_a^b \left[\mathbf{h}' \cdot \mathbf{P} \mathbf{h}' + \mathbf{h}' \cdot \mathbf{C}^T \mathbf{h} + \mathbf{h} \cdot \mathbf{C} \mathbf{h}' + \mathbf{h} \cdot \mathbf{Q} \mathbf{h} \right] \, \mathrm{d}s, \tag{2.5}$$

where

$$\mathbf{P} = \mathcal{L}_{\mathbf{q}'\mathbf{q}'}, \quad \mathbf{C} = \mathcal{L}_{\mathbf{q}\mathbf{q}'}, \quad \text{and} \quad \mathbf{Q} = \mathcal{L}_{\mathbf{q}\mathbf{q}}.$$

The variations $\mathbf{h} \in \mathbb{R}^p$ must satisfy the linearised constraints

$$\int_a^b \mathbf{h} \cdot \mathbf{T}_k \, \mathrm{d}s = 0, \quad k = 1, \ldots, m,$$

where

$$\mathbf{T}_k = \frac{\partial g_k}{\partial \mathbf{q}}.$$

Note that $\mathbf{P}$, $\mathbf{C}$, $\mathbf{Q}$, and $\mathbf{T}_k$ are all functions of $\mathbf{q}$, evaluated at a critical point.

Let us define the following spaces:

$$\mathcal{T} \quad \equiv \quad \mathrm{span}(\mathbf{T}_1, \ldots, \mathbf{T}_m), \tag{2.6}$$

$$\mathcal{H}(\sigma) \quad \equiv \quad \left\{ \mathbf{h} \in H^2(a, \sigma) \ : \ \mathbf{h}(a) = \mathbf{h}(\sigma) = \mathbf{0} \right\}, \tag{2.7}$$

$$\mathcal{H}_{(con)}(\sigma) \quad \equiv \quad \left\{ \mathbf{h} \in \mathcal{H}(\sigma) \ : \ \langle \mathbf{h}, \mathbf{T}_k \rangle_\sigma = 0, \quad k = 1, \ldots, m \right\}, \tag{2.8}$$

where $\sigma \in [a, b]$, and H^2 defines the Sobolev space of functions with integrable weak second derivatives. Here, $\langle \cdot, \cdot \rangle_\sigma$ denotes the standard L^2 inner product on $[a, \sigma]$. We will denote $\langle \cdot, \cdot \rangle_b$ as simply $\langle \cdot, \cdot \rangle$.

A necessary condition for an extremal to be a local minimum is that the second variation be non-negative for all $\mathbf{h}$ in $\mathcal{H}_{(con)}(b)$.

The second variation $\delta^2 E[\mathbf{h}]$ can be written as

$$\delta^2 E[\mathbf{h}] = \frac{1}{2} \langle \mathcal{S} \mathbf{h}, \mathbf{h} \rangle,$$

where $\mathcal{S}$ is the Jacobi operator

$$\mathcal{S} \mathbf{h} \equiv - \left(\mathbf{P} \mathbf{h}' + \mathbf{C}^T \mathbf{h} \right)' + \mathbf{C} \mathbf{h}' + \mathbf{Q} \mathbf{h}.$$

If the matrix $\mathbf{P}$ is positive definite, and the critical point $\mathbf{q}$ has no *isoperimetric conjugate point*, then

$$\delta^2 E[\mathbf{h}] > 0, \quad \mathbf{h} \in \mathcal{H}_{(con)}(b) \tag{2.9}$$

where an isoperimetric conjugate point is defined as follows:

Definition 2.1.1. *A point σ, $a < \sigma < b$, is an isoperimetric conjugate point to a with respect to the functional $\delta^2 E[\mathbf{h}]$ if there is a nontrivial solution to*

$$\mathcal{S} \mathbf{h} = \sum_{k=1}^{m} \hat{c}_k \mathbf{T}_k, \tag{2.10}$$

$$\mathbf{h}(a) = \mathbf{h}(\sigma) = \mathbf{0}, \tag{2.11}$$

$$\int_a^\sigma \mathbf{h} \cdot \mathbf{T}_k \, \mathrm{d}s = 0, \quad k = 1, \ldots, m, \tag{2.12}$$

for some constants $\hat{c}_k \in \mathbb{R}$.

This condition is equivalent to Bolza's condition for the second variation to be positive definite [3]. It is an extension to Jacobi's necessary condition for an unconstrained functional to have a weak minimum, which can be found in many standard books on the calculus of variations, (e.g. [12] or [37]).

In the case of no constraints, the unconstrained index is equal to the number of negative eigenvalues of

$$\mathcal{S}\mathbf{h} = \rho(\sigma)\mathbf{h}, \quad \mathbf{h} \in \mathcal{H}(\sigma), \tag{2.13}$$

for which the standard Jacobi condition states is equal to the number of conjugate points (zero eigenvalues) in $[a, b]$. We now seek a suitable self-adjoint, orthogonal projection $\mathcal{Q} : H^2 \to \mathcal{T}^\perp(\sigma)$, of the unconstrained eigenvalue problem (2.13), for which

$$\delta^2 E[\mathbf{h}] > 0 \,\forall \mathbf{h} \in \mathcal{H}(b) \iff \delta^2 E[\mathcal{Q}\mathbf{h}] > 0 \,\forall \mathbf{h} \in \mathcal{H}_{(con)}(b). \tag{2.14}$$

Here, $\mathcal{T}^\perp(\sigma)$ denotes the orthogonal complement of $\mathcal{T}$ on the inner product $\langle \cdot, \cdot \rangle_\sigma$.

Let $\mathcal{Q} = \mathcal{I} - \mathcal{P}$, where $\mathcal{P} : H^2 \to \mathcal{T}$ has kernal $\mathcal{T}^\perp(\sigma)$, $\mathcal{I}$ is the identity operator, and $\mathcal{Q}$ has kernal $\mathcal{T}$, then

$$\mathcal{Q}\mathbf{T} = \mathbf{0}, \quad \forall \mathbf{T} \in \mathcal{T}, \tag{2.15}$$

$$\mathcal{Q}\mathbf{h} = \mathbf{h}, \quad \forall \mathbf{h} \in \mathcal{H}_{(con)}(\sigma) \subset \mathcal{T}^\perp(\sigma). \tag{2.16}$$

For $\mathbf{h} \in \mathcal{H}_{(con)}$, we have $\delta^2 E[\mathbf{h}] = \delta^2 E[\mathbf{Q}\mathbf{h}]$, and as $\mathcal{Q}$ is self-adjoint we can write

$$\langle \mathcal{S}\mathbf{h}, \mathbf{h} \rangle = \langle \mathcal{Q}\mathcal{S}\mathcal{Q}\mathbf{h}, \mathbf{h} \rangle \quad \forall \mathbf{h} \in \mathcal{H}_{(con)}(b). \tag{2.17}$$

The conjugate point definition (2.1.1) can be extended to an eigenvalue problem by writing (2.10) as

$$\mathcal{S}\mathbf{h} + \sum_{k=1}^{m} \hat{c}_k \mathbf{T}_k = \rho(\sigma)\mathbf{h}, \quad \mathbf{h} \in \mathcal{H}_{(con)}(\sigma). \tag{2.18}$$

Since $(\mathcal{S}\mathbf{h} - \rho(\sigma)\mathbf{h}) \in \mathcal{T}$, we have

$$\mathcal{Q}(\mathcal{S}\mathbf{h} - \rho(\sigma)\mathbf{h}) = \mathbf{0}. \tag{2.19}$$

Therefore, using (2.15) and (2.16), we see that (2.18) is equivalent to

$$\mathcal{Q}\mathcal{S}\mathcal{Q}\mathbf{h} = \rho(\sigma)\mathbf{h}, \quad \mathbf{h} \in \mathcal{H}_{(con)}(\sigma), \tag{2.20}$$

Rogers [36] showed that the conjugate points defined by (2.18) are equal to the zero eigenvalues of (2.20) as long a the projection $\mathcal{QSQ}$ retains it's spectral properties.

One such suitable projection $\mathcal{Q}$ is given by

$$\mathcal{Q}\mathbf{h} \equiv \mathbf{h} - \sum_{i,j=1}^{m} \mathbf{T}_i \chi_{ij} \left\langle \mathbf{h}, \mathbf{T}_j \right\rangle_\sigma, \tag{2.21}$$

where the matrix $\boldsymbol{\chi} = \{\chi_{ij}\}$ is defined by $\boldsymbol{\chi}^{-1} \equiv \left\{\left\langle \mathbf{T}_i, \mathbf{T}_j \right\rangle_\sigma\right\}$.

The *isoperimetric index* I is defined as the number of isoperimetric conjugate points counted according to multiplicity. I is equal to the dimension of the subspace of constrained variations for which the second variation is negative, assuming both the continuity of $\rho(\sigma)$ with respect to σ, and the isolation of conjugate points [36]. Therefore, the definition of an isoperimetric index is analogous to that of an unconstrained index, first introduced by Morse [32]. If $I = 0$ then the condition (2.9) holds and the critical point $\mathbf{q}$ is stable. Central to showing this analogous extension from the unconstrained to the constrained case to be true, is proving that the projected operator $\mathcal{QSQ}$ has the following three properties:

1. For prescribed σ, the operator $\mathcal{QSQ}$ has a countable infinity of isolated eigenvalues $\rho_1(\sigma) \le \rho_2(\sigma) \le \cdots$, each with finite multiplicity.

2. Each eigenvalue $\rho_j(\sigma)$ is a monotonically decreasing function of σ.

3. For σ sufficiently close to a, $\rho_j(\sigma) > 0$, for all j.

The proofs of these properties can be found in Rogers [36] or Manning, Rogers and Maddocks [31]. Given the properties 1 - 3, the number of conjugate points is equal to the number of eigenvalues $\rho_j(b)$ that are negative.

2.2 Neumann Boundary Conditions

We shall briefly look at how changing the Dirichlet boundary conditions (2.2) to the Neumann conditions

$$\mathbf{q}'(a) = \mathbf{f}_a, \quad \mathbf{q}'(b) = \mathbf{f}_b, \tag{2.22}$$

affects the conjugate point theory discussed above.

Here, we assume that there exists a solution $\mathbf{q}^{(0)}(s)$, to the Euler-Lagrange equations, and that

$$\left[\mathcal{L}_{\mathbf{q'}}(s)\right]_a^b = 0, \quad \text{and} \quad \left[\mathcal{L}_{\mathbf{q'q}}(s)\right]_a^b = 0, \tag{2.23}$$

which allows us to write the second variation in it's inner product form. These conditions will hold for the rod examples shown in this thesis with Neumann boundary conditions.

If properties 1 - 3 hold, then if there is a zero eigenvalue $\rho_j(\sigma)$, it is becoming negative and therefore, since there are no negative eigenvalues for σ close to a, the number of conjugate points is equal to the number of negative eigenvalues at b. However, properties 2 and 3 are only strictly true for Dirichlet boundary conditions [27]. In the case of Neumann boundary conditions, there may be eigenvalues which are becoming positive. There may also be negative eigenvalues for σ close to a (we see an example of this in chapter 5). Therefore we must use a revised expression for the index I.

$$I = N_i + N_n - N_p, \tag{2.24}$$

where

$$N_i = \left| \left\{ \rho_j(\sigma) \ : \ \lim_{\sigma \to a} \rho_j(\sigma) < 0 \right\} \right|,$$

which we call the negative *inborn eigenvalues*, and

$$N_n = \left| \left\{ \rho_j(\sigma) \ : \ \rho_j(\sigma) = 0, \ \frac{\partial}{\partial \sigma}\rho_j(\sigma) < 0, \ a < \sigma < b \right\} \right|,$$
$$N_p = \left| \left\{ \rho_j(\sigma) \ : \ \rho_j(\sigma) = 0, \ \frac{\partial}{\partial \sigma}\rho_j(\sigma) > 0, \ a < \sigma < b \right\} \right|.$$

Therefore, N_n is the number of zero eigenvalues with negative velocity with respect to σ, and N_p is the number of zero eigenvalues with positive velocity with respect to σ.

This new index definition is required for Neumann problems because the Jacobi operator (either the standard unconstrained operator or the orthogonal projection) no longer strictly satisfy the properties 1 - 3, from section 2.1. In the case of a discontinuous integrand, we can still use the index definition (in both Dirichlet and Neumann problems) as long as the analogous second order operator keeps the same properties as in the continuous case.

2.3 Discontinuous Integrand

In this section, we shall look at the problem of a discontinuous integrand, first for the unconstrained problem, and then for the constrained variational problem. Divide the region $[a, b]$ into n partitions so that $a = s_0 < s_1 < \cdots < s_n = b$, and consider the discontinuous function

$$W(\mathbf{q}, \mathbf{q}') = \begin{cases} W^{(1)}(\mathbf{q}, \mathbf{q}') & s_0 \leq s < s_1 \\ \vdots & \vdots \\ W^{(n)}(\mathbf{q}, \mathbf{q}') & s_{n-1} \leq s \leq s_n \end{cases}, \quad \mathbf{q}(s) \in \mathbb{R}^p.$$

We wish to minimise the functional

$$E[\mathbf{q}] \quad = \quad \int_a^b W(\mathbf{q}, \mathbf{q}') \, \mathrm{d}s \quad = \quad \sum_{i=1}^n \int_{s_{i-1}}^{s_i} W^{(i)}(\mathbf{q}, \mathbf{q}') \, \mathrm{d}s, \tag{2.25}$$

$$\mathbf{q}(a) = \mathbf{f}_a, \quad \mathbf{q}(b) = \mathbf{f}_b. \tag{2.26}$$

Define $E_i[\mathbf{q}]$ by

$$E_i[\mathbf{q}] := \int_{s_{i-1}}^{s_i} W^{(i)}(\mathbf{q}, \mathbf{q}') \, \mathrm{d}s.$$

2.3.1 The First Variation

We seek critical points $\mathbf{q}$, such that the first variation $\delta E[\mathbf{h}]$ vanishes for all $\mathbf{h}$ belonging to a set of continuous variations satisfying homogeneous Dirichlet boundary conditions

$$\mathcal{H}_d \equiv \left\{ \mathbf{h} \in H^2(a, b) \ : \ \mathbf{h}(a) = \mathbf{h}(b) = \mathbf{0} \right\}. \tag{2.27}$$

The first variation of the functional $E[\mathbf{q}]$ is

$$\begin{aligned} \delta E[\mathbf{h}] \quad &= \quad \int_a^b \left[\mathbf{h} \cdot W_{\mathbf{q}} + \mathbf{h}' \cdot W_{\mathbf{q}'} \right] \, \mathrm{d}s \\ &= \quad \sum_{i=1}^n \int_{s_{i-1}}^{s_i} \left[\mathbf{h} \cdot W_{\mathbf{q}}^{(i)} + \mathbf{h}' \cdot W_{\mathbf{q}'}^{(i)} \right] \, \mathrm{d}s. \end{aligned} \tag{2.28}$$

By integrating by parts, and using the boundary conditions and the continuity of $\mathbf{h}$, we now require

$$
\begin{aligned}
\delta E[\mathbf{h}] \;=\; & \sum_{i=1}^{n} \int_{s_{i-1}}^{s_i} \mathbf{h} \cdot \left[W_{\mathbf{q}}^{(i)} - \frac{\mathrm{d}}{\mathrm{d}s} W_{\mathbf{q}'}^{(i)} \right] \, \mathrm{d}s \\
& + \sum_{i=1}^{n-1} \mathbf{h}(s_i) \cdot \left[W_{\mathbf{q}'}^{(i)}(s_i-) - W_{\mathbf{q}'}^{(i+1)}(s_i+) \right] = 0, \quad \forall \mathbf{h} \in \mathcal{H}_d. \quad (2.29)
\end{aligned}
$$

One can construct a family of functions $\left\{ \tilde{\mathbf{h}}_i(s) \right\} \in \mathcal{H}_d$, which are zero everywhere except in the region (s_{i-1}, s_i). Then $\delta E\left[\tilde{\mathbf{h}}_i \right] = 0$ only if $W_{\mathbf{q}}^{(i)} - \frac{\mathrm{d}}{\mathrm{d}s} W_{\mathbf{q}'}^{(i)} = \mathbf{0}$. Therefore, for the first variation to vanish for all $\mathbf{h} \in \mathcal{H}_d$, we must have

$$
\sum_{i=1}^{n-1} \mathbf{h}(s_i) \cdot \left[W_{\mathbf{q}'}^{(i)}(s_i-) - W_{\mathbf{q}'}^{(i+1)}(s_i+) \right] = 0 \quad \forall \mathbf{h} \in \mathcal{H}_d.
$$

Now, by constructing a family of functions $\left\{ \hat{\mathbf{h}}_i(s) \right\} \in \mathcal{H}_d$, which are zero everywhere except in the neighbourhood of s_i, $i = 1, \ldots, n-1$, we see that we must have

$$
\begin{aligned}
W_{\mathbf{q}}^{(i)} \;&=\; \frac{\mathrm{d}}{\mathrm{d}s} W_{\mathbf{q}'}^{(i)}, \quad \text{for} \quad i = 1, \ldots, n, \quad \text{and} & (2.30) \\
W_{\mathbf{q}'}^{(i)}(s_i-) \;&=\; W_{\mathbf{q}'}^{(i+1)}(s_i+), \quad \text{for} \quad i = 1, \ldots, n-1. & (2.31)
\end{aligned}
$$

These are the Euler-Lagrange equations for each E_i, as well as the first Weierstrass-Erdmann corner conditions for a fixed point variational problem with a broken extremal, which is differentiable at all points of s in the neighbourhood of s_j, but which is not differentiable at s_j itself. These results agree with the work of Cole [7], Bliss and Mason [2], and Graves [14], in which the calculus of variations problem with a discontinuous integrand is considered.

The second Weierstrass-Erdmann corner condition requires the continuity of the expression $\mathbf{q}' \cdot W_{\mathbf{q}'} - W$ (the Hamiltonian). However, since we are concerned with the discontinuous function W, this is not a required condition for our problem. This is also the case in [2],[7], and [14]. Indeed, in the case of elastic rods formulated in the next chapter, for continuous $\mathbf{q}$, the discontinuity of W implies the discontinuity of the Hamiltonian.

Note that if $W^{(i)}_{\mathbf{q'q'}} > 0$ for all s in (s_{i-1}, s_i), then the function $W^{(i)}$ is strictly convex with respect to $\mathbf{q}'$, and therefore does not have an extremal with corner points within (s_{i-1}, s_i).

2.3.2 The Second Variation

The second variation of $E[\mathbf{q}]$ is

$$\delta^2 E[\mathbf{h}] = \frac{1}{2} \int_a^b \left[\mathbf{h'} \cdot \mathbf{P}\mathbf{h'} + \mathbf{h'} \cdot \mathbf{C}^T \mathbf{h} + \mathbf{h} \cdot \mathbf{C}\mathbf{h'} + \mathbf{h} \cdot \mathbf{Q}\mathbf{h} \right] \, \mathrm{d}s, \tag{2.32}$$

which we can write as

$$\delta^2 E[\mathbf{h}] = \frac{1}{2} \sum_{i=1}^n \int_{s_{i-1}}^{s_i} \left[\mathbf{h'} \cdot \mathbf{P}\mathbf{h'} + \mathbf{h'} \cdot \mathbf{C}^T \mathbf{h} + \mathbf{h} \cdot \mathbf{C}\mathbf{h'} + \mathbf{h} \cdot \mathbf{Q}\mathbf{h} \right] \, \mathrm{d}s, \tag{2.33}$$

Alternatively, we can write the second variation $\delta^2 E[\mathbf{h}]$ as

$$\delta^2 E[\mathbf{h}] \;=\; \frac{1}{2} \langle \mathcal{S}\mathbf{h}, \mathbf{h} \rangle \;=\; \frac{1}{2} \sum_{i=1}^n \langle \mathcal{S}\mathbf{h}, \mathbf{h} \rangle_i \tag{2.34}$$

where $\mathcal{S}$ is the Jacobi operator

$$\mathcal{S}\mathbf{h} \equiv - \left(\mathbf{P}\mathbf{h'} + \mathbf{C}^T \mathbf{h} \right)' + \mathbf{C}\mathbf{h'} + \mathbf{Q}\mathbf{h}, \tag{2.35}$$

and $\langle \cdot, \cdot \rangle$ denotes the standard L^2 inner product on $[a, b]$, and $\langle \cdot, \cdot \rangle_i$ denotes the L^2 inner product on $[s_{i-1}, s_i]$.

Note that if the matrix $\mathbf{P}$ is positive definite and if $\mathbf{v}(s_i-) = \mathbf{v}(s_i+)$ for $i = 1, \ldots, n-1$, where

$$\mathbf{v}(s) := \mathbf{P}\mathbf{h'} + \mathbf{C}^T \mathbf{h}, \tag{2.36}$$

then the Jacobi operator $\mathcal{S}$ is regular and self-adjoint, as in the case of W being a smooth and continuous function. Now let us introduce a revised definition for a conjugate point.

Definition 2.3.1. *A point $\sigma \in [s_\ell, s_{\ell+1}] \subset [a, b]$, is conjugate to a with respect to the functional $\delta^2 E[\mathbf{h}]$ if there is a nontrivial solution to*

$$\mathcal{S}\mathbf{h} \;=\; \mathbf{0}, \tag{2.37}$$

$$\mathbf{h}(a) \;=\; \mathbf{h}(\sigma) = \mathbf{0}, \tag{2.38}$$

$$\mathbf{v}(s_i-) \;=\; \mathbf{v}(s_i+), \quad i = 1, \ldots, \ell. \tag{2.39}$$

For a critical point $\mathbf{q}$ to be a local minimum of $E[\mathbf{q}]$, we must have $\delta^2 E[\mathbf{h}] \geq 0$ $\forall \mathbf{h} \in \mathcal{H}_d$. Let us now assume that $\delta^2 E[\mathbf{h}] > 0$, then we can reduce it to the form

$$\delta^2 E[\mathbf{h}] = \int_a^b \boldsymbol{\varphi} \cdot \boldsymbol{\varphi} \, \mathrm{d}s, \tag{2.40}$$

where $\boldsymbol{\varphi}$ is a function which cannot be identically zero unless $\mathbf{h} \equiv \mathbf{0}$. We attempt to express $\delta^2 E[\mathbf{h}]$ in the form (2.40) by adding the quantity $\frac{\mathrm{d}}{\mathrm{d}s}(\mathbf{h} \cdot \mathbf{U}\mathbf{h})$ to the integrand, where $\mathbf{U}$ is a real symmetric matrix. First observe that

$$\int_a^b \frac{\mathrm{d}}{\mathrm{d}s}(\mathbf{h} \cdot \mathbf{U}\mathbf{h}) \, \mathrm{d}s = \sum_{i=1}^{n-1} \left\{ \, [\mathbf{h} \cdot \mathbf{U}\mathbf{h}](s_i-) - [\mathbf{h} \cdot \mathbf{U}\mathbf{h}](s_i+) \, \right\}.$$

Therefore, adding the expression $(\mathbf{h} \cdot \mathbf{U}\mathbf{h})'$ to the integrand, will not change the value of $\delta^2 E$ as long as

$$[\mathbf{h} \cdot \mathbf{U}\mathbf{h}](s_i-) = [\mathbf{h} \cdot \mathbf{U}\mathbf{h}](s_i+), \quad i = 1, \ldots, n-1. \tag{2.41}$$

If (2.41) holds, then continuity of $\mathbf{h}$ means

$$\mathbf{U}(s_i-)\,\mathbf{h}(s_i-) = \mathbf{U}(s_i+)\,\mathbf{h}(s_i+), \quad i = 1, \ldots, n-1. \tag{2.42}$$

Now, after some trivial manipulation, it can be shown that

$$\delta^2 E = \int_a^b \left(\mathbf{P}^{1/2}\mathbf{h}' + \mathbf{P}^{-1/2}\left(\mathbf{U} + \mathbf{C}^T\right)\mathbf{h} \right) \cdot \left(\mathbf{P}^{1/2}\mathbf{h}' + \mathbf{P}^{-1/2}\left(\mathbf{U} + \mathbf{C}^T\right)\mathbf{h} \right) \, \mathrm{d}s.$$

This is only true if $\mathbf{U}$ is chosen to be a solution to the following differential equation

$$\mathbf{Q} + \mathbf{U}' = (\mathbf{U} + \mathbf{C})\,\mathbf{P}^{-1}\left(\mathbf{U} + \mathbf{C}^T\right). \tag{2.43}$$

Therefore, if (2.43) has a solution which does not vanish in $[a, b]$, which satisfies the matching conditions (2.42), then $\delta^2 E > 0$. If we make the substitution

$$\mathbf{U} + \mathbf{C}^T = -\mathbf{P}\mathbf{H}'\mathbf{H}^{-1},$$

where $\mathbf{H} := (\mathbf{h}_1, \ldots, \mathbf{h}_p)$, and $\mathbf{h}_j$ $(j = 1, \ldots, p)$, are linearly independent solutions to (2.37)-(2.39), then equation (2.43) reduces to

$$-\left(\mathbf{P}\mathbf{H}' + \mathbf{C}^T\mathbf{H}\right)' + \mathbf{C}\mathbf{H}' + \mathbf{Q}\mathbf{H} = \mathbf{0},$$

which is the Jacobi equation, and (2.42) becomes

$$\mathbf{v}\left(s_i-\right) = \mathbf{v}\left(s_i+\right), \quad i = 1, \ldots, n-1.$$

Therefore, if there are no points in $[a, b]$ conjugate to a with respect to $\delta^2 E[\mathbf{h}]$, then there exists a solution to (2.43) which does not vanish in $[a, b]$. Hence $\delta^2 E[\mathbf{h}] > 0$. Thus we have proved the following theorem:

Theorem 2.3.2. *If* **P** *is positive definite, and the interval* $[a, b]$ *contains no points conjugate to* a*, then the functional* $\delta^2 E[\mathbf{h}] > 0$ *for all continuous* **h** *such that* $\mathbf{h}(a) = \mathbf{h}(b) = \mathbf{0}$ *and* $\mathbf{v}(s_i-) = \mathbf{v}(s_i+)$*, for* $i = 1, \cdots, n-1$*.*

The converse of theorem (2.3.2) can also be proved. First observe the following lemma:

Lemma 2.3.3. *If the function* **h** *satisfies*

$$-\left(\mathbf{P}\mathbf{h}' + \mathbf{C}^T\mathbf{h}\right)' + \mathbf{C}\mathbf{h}' + \mathbf{Q}\mathbf{h} = \mathbf{0},$$

with the conditions

$$\begin{aligned} \mathbf{h}(a) &= \mathbf{h}(b) = \mathbf{0}, \\ \mathbf{v}(s_i-) &= \mathbf{v}(s_i+), \quad i = 1, \ldots, n-1, \end{aligned}$$

then

$$\int_a^b \left[\mathbf{h}' \cdot \mathbf{P}\mathbf{h}' + \mathbf{h}' \cdot \mathbf{C}^T\mathbf{h} + \mathbf{h} \cdot \mathbf{C}\mathbf{h}' + \mathbf{h} \cdot \mathbf{Q}\mathbf{h}\right] \, \mathrm{d}s = 0$$

Proof. This is easily shown by integrating by parts and applying the boundary conditions. □

Theorem 2.3.4. *If the functional*

$$\int_a^b \left[\mathbf{h}' \cdot \mathbf{P}\mathbf{h}' + \mathbf{h}' \cdot \mathbf{C}^T\mathbf{h} + \mathbf{h} \cdot \mathbf{C}\mathbf{h}' + \mathbf{h} \cdot \mathbf{Q}\mathbf{h}\right] \, \mathrm{d}s > 0 \qquad (2.44)$$

for all **h***, such that* $\mathbf{h}(a) = \mathbf{h}(b) = \mathbf{0}$*,* $\mathbf{v}(s_i-) = \mathbf{v}(s_i+)$*,* $i = 1, \ldots, n-1$*, and* **P** *is positive definite, then the interval* $[a, b]$ *contains no points conjugate to* a*, with respect to* $\delta^2 E$*.*

Proof. Construct a family of positive definite functionals:

$$\int_a^b t\left[\mathbf{h}' \cdot \mathbf{P}\mathbf{h}' + \mathbf{h}' \cdot \mathbf{C}^T\mathbf{h} + \mathbf{h} \cdot \mathbf{C}\mathbf{h}' + \mathbf{h} \cdot \mathbf{Q}\mathbf{h}\right] \; + \; (1-t)\left[\mathbf{h}' \cdot \mathbf{h}'\right] \quad \mathrm{d}s \qquad (2.45)$$

dependent on a parameter t, which for $t = 1$, gives the functional (2.44), and $t = 0$ gives

$$\int_a^b \mathbf{h}' \cdot \mathbf{h}' \; \mathrm{d}s. \qquad (2.46)$$

The Jacobi equation for (2.45) is

$$t\left[\left(\mathbf{P}\mathbf{h}' + \mathbf{C}^T\mathbf{h}\right)' + \mathbf{C}\mathbf{h}' + \mathbf{Q}\mathbf{h}\right] \; + \; (1-t)\left[\mathbf{h}''\right] = \mathbf{0}. \qquad (2.47)$$

For $t = 0$, it is obvious that there is no conjugate point in $[a, b]$.

To prove the theorem, we show that as t is varied continuously from 0 to 1, no conjugate points can appear in $[a, b]$. Let $\{\mathbf{h}_j(s,t), \; j = 1, \ldots, p\}$ be the set of linearly independent solutions of (2.47), such that

$$\mathbf{h}_j(a,t) \;=\; \mathbf{0}, \quad \forall t \qquad (2.48)$$

$$\mathbf{h}_j'(a,t) \;=\; \mathbf{e}_j, \quad \forall t \qquad (2.49)$$

$$\mathbf{v}\left[\mathbf{h}_j(s_i-,t)\right] \;=\; \mathbf{v}\left[\mathbf{h}_j(s_i+,t)\right], \quad i = 1, \ldots, n-1, \quad \forall t \qquad (2.50)$$

Now, suppose that $[a, b]$ contains a point σ conjugate to a. If $\sigma = b$ then, from the lemma, the functional (2.44) would be zero, which contradicts the original assumption of positive definiteness of (2.44). Therefore we assume $\sigma \in (a, b)$. Now, for a given solution $\mathbf{h}_j(s,t)$, consider the set of all points

$$\{(s,t) : \mathbf{h}_j(s,t) = \mathbf{0}\}. \qquad (2.51)$$

If this set is nonempty, it represents a continuous curve $s = s(t)$. By hypothesis, the point $(\sigma, 1)$ lies on this curve. Thus starting from the point $(\sigma, 1)$, the curve

A. Cannot terminate inside the rectangle $a \leq s \leq b$, $0 \leq t \leq 1$, since this would contradict the continuous dependence of the solution $\mathbf{h}_j(s,t)$ on the parameter t;

B. Cannot intersect the segment $s = b$, since on this line (2.45) is equal to zero for all t;

C. Cannot intersect the segment $t = 1$, since then for some t we would have $\mathbf{h}_j(s,t) = \mathbf{h}'_j(s,t) = \mathbf{0}$, which could only be true if $\mathbf{h}_j(s,t) \equiv \mathbf{0}$ for all s;

D. Cannot intersect the segment $t = 0$, since equation (2.47) would be $\mathbf{h}''_j = \mathbf{0}$, whose solution $\mathbf{h}_j = (s - a)\boldsymbol{e}_j$ would only vanish for $s = a$;

E. Cannot intersect the segment $s = a$, since the limit of $\mathbf{h}'_j(a + \epsilon, t)$ as $\epsilon \to 0$, is $\mathbf{0}$.

Therefore no such curve can exist and hence there can be no conjugate points. □

We have shown that a necessary condition for a critical point $\mathbf{q}$ to be stable is that there is no conjugate point to a in the interval $[a, b]$ with respect to $\delta^2 E[\mathbf{h}]$, where the conjugate point definition (2.3.1) is the same as in the case of a continuous integrand except for the following conditions at $s = s_i$, where W has a jump in continuity:

$$\mathbf{v}(s_i-) = \mathbf{v}(s_i+). \tag{2.52}$$

The proofs of theorems (2.3.2) and (2.3.4) are an adaptation of those found in [12], where here we do not assume the continuity of W, nor the symmetry of the matrix $\mathbf{C}$. The conditions (2.52) agree with the work of Cole [7], in which an index is established for the calculus of variations problem with a discontinuous integrand. Cole [7] shows that the index of the Jacobi operator $\mathcal{S}$, defined to be the maximal dimension of the subspace of variations on which $\delta^2 E[\mathbf{h}] < 0$, is equal to the sum of the orders of the conjugate points defined in definition (2.3.1).

2.3.3 The Isoperimetric Problem

Since the linear operator $\mathcal{S}$ is regular and self-adjoint, the notion of an index can be extended to isoperimetric problem by taking a suitable projection of the unconstrained eigenvalue problem and showing that the properties 1 - 3 still hold.

Now let us introduce a new definition for an isoperimetric conjugate point for a discontinuous integrand.

Definition 2.3.5. *A point $\sigma \in [s_\ell, s_{\ell+1}] \subset [a, b]$, is an isoperimetric conjugate point to a with respect to the functional $\delta^2 E[\mathbf{h}]$ if there is a nontrivial solution to*

$$\mathcal{S}\mathbf{h} = \sum_{k=1}^{m} \hat{c}_k \mathbf{T}_k, \tag{2.53}$$

$$\mathbf{h}(a) = \mathbf{h}(\sigma) = \mathbf{0}, \tag{2.54}$$

$$\mathbf{v}(s_i-) = \mathbf{v}(s_i+), \quad i = 1, \dots, \ell, \tag{2.55}$$

$$\int_a^\sigma \mathbf{h} \cdot \mathbf{T}_k \, \mathrm{d}s = 0, \quad k = 1, \dots, m. \tag{2.56}$$

2.4 Numerical Implementation

The stability index can be obtained by counting the conjugate points, which are found by solving the initial value problem

$$\mathcal{S}\mathbf{h} = \sum_{k=1}^{m} \hat{c}_k \mathbf{T}_k, \quad \mathbf{h}(a) = \mathbf{0}.$$

The number of conjugate points is then equal to the number of times $\mathbf{h}(\sigma) = \mathbf{0}$ for $a < \sigma < b$, subject to the constraints (2.56). Given the initial conditions, we seek the solution $\mathbf{h}$ of the form

$$\mathbf{h} = c_1 \mathbf{h}_1 + \cdots + c_p \mathbf{h}_p + \hat{c}_1 \hat{\mathbf{h}}_1 + \cdots + \hat{c_m} \hat{\mathbf{h}}_m.$$

In order to find the individual linearly independent solutions, we solve the system of initial value problems

$$\mathcal{S}\mathbf{h}_j = \mathbf{0}, \quad \mathbf{h}_j(a) = \mathbf{0}, \quad \mathbf{h}_j'(a) = \boldsymbol{e}_j, \quad j = 1, \dots, p,$$
$$\mathcal{S}\hat{\mathbf{h}}_k = \hat{c}_k \mathbf{T}_k, \quad \hat{\mathbf{h}}_k(a) = \mathbf{0}, \quad \hat{\mathbf{h}}_k'(a) = \mathbf{0}, \quad k = 1, \dots, m.$$

The boundary conditions $\mathbf{h}_j'(a) = \boldsymbol{e}_j$ ensures linearly independent solutions of the homogeneous equations. Note that we can write the eigenvalue boundary value problem as an initial value problem as a standard consequence of the Jacobi condition, see e.g. theorem 6.2(c) in Maddocks [24].

Conjugate points are then values of $\sigma \in (a, b)$ for which

$$\mathcal{A}(\sigma) \begin{bmatrix} c_1 \\ \vdots \\ \hat{c}_m \end{bmatrix} = \mathbf{0},$$

where

$$\mathcal{A} = \begin{pmatrix} \mathbf{h}_1(\sigma) & \cdots & \mathbf{h}_p(\sigma) & \hat{\mathbf{h}}_1(\sigma) & \cdots & \hat{\mathbf{h}}_m(\sigma) \\ \int_a^\sigma \mathbf{h}_1 \cdot \mathbf{T}_1 \, \mathrm{d}s & \cdots & \int_a^\sigma \mathbf{h}_p \cdot \mathbf{T}_1 \, \mathrm{d}s & \int_a^\sigma \hat{\mathbf{h}}_1 \cdot \mathbf{T}_1 \, \mathrm{d}s & \cdots & \int_a^\sigma \hat{\mathbf{h}}_m \cdot \mathbf{T}_1 \, \mathrm{d}s \\ \vdots & & \vdots & \vdots & & \vdots \\ \int_a^\sigma \mathbf{h}_1 \cdot \mathbf{T}_m \, \mathrm{d}s & \cdots & \int_a^\sigma \mathbf{h}_p \cdot \mathbf{T}_m \, \mathrm{d}s & \int_a^\sigma \hat{\mathbf{h}}_1 \cdot \mathbf{T}_m \, \mathrm{d}s & \cdots & \int_a^\sigma \hat{\mathbf{h}}_m \cdot \mathbf{T}_m \, \mathrm{d}s \end{pmatrix}.$$

Therefore if

$$|\mathcal{A}(\sigma)| = 0,$$

then σ is a conjugate point. Here, $|\cdot|$ denotes the matrix determinant.

To account for the matching conditions (2.55), we solve the initial value problem for each subsection of the interval $[a, b]$:

$$\mathcal{S}\mathbf{h}_j^{(0)} = \mathbf{0}, \qquad \mathbf{h}_j^{(0)}(a) = \mathbf{0}, \qquad \mathbf{h}_j^{'(0)}(a) = \boldsymbol{e}_j,$$

$$\mathcal{S}\hat{\mathbf{h}}_k^{(0)} = \hat{c}_k \mathbf{T}_k, \quad \hat{\mathbf{h}}_k^{(0)}(a) = \mathbf{0}, \qquad \hat{\mathbf{h}}_k^{'(0)}(a) = \mathbf{0},$$

$$\mathcal{S}\mathbf{h}_j^{(i)} = \mathbf{0}, \qquad \mathbf{h}_j^{(i)}(s_i) = \mathbf{h}_j^{(i-1)}(s_i), \quad \mathbf{v}[\mathbf{h}_j^{(i)}(s_i)] = \mathbf{v}[\mathbf{h}_j^{(i-1)}(s_i)],$$

$$\mathcal{S}\hat{\mathbf{h}}_k^{(i)} = \hat{c}_k \mathbf{T}_k, \quad \hat{\mathbf{h}}_k^{(i)}(s_i) = \hat{\mathbf{h}}_k^{(i-1)}(s_i), \quad \mathbf{v}[\hat{\mathbf{h}}_k^{(i)}(s_i)] = \mathbf{v}[\hat{\mathbf{h}}_k^{(i-1)}(s_i)],$$

for $i = 1, \ldots, n-1$, $j = 1, \ldots, p$, and $k = 1, \ldots, m$. Conjugate points are then values of σ for which

$$\left|\bar{\mathcal{A}}(\sigma)\right| = 0, \tag{2.57}$$

where

$$\bar{\mathcal{A}}(\sigma) = \begin{cases} \mathcal{A}^{(0)} & : & s_0 < \sigma \leq s_1 \\ \vdots & & \\ \mathcal{A}^{(n-1)} & : & s_{n-1} \leq \sigma < s_n \end{cases},$$

and $\mathcal{A}^{(i)}$, for $i = 0, \ldots, n-1$, is given by

$$\mathcal{A}^{(i)} = \begin{pmatrix} \mathbf{h}_1^{(i)}(\sigma) & \cdots & \mathbf{h}_p^{(i)}(\sigma) & \hat{\mathbf{h}}_1^{(i)}(\sigma) & \cdots & \hat{\mathbf{h}}_m^{(i)}(\sigma) \\ \int_a^\sigma \mathbf{h}_1^{(i)} \cdot \mathbf{T}_1 \, \mathrm{d}s & \cdots & \int_a^\sigma \mathbf{h}_p^{(i)} \cdot \mathbf{T}_1 \, \mathrm{d}s & \int_a^\sigma \hat{\mathbf{h}}_1^{(i)} \cdot \mathbf{T}_1 \, \mathrm{d}s & \cdots & \int_a^\sigma \hat{\mathbf{h}}_m^{(i)} \cdot \mathbf{T}_1 \, \mathrm{d}s \\ \vdots & & \vdots & \vdots & & \vdots \\ \int_a^\sigma \mathbf{h}_1^{(i)} \cdot \mathbf{T}_m \, \mathrm{d}s & \cdots & \int_a^\sigma \mathbf{h}_p^{(i)} \cdot \mathbf{T}_m \, \mathrm{d}s & \int_a^\sigma \hat{\mathbf{h}}_1^{(i)} \cdot \mathbf{T}_m \, \mathrm{d}s & \cdots & \int_a^\sigma \hat{\mathbf{h}}_m^{(i)} \cdot \mathbf{T}_m \, \mathrm{d}s \end{pmatrix}.$$

Chapter 3

Cosserat Theory of Elastic Rods

In this chapter we will determine the static equilibrium equations for an elastic rod which is inextensible and unshearable. The Cosserat theory of elastic rods can be found in many books and articles. A review of the theory of intrinsically straight, inextensible, unshearable elastic rods undergoing bending and torsion can be found in [42]. A comprehensive overview of the dynamic rod equations can be found in Antman [1]. Although here we look at static deformations of the rod, inextensibility lets us treat the arclength s as an independent 'time' variable, and so the static rod equations lead to a dynamical system in the mathematical sense.

3.1 Kinematic Equations

The rod is determined by a centreline

$$\boldsymbol{r}(s) : [0, L] \to \mathbb{R}^3, \tag{3.1}$$

and

$$\boldsymbol{d}_1(s) : [0, L] \to \mathbb{R}^3, \tag{3.2}$$

which is a unit vector in the normal cross-section of the rod. The rod is parametrised by $s \in [0, L]$. Since the rod is inextensible, $\boldsymbol{r}'(s)$ is a vector function describing the tangent to the centreline at s. Inextensibility implies that s can be treated as the arclength of the rod of length L. Unshearability implies that the tangent to the centreline $\boldsymbol{r}'(s)$ be

normal to $\boldsymbol{d}_1$. Let $\boldsymbol{d}_3$ describe the tangent vector, then by introducing $\boldsymbol{d}_2 := \boldsymbol{d}_3 \times \boldsymbol{d}_1$, we get an orthonormal set of *directors*

$$\{\boldsymbol{d}_1(s), \boldsymbol{d}_2(s), \boldsymbol{d}_3(s)\}, \tag{3.3}$$

describing the orientation of the cross-section of the rod at s (see figure 3.1).

The function $\boldsymbol{r}(s)$ can be found by solving the differential equation

$$\boldsymbol{r}' = \boldsymbol{d}_3, \quad \boldsymbol{r}(0) = \boldsymbol{0}. \tag{3.4}$$

Since the set of directors $\{\boldsymbol{d}_i\}$ is orthonormal, there exists a vector $\boldsymbol{u}(s)$ such that
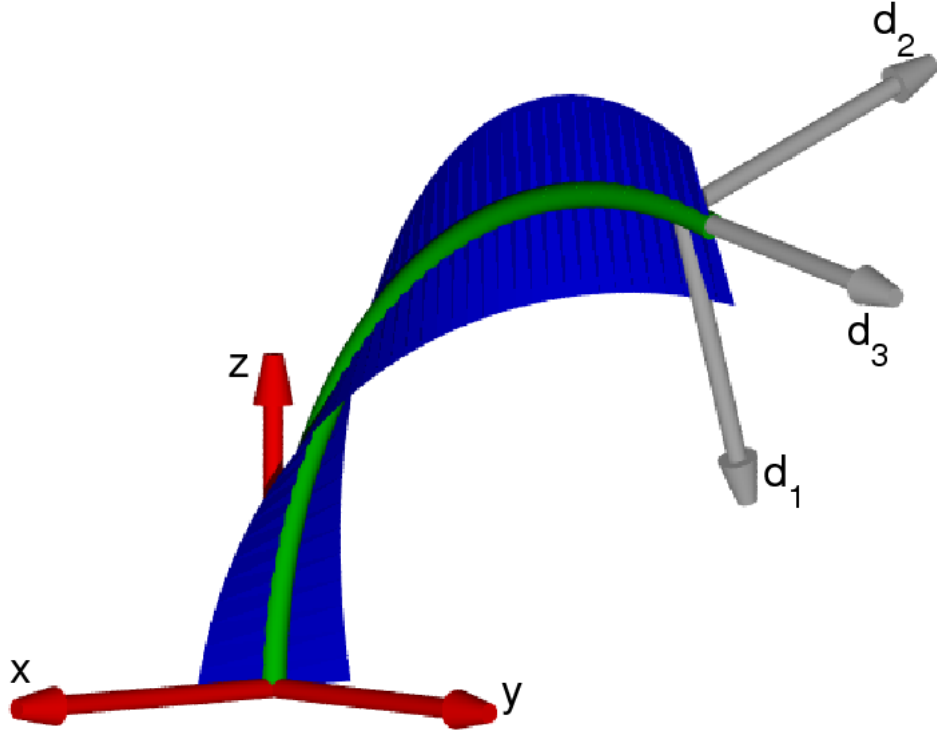
Figure 3.1: The centreline of the rod (green) with the directors. The vector $\boldsymbol{d}_3$ points in the same direction as $\boldsymbol{r}'$, the tangent to the centreline. The directors $\boldsymbol{d}_1$ and $\boldsymbol{d}_2$ are normal to $\boldsymbol{d}_3$ and make up the orthonormal basis for the moving frame. The blue ribbon is in line with $\boldsymbol{d}_1$, illustrating the twist of the rod along the arclength. Image taken from [30].

$$\boldsymbol{d}_i' = \boldsymbol{u} \times \boldsymbol{d}_i, \quad \text{for} \quad i = 1, 2, 3. \tag{3.5}$$

If we express $\boldsymbol{u}(s)$ as

$$\boldsymbol{u} := u_1(s)\boldsymbol{d}_1(s) + u_2(s)\boldsymbol{d}_2(s) + u_3(s)\boldsymbol{d}_3(s), \tag{3.6}$$

then we shall call (u_1, u_2, u_3) the *strains*. u_1 and u_2 are the strains with respect to bending, and they represent the curvatures of the centreline on the planes $(\boldsymbol{d}_2, \boldsymbol{d}_3)$ and $(\boldsymbol{d}_1, \boldsymbol{d}_3)$ respectively. u_3 represents the rate of rotation about the body axis of the rod.

3.2 Balance Equations

In this section we introduce the static equilibrium balance equations for the rod. Let $\boldsymbol{n}(s)$ be the contact force, and $\boldsymbol{m}(s)$ be the contact moment exerted by the material of $(s, L]$ on to that of $[0, s]$. The force and moment balance equations are

$$\boldsymbol{n}' = \boldsymbol{0}, \tag{3.7}$$

$$\boldsymbol{m}' = \boldsymbol{n} \times \boldsymbol{r}'. \tag{3.8}$$

Since $\boldsymbol{n}$ is an integral to equation (3.7), we choose the fixed orthonormal basis $\{\boldsymbol{e}_1, \boldsymbol{e}_2, \boldsymbol{e}_3\}$ such that the direction of $\boldsymbol{e}_3$ is the same as the direction of $\boldsymbol{n}$. Therefore

$$\boldsymbol{n} = T\boldsymbol{e}_3, \quad T > 0, \tag{3.9}$$

where T is the magnitude of the force, and we can write (3.8) as

$$\boldsymbol{m}' = T\boldsymbol{e}_3 \times \boldsymbol{d}_3. \tag{3.10}$$

These co-ordinate free equations (3.9) and (3.10) can provide relationships between boundary conditions at $s = 0$ and $s = L$. Integrating (3.10) and using (3.4), we get

$$\boldsymbol{m} - T\boldsymbol{e}_3 \times \boldsymbol{r} = \boldsymbol{m}(0), \tag{3.11}$$

and we can write

$$\boldsymbol{m}(L) \cdot \boldsymbol{n} = \boldsymbol{m}(0) \cdot \boldsymbol{n}. \tag{3.12}$$

These relationships will be of importance when solving the rod equilibrium equations numerically, since to avoid non isolated solutions, we must know which conditions have been imposed, and which conditions are implied by the balance of external forces.

33

3.3 Constitutive Relations

In order to complete the formulation of the elastic rod, we must introduce constitutive relations between the strains $\boldsymbol{u}(s)$ and the moment $\boldsymbol{m}(s)$. If we make the assumption of a *hyperelastic* rod, then we can introduce a strain energy density function $W(u_1 - \hat{u}_1, u_2 - \hat{u}_2, u_3 - \hat{u}_3; s)$, where $\hat{u}_i$ are the intrinsic strains, i.e. the strains of the rod in an unstressed state. The strains u_i determine the local moment m_i acting on the cross-section of the rod by the relation

$$\frac{\partial W}{\partial u_i} = m_i, \quad i = 1, 2, 3, \tag{3.13}$$

where

$$m_i := \boldsymbol{m} \cdot \boldsymbol{d}_i, \quad i = 1, 2, 3. \tag{3.14}$$

For a linearly elastic rod, we have

$$W = \frac{1}{2} \sum_{i=1}^{3} B_i (u_i - \hat{u}_i)^2, \tag{3.15}$$

where B_i are the bending stiffnesses $(i = 1, 2)$, and the torsional stiffness $(i = 3)$, assumed to be constant. Here, $B_1 = Y I_1$ and $B_2 = Y I_2$, where Y is Young's modulus of the material and I_1 and I_2 are the moments of inertia about $\boldsymbol{d}_1$ and $\boldsymbol{d}_2$. $B_3 = G I_3$, where I_3 is the moment of inertia about the $\boldsymbol{d}_3$ axis, and

$$G = \frac{Y}{2(1 + \nu)} \tag{3.16}$$

is the shear modulus, where ν is the Poisson ratio of the material. For an intrinsically straight rod with no intrinsic twist, the constitutive relations are then

$$m_i = B_i u_i, \quad i = 1, 2, 3. \tag{3.17}$$

If we introduce the components of the force with respect to the directors

$$n_i = \boldsymbol{n} \cdot \boldsymbol{d}_i, \quad i = 1, 2, 3, \tag{3.18}$$

and let

$$\mathsf{m} = (m_1, m_2, m_3)^T, \tag{3.19}$$

$$\mathsf{u} = (u_1, u_2, u_3)^T, \tag{3.20}$$

$$\mathsf{n} = (n_1, n_2, n_3)^T, \tag{3.21}$$

then we can write the full rod equations as

$$\boldsymbol{r}' = \boldsymbol{d}_3, \tag{3.22}$$

$$\boldsymbol{d}_i' = \boldsymbol{u} \times \boldsymbol{d}_i, \quad i = 1, 2, 3, \tag{3.23}$$

$$\mathsf{m}' = \mathsf{m} \times \mathsf{u} + \mathsf{n} \times \boldsymbol{e}_3, \tag{3.24}$$

$$\mathsf{n}' = \mathsf{n} \times \mathsf{u}. \tag{3.25}$$

3.4 Euler Parameters

We follow the approach of Dichmann, Li, and Maddocks [9] and parametrise the directors $\{\boldsymbol{d}_1, \boldsymbol{d}_2, \boldsymbol{d}_3\}$ relative to the fixed frame $\{\boldsymbol{e}_1, \boldsymbol{e}_2, \boldsymbol{e}_3\}$ by the use of Euler parameters (or quaternions). These are a quadruple of real numbers $\mathsf{q} = (q_1, q_2, q_3, q_4)$ which satisfy the condition

$$\mathsf{q} \cdot \mathsf{q} = 1. \tag{3.26}$$

The use of Euler parameters avoids any singularities which can occur if we parametrise with Euler angles. Also, the expressions for the strains u_i and the directors $\boldsymbol{d}_i$ in terms of the Euler parameters are polynomial, which is computationally more efficient to deal with than the trigonomic expressions derived from using Euler angles.

The directors can be written in terms of Euler parameters as follows:

$$\boldsymbol{d}_1 = \frac{1}{|\mathsf{q}|^2} \begin{pmatrix} q_1^2 - q_2^2 - q_3^2 + q_4^2 \\ 2(q_1 q_2 + q_3 q_4) \\ 2(q_1 q_3 - q_2 q_4) \end{pmatrix}, \tag{3.27}$$

$$\boldsymbol{d}_2 = \frac{1}{|\mathsf{q}|^2} \begin{pmatrix} 2(q_1 q_2 - q_3 q_4) \\ -q_1^2 + q_2^2 - q_3^2 + q_4^2 \\ 2(q_1 q_4 + q_2 q_3) \end{pmatrix}, \tag{3.28}$$

$$\boldsymbol{d}_3 = \frac{1}{|\mathsf{q}|^2} \begin{pmatrix} 2(q_1 q_3 + q_2 q_4) \\ 2(-q_1 q_4 + q_2 q_3) \\ -q_1^2 - q_2^2 + q_3^2 + q_4^2 \end{pmatrix}. \tag{3.29}$$

The strains of the rod in terms of Euler parameters are

$$u_i = \frac{2}{|\mathbf{q}|^2} D_i \mathbf{q} \cdot \mathbf{q}', \quad \text{for} \quad i = 1, 2, 3, \tag{3.30}$$

where the skew-symmetric rotation matrices D_i are

$$D_1 = \begin{pmatrix} 0 & 0 & 0 & 1 \\ 0 & 0 & 1 & 0 \\ 0 & -1 & 0 & 0 \\ -1 & 0 & 0 & 0 \end{pmatrix}, \quad D_2 = \begin{pmatrix} 0 & 0 & -1 & 0 \\ 0 & 0 & 0 & 1 \\ 1 & 0 & 0 & 0 \\ 0 & -1 & 0 & 0 \end{pmatrix}, \quad D_3 = \begin{pmatrix} 0 & 1 & 0 & 0 \\ -1 & 0 & 0 & 0 \\ 0 & 0 & 0 & 1 \\ 0 & 0 & -1 & 0 \end{pmatrix}.$$

When analysing the stability of a static deformation of an elastic rod, it will be convenient to express the energy functional in terms of $\mathbf{q}$:

$$E[\mathbf{q}] = \int_0^L W \left[u_1(\mathbf{q}, \mathbf{q}'), u_2(\mathbf{q}, \mathbf{q}'), u_3(\mathbf{q}, \mathbf{q}'); s \right] \, ds. \tag{3.31}$$

By writing the energy in this form we adopt the methods used in [19], [28], [36], although variational formulations for the rod equations as well as stability analysis has been derived in [6] by taking variations of the rotation matrix $R := (\boldsymbol{d}_1, \boldsymbol{d}_2, \boldsymbol{d}_3)$.

3.5   Boundary Conditions

Let us look at some of the various boundary conditions that can be imposed on an elastic rod. For each set of boundary conditions, we will look at two distinct options - unconstrained, or constrained. In the unconstrained case, the end at $s = L$ is able to move freely, whereas in the constrained case the end of the rod at $s = L$ is forced to lie on the 'vertical' axis $\boldsymbol{e}_3$.

For constrained problems, we let

$$\boldsymbol{r}(L) = (0, 0, *), \quad \boldsymbol{f} = (*, *, \lambda). \tag{3.32}$$

For unconstrained problems, we let

$$\boldsymbol{r}(L) = (*, *, *), \quad \boldsymbol{f} = (0, 0, \lambda). \tag{3.33}$$

For all boundary value problems, we take $\boldsymbol{r}(0) = \boldsymbol{0}$. In either the constrained or unconstrained case, we have specified 6 conditions, and therefore need to specify an additional 7 conditions.

3.5.1 Clamped-Sleeved

For the clamped-sleeved boundary value problem, the rod is taken to be in line with the fixed frame at $s = 0$, i.e. $\boldsymbol{d}_i = \boldsymbol{e}_i$ for $i = 1, 2, 3$. At the other end, the tangent of the centreline remains in line with the vertical axis, i.e. $\boldsymbol{d}_3 = \boldsymbol{e}_3$. In terms of the Euler parameters, we have

$$\mathbf{q}(0) = (0, 0, 0, 1), \quad \mathbf{q}(L) = \left(0, 0, \sin\left(\frac{\phi}{2}\right), \cos\left(\frac{\phi}{2}\right)\right), \tag{3.34}$$

where ϕ is the twist angle with respect to the plane $(\boldsymbol{e}_1, \boldsymbol{e}_2)$. This gives us 14 boundary conditions - one more than necessary. However, since the norm condition $|\mathbf{q}|^2 = 1$ is satisfied through the boundary condition at $s = 0$, the condition $q_4(L) = \cos\left(\frac{\phi}{2}\right)$ is already implied. Thus, we have the 7 necessary boundary conditions. If $\phi = 0$, then this is reduced to a clamped-clamped boundary value problem.

3.5.2 Pinned

Pinned boundary conditions describe ends of the rod that have zero moment, so we have

$$\mathsf{m}(0) = \mathbf{0}, \quad \mathsf{m}(L) = \mathbf{0}. \tag{3.35}$$

In addition to these conditions, the norm condition is specified at one end, $|\mathbf{q}|^2(L) = 1$. This problem has non-isolated solutions, which prohibit numerical solutions via parameter continuation methods. To avoid this, we impose the condition $d_{1y}(L) := \boldsymbol{d}_1 \cdot \boldsymbol{e}_2(L) = 0$, which selects a single family of possible values for the directors. In the constrained case, both ends of the rod are in line with the vertical axis, thus the condition $m_3(L) = 0$ is implied though the moment balance equation (3.8). The additional 7 boundary conditions required for a pinned boundary value problem are then

$$\mathsf{m}(0) = \mathbf{0}, \quad \mathsf{m}(L) = (0, 0, *), \quad (q_1 q_2 + q_3 q_4)(L) = 0, \quad |\mathbf{q}|^2(L) = 1. \tag{3.36}$$

3.6 Matching Conditions

At a point $s = s_c$, where W is discontinuous, the matching conditions

$$W_{\mathbf{q}'}(s_c+) - W_{\mathbf{q}'}(s_c-) = 0,$$

must be satisfied. This is a result from section 2.3.1, and must hold in order that the first variation of the energy functional be zero for all allowed variations. For the strain energy density function (3.15), the function $W_{\mathbf{q}'}$ becomes

$$W_{\mathbf{q}'} = \frac{B_1 u_1}{|\mathbf{q}|^2} \begin{pmatrix} q_4 \\ q_3 \\ -q_2 \\ -q_1 \end{pmatrix} + \frac{B_2 u_2}{|\mathbf{q}|^2} \begin{pmatrix} -q_3 \\ q_4 \\ q_1 \\ -q_2 \end{pmatrix} + \frac{B_3 u_3}{|\mathbf{q}|^2} \begin{pmatrix} q_2 \\ -q_1 \\ q_4 \\ -q_3 \end{pmatrix}.$$

If the directors $\mathbf{q}$ are continuous then this condition is the continuity of the local moment components:

$$m_1(s_c+) = m_1(s_c-), \qquad (3.37)$$

$$m_2(s_c+) = m_2(s_c-), \qquad (3.38)$$

$$m_3(s_c+) = m_3(s_c-). \qquad (3.39)$$

Chapter 4

Stability Analysis of an Elastic Strut

In this chapter we consider a rod of length L, with a discontinuity in the bending or torsional stiffnesses at the point $s = L_1$, but on which the bending stiffnesses are constant over the regions $[0, L_1)$ and $(L_1, L]$. We consider an intrinsically straight rod with clamped-clamped boundary conditions, undergoing a vertical compression λ_3 in the $\boldsymbol{e}_3$ direction, with the end at $s = L$ constrained to lie on the $\boldsymbol{e}_3$-axis. We perform bifurcation analysis on the simpler planar rod, as well as the three-dimensional elastic strut. In section 4.6, we focus on a specific class of discontinuous rods in which the cross-section of each partition is an ellipse with the same circumference, but different eccentricity. The aim is to model a nanotube, in which part of the tube has been deformed by axial compression, to create a nanotube junction. Also in this section, we will consider the case where the load parameter λ_3 is replaced by an end displacement condition (hard loading), and the end rotation of the rod is varied.

The post-buckling analysis of an elastic strut has been widely studied, e.g. by van der Heijden and colleagues [39], [40], [43], and Hoffman, Manning and Paffenroth [20], in which the stability index of solutions of the twisted elastic strut are computed using conjugate point theory. Results in this chapter agree with those found in [20] for the case of no discontinuities. For the hard loaded problem in section 4.6, our results agree with van der Heijden, Neukirch and Thomson [40], in which stability analysis is performed

on clamped anisotropic rods.

4.1   Second Variation

Consider a rod with clamped-clamped boundary conditions from chapter 3

$$\mathbf{q}(0) = \mathbf{q}(L) = (0,0,0,1),$$

which is subject to constraints

$$\boldsymbol{r}(L) = (0,0,*).$$

We use the equation from chapter 3

$$\boldsymbol{r}' = \boldsymbol{d}_3, \quad \boldsymbol{r}(0) = \mathbf{0},$$

to write the constraints in isoperimetric form

$$\int_0^L d_{3x}(s) \; \mathrm{d}s = 0, \quad \int_0^L d_{3y}(s) \; \mathrm{d}s = 0. \tag{4.1}$$

Here, and throughout this thesis, we define

$$\begin{aligned}
\boldsymbol{d}_{ix} &:= \boldsymbol{d}_i \cdot \boldsymbol{e}_1, \\
\boldsymbol{d}_{iy} &:= \boldsymbol{d}_i \cdot \boldsymbol{e}_2, \\
\boldsymbol{d}_{iz} &:= \boldsymbol{d}_i \cdot \boldsymbol{e}_3.
\end{aligned}$$

The strain energy density function is chosen to be discontinuous

$$W(\mathbf{q}, \mathbf{q}') = \left\{ \begin{array}{lll} W^{(1)}(\mathbf{q}, \mathbf{q}') & : & 0 \leq s \leq L_1 \\ W^{(2)}(\mathbf{q}, \mathbf{q}') & : & L_1 < s \leq L \end{array} \right. ,$$

where

$$\begin{aligned}
W^{(1)}(\mathbf{q}, \mathbf{q}') &= \frac{1}{2} \sum_{j=1}^{3} B_j \left[u_j(\mathbf{q}, \mathbf{q}') \right]^2 + \lambda_3 d_{3z}(\mathbf{q}), \\
W^{(2)}(\mathbf{q}, \mathbf{q}') &= \frac{1}{2} \sum_{j=1}^{3} C_j \left[u_j(\mathbf{q}, \mathbf{q}') \right]^2 + \lambda_3 d_{3z}(\mathbf{q}),
\end{aligned}$$

and λ_3 is an external force pushing downward on the strut. B_j and C_j are the bending ($j = 1, 2$) and torsional ($j = 3$) stiffnesses of the rod for each partition. Adding the

constraints to the energy functional by means of the multiplier rule, the elastic energy is given by

$$E[\mathbf{q}] \;=\; \int_0^{L_1} W^{(1)}(\mathbf{q},\mathbf{q}') + \boldsymbol{\lambda} \cdot \boldsymbol{d}_3(\mathbf{q}) \; \mathrm{d}s \;+\; \int_{L_1}^{L} W^{(2)}(\mathbf{q},\mathbf{q}') + \boldsymbol{\lambda} \cdot \boldsymbol{d}_3(\mathbf{q}) \; \mathrm{d}s,$$

where $\boldsymbol{\lambda} = (\lambda_1, \lambda_2, \lambda_3)^T$. The constants λ_1 and λ_2 are Lagrange multipliers from the isoperimetric constraints (4.1). Let $\mathbf{h} \in \mathbb{R}^4$ be the variation of $\mathbf{q}$. The second variation of the energy functional is given by

$$\delta^2 E[\mathbf{h}] = \frac{1}{2} \int_0^{L_1} \mathbf{h} \cdot \mathcal{S}\mathbf{h} \; \mathrm{d}s \;+\; \frac{1}{2} \int_{L_1}^{L} \mathbf{h} \cdot \mathcal{S}\mathbf{h} \; \mathrm{d}s,$$

where

$$\mathcal{S}\mathbf{h} \equiv \left(\mathbf{P}\mathbf{h}' + \mathbf{C}^T\mathbf{h}\right)' + \mathbf{C}\mathbf{h}' + \mathbf{Q}\mathbf{h},$$

and

$$\mathbf{P} = \mathcal{L}_{\mathbf{q}'\mathbf{q}'} \quad \mathbf{C} = \mathcal{L}_{\mathbf{q}\mathbf{q}'} \quad \mathbf{Q} = \mathcal{L}_{\mathbf{q}\mathbf{q}},$$

where $\mathcal{L} = W + \boldsymbol{\lambda} \cdot \boldsymbol{d}_3$. For a critical point to be stable, the second variation must be non-negative,

$$\delta^2 E[\mathbf{h}] \geq 0,$$

for all variations $\mathbf{h}$ satisfying $\mathbf{h}(0) = \mathbf{h}(L) = 0$, as well as the linearised constraints

$$\int_0^L \mathbf{h} \cdot (d_{3x})_{\mathbf{q}} \; \mathrm{d}s = 0, \quad \text{and} \quad \int_0^L \mathbf{h} \cdot (d_{3y})_{\mathbf{q}} \; \mathrm{d}s = 0.$$

Assuming Legendre's strengthend condition that $\mathbf{P}$ is positive definite, this is equivalent to there being no isoperimetric conjugate points.

4.2   Projection of Variations

A simple calculation of the matrix $\mathbf{P}$ evaluated for the trivial unstressed rod gives

$$\mathbf{P} = \begin{cases} 4\begin{pmatrix} B_1 & 0 & 0 & 0 \\ 0 & B_2 & 0 & 0 \\ 0 & 0 & B_3 & 0 \\ 0 & 0 & 0 & 0 \end{pmatrix} & : \;\; 0 \leq s \leq L_1 \\[2em] 4\begin{pmatrix} C_1 & 0 & 0 & 0 \\ 0 & C_2 & 0 & 0 \\ 0 & 0 & C_3 & 0 \\ 0 & 0 & 0 & 0 \end{pmatrix} & : \;\; L_1 < s \leq L \end{cases},$$

which is not positive definite. Since Legendre's strengthend condition does not hold for the trivial rod configuration, we can not find the index by counting the number of conjugate points.

This problem is a result of the use of $\mathbf{q} \in \mathbb{R}^4$ to parametrise the three-dimensional space of directors. To fix this problem, we follow the methods used in [20] and [28] by only considering variations $\mathbf{h}$ that are orthogonal to $\mathbf{q}$.

Let $\mathbf{h} = \psi(\sigma)\mathbf{q}(\sigma) + \boldsymbol{w}(\sigma)$, where $\boldsymbol{w}(\sigma)$ is orthogonal to $\mathbf{q}(\sigma)$. Then

$$E\left[\mathbf{q} + \epsilon \mathbf{h}\right] = E\left[(1 + \epsilon\psi)\mathbf{q} + \epsilon\boldsymbol{w}\right].$$

Since $E[\mathbf{q}] = E[c\mathbf{q}]$ for any $c \in \mathbb{R}$, the above expression is equal to

$$E\left[\mathbf{q} + \frac{\epsilon\boldsymbol{w}}{(1 + \epsilon\psi)}\right].$$

Therefore

$$E\left[\mathbf{q} + \epsilon \mathbf{h}\right] < E\left[\mathbf{q}\right] \iff E\left[\mathbf{q} + \epsilon\boldsymbol{w}\right] < E\left[\mathbf{q}\right]$$

for ϵ sufficiently small. If we define a projection matrix $\boldsymbol{\Pi} = (D_1\mathbf{q}, D_2\mathbf{q}, D_3\mathbf{q}) \in \mathbb{R}^{4\times3}$, then

$$\mathbf{q} \cdot (\boldsymbol{\Pi}\boldsymbol{\zeta}) = \sum_{i=1}^{3} \zeta_i \mathbf{q} \cdot D_i\mathbf{q} = 0$$

for any $\boldsymbol{\zeta} := (\zeta_1, \zeta_2, \zeta_3)^T \in \mathbb{R}^3$. Therefore, we make the substitution $\mathbf{q} = \boldsymbol{\Pi}\boldsymbol{\zeta}$. For a critical point $\mathbf{q}$ to be a local minimum, we now require

$$\delta^2 E\left[\boldsymbol{\Pi}\boldsymbol{\zeta}\right] \geq 0,$$

for all $\boldsymbol{\zeta}$ satisfying the boundary conditions

$$\boldsymbol{\Pi}\boldsymbol{\zeta}(0) = \boldsymbol{\Pi}\boldsymbol{\zeta}(L) = \mathbf{0},$$

as well as the projected, linearised constraints

$$\int_0^L \boldsymbol{\Pi}\boldsymbol{\zeta} \cdot (d_{3x})_{\mathbf{q}} \, \mathrm{d}s = 0, \quad \text{and} \quad \int_0^L \boldsymbol{\Pi}\boldsymbol{\zeta} \cdot (d_{3y})_{\mathbf{q}} \, \mathrm{d}s = 0.$$

The second variation can be expressed as

$$\delta^2 E\left[\boldsymbol{\Pi}\boldsymbol{\zeta}\right] = \left\langle \bar{\mathcal{S}}\boldsymbol{\zeta}, \boldsymbol{\zeta} \right\rangle,$$

where

$$\bar{\mathcal{S}}\boldsymbol{\zeta} \equiv -\left(\bar{\mathbf{P}}\boldsymbol{\zeta}' + \bar{\mathbf{C}}^T\boldsymbol{\zeta}\right)' + \bar{\mathbf{C}}\boldsymbol{\zeta}' + \bar{\mathbf{Q}}\boldsymbol{\zeta}, \tag{4.2}$$

for

$$\begin{aligned}
\bar{\mathbf{P}} &:= \boldsymbol{\Pi}^T\mathbf{P}\boldsymbol{\Pi}, \\
\bar{\mathbf{C}} &:= \boldsymbol{\Pi}^T\mathbf{C}\boldsymbol{\Pi} + \boldsymbol{\Pi}'^T\mathbf{P}\boldsymbol{\Pi}, \\
\bar{\mathbf{Q}} &:= \boldsymbol{\Pi}^T\mathbf{C}\boldsymbol{\Pi}' + \boldsymbol{\Pi}'^T\mathbf{C}^T\boldsymbol{\Pi} + \boldsymbol{\Pi}^T\mathbf{Q}\boldsymbol{\Pi} + \boldsymbol{\Pi}'^T\mathbf{P}\boldsymbol{\Pi}'.
\end{aligned}$$

A conjugate point is a value $\sigma \in (0, L)$ for which

$$\begin{aligned}
\bar{\mathcal{S}}\boldsymbol{\zeta} &= \hat{c}_1\mathbf{T}_1 + \hat{c}_2\mathbf{T}_2, \\
\boldsymbol{\zeta}(0) = \boldsymbol{\zeta}(\sigma) &= \mathbf{0}, \\
\bar{\mathbf{P}}\boldsymbol{\zeta}'(L_1-) &= \bar{\mathbf{P}}\boldsymbol{\zeta}'(L_1+), \\
\int_0^L \boldsymbol{\zeta} \cdot \mathbf{T}_k \,\mathrm{d}s &= 0, \quad k = 1, 2,
\end{aligned} \tag{4.3}$$

where

$$\mathbf{T}_1 = \boldsymbol{\Pi}^T\left(d_{3x}\right)_{\mathbf{q}}, \quad \mathbf{T}_2 = \boldsymbol{\Pi}^T\left(d_{3y}\right)_{\mathbf{q}}.$$

4.3 Stability of the Unbuckled Rod

For the purposes of numerical implementation, we define the functions $\boldsymbol{\varphi}[0, L_1] \to \mathbb{R}^3$ and $\boldsymbol{\eta}[L_1, L] \to \mathbb{R}^3$ by

$$\begin{aligned}
\boldsymbol{\varphi}(s) &= \boldsymbol{\zeta}(s), \quad 0 \le s \le L_1, \\
\boldsymbol{\eta}(s) &= \boldsymbol{\zeta}(s), \quad L_1 < s \le L, \\
\boldsymbol{\eta}(L_1) &= \lim_{\epsilon \to 0} \boldsymbol{\zeta}(L_1 + \epsilon);
\end{aligned}$$

$\mathbf{T}_{k1}[0, L_1] \to \mathbb{R}^3$ and $\mathbf{T}_{k2}[L_1, L] \to \mathbb{R}^3$ $(k = 1, 2)$ by

$$\begin{aligned}
\mathbf{T}_{k1}(s) &= \mathbf{T}_k(s), \quad 0 \le s \le L_1, \\
\mathbf{T}_{k2}(s) &= \mathbf{T}_k(s), \quad L_1 < s \le L, \\
\mathbf{T}_{k2}(L_1) &= \lim_{\epsilon \to 0} \mathbf{T}_k(L_1 + \epsilon);
\end{aligned}$$

$\bar{\mathbf{P}}_1[0, L_1] \to \mathbb{R}^{3\times 3}$ and $\bar{\mathbf{P}}_2[L_1, L] \to \mathbb{R}^{3\times 3}$ by

$$
\begin{aligned}
\bar{\mathbf{P}}_1(s) &= \bar{\mathbf{P}}(s), \quad 0 \leq s \leq L_1, \\
\bar{\mathbf{P}}_2(s) &= \bar{\mathbf{P}}(s), \quad L_1 < s \leq L, \\
\bar{\mathbf{P}}_2(L_1) &= \lim_{\epsilon \to 0} \bar{\mathbf{P}}(L_1 + \epsilon),
\end{aligned}
$$

and we define $\bar{\mathbf{C}}_1, \bar{\mathbf{C}}_2, \bar{\mathbf{Q}}_1, \bar{\mathbf{Q}}_2$ in the same way.

The second order Jacobi equation can now be written as

$$\bar{\mathcal{S}}_1 \boldsymbol{\varphi} \equiv - \left(\bar{\mathbf{P}}_1 \boldsymbol{\varphi}' + \bar{\mathbf{C}}_1^T \boldsymbol{\varphi} \right)' + \bar{\mathbf{C}}_1 \boldsymbol{\varphi}' + \bar{\mathbf{Q}}_1 \boldsymbol{\varphi} = \hat{c}_1 \mathbf{T}_{11} + \hat{c}_2 \mathbf{T}_{21}, \quad 0 \leq s \leq L_1, \qquad (4.4)$$

$$\bar{\mathcal{S}}_2 \boldsymbol{\eta} \equiv - \left(\bar{\mathbf{P}}_2 \boldsymbol{\eta}' + \bar{\mathbf{C}}_2^T \boldsymbol{\eta} \right)' + \bar{\mathbf{C}}_2 \boldsymbol{\eta}' + \bar{\mathbf{Q}}_2 \boldsymbol{\eta} = \hat{d}_1 \mathbf{T}_{12} + \hat{d}_2 \mathbf{T}_{22}, \quad L_1 \leq s \leq L, \qquad (4.5)$$

with boundary conditions

$$
\begin{aligned}
\boldsymbol{\varphi}(0) &= \mathbf{0}, & (4.6) \\
\boldsymbol{\eta}(L) &= \mathbf{0}, & (4.7) \\
\boldsymbol{\varphi}(L_1) &= \boldsymbol{\eta}(L_1), & (4.8) \\
\bar{\mathbf{P}}_1(L_1) \boldsymbol{\varphi}'(L_1) &= \bar{\mathbf{P}}_2(L_1) \boldsymbol{\eta}'(L_1). & (4.9)
\end{aligned}
$$

If we express the general solution, which in this case, is the sum of the 6 linearly independent homogeneous solutions and the 2 particular solutions as

$$
\begin{aligned}
\boldsymbol{\varphi}(s) &= a_1 \boldsymbol{\varphi}_1 + \cdots + a_n \boldsymbol{\varphi}_n, \\
\boldsymbol{\eta}(s) &= b_1 \boldsymbol{\eta}_1 + \cdots + b_n \boldsymbol{\eta}_n,
\end{aligned}
$$

then we find branch points occur when

$$|\mathcal{A}| = 0,$$

where $\mathcal{A}$ is the $2n \times 2n$ matrix, incorporating the boundary conditions and constraints,

given by

$$
\mathcal{A} = \begin{pmatrix}
\boldsymbol{\varphi}_1(0) & \cdots & \boldsymbol{\varphi}_n(0) & 0 & \cdots & 0 \\
0 & \cdots & 0 & \boldsymbol{\eta}_1(L) & \cdots & \boldsymbol{\eta}_n(L) \\
\boldsymbol{\varphi}_1(L_1) & \cdots & \boldsymbol{\varphi}_n(L_1) & -\boldsymbol{\eta}_1(L_1) & \cdots & -\boldsymbol{\eta}_n(L_1) \\
\bar{\mathbf{P}}_1\boldsymbol{\varphi}_1'(L_1) & \cdots & \bar{\mathbf{P}}_1\boldsymbol{\varphi}_n'(L_1) & -\bar{\mathbf{P}}_2\boldsymbol{\eta}_1'(L_1) & \cdots & -\bar{\mathbf{P}}_2\boldsymbol{\eta}_n'(L_1) \\
f_{11}(0) & \cdots & f_{1n}(0) & -g_{11}(L) & \cdots & -g_{1n}(L) \\
f_{11}(L_1) & \cdots & f_{1n}(L_1) & -g_{11}(L_1) & \cdots & -g_{1n}(L_1) \\
f_{21}(0) & \cdots & f_{2n}(0) & -g_{21}(L) & \cdots & -g_{2n}(L) \\
f_{21}(L_1) & \cdots & f_{2n}(L_1) & -g_{21}(L_1) & \cdots & -g_{2n}(L_1)
\end{pmatrix},
$$

where

$$
f_{ij}(s) = \int \mathbf{T}_i \cdot \boldsymbol{\varphi}_j \, \mathrm{d}s,
$$

$$
g_{ij}(s) = \int \mathbf{T}_i \cdot \boldsymbol{\eta}_j \, \mathrm{d}s,
$$

for $i = 1, 2$, and $j = 1, \ldots, n$.

4.3.1 Pure Compression Buckling

For the trivial critical point $\mathbf{q} = (0, 0, 0, 1)$, the Jacobi equation becomes

$$
-4 \begin{pmatrix} B_1 & 0 & 0 \\ 0 & B_2 & 0 \\ 0 & 0 & B_3 \end{pmatrix} \boldsymbol{\varphi}'' - 4\lambda_3 \begin{pmatrix} 1 & 0 & 0 \\ 0 & 1 & 0 \\ 0 & 0 & 0 \end{pmatrix} \boldsymbol{\varphi} = \hat{c}_1 \begin{pmatrix} 0 \\ 2 \\ 0 \end{pmatrix} + \hat{c}_2 \begin{pmatrix} -2 \\ 0 \\ 0 \end{pmatrix},
$$

$$
-4 \begin{pmatrix} C_1 & 0 & 0 \\ 0 & C_2 & 0 \\ 0 & 0 & C_3 \end{pmatrix} \boldsymbol{\eta}'' - 4\lambda_3 \begin{pmatrix} 1 & 0 & 0 \\ 0 & 1 & 0 \\ 0 & 0 & 0 \end{pmatrix} \boldsymbol{\eta} = \hat{d}_1 \begin{pmatrix} 0 \\ 2 \\ 0 \end{pmatrix} + \hat{d}_2 \begin{pmatrix} -2 \\ 0 \\ 0 \end{pmatrix}.
$$

Boundary conditions (4.6) - (4.9) lead to

$$
\nu_3(s) \equiv 0, \quad \text{and} \quad \eta_3(s) \equiv 0.
$$

Therefore we only consider the first two components of $\boldsymbol{\varphi}$ and $\boldsymbol{\eta}$. Let

$$
\bar{\boldsymbol{\varphi}} := \begin{pmatrix} \boldsymbol{\varphi} \cdot \mathbf{e}_1 \\ \boldsymbol{\varphi} \cdot \mathbf{e}_2 \end{pmatrix} \quad \text{and} \quad \bar{\boldsymbol{\eta}} := \begin{pmatrix} \boldsymbol{\eta} \cdot \mathbf{e}_1 \\ \boldsymbol{\eta} \cdot \mathbf{e}_2 \end{pmatrix}.
$$

The general solution to the above equation is

$$\bar{\boldsymbol{\varphi}} = \begin{pmatrix} a_1 \cos(\mu_1 s) + a_2 \sin(\mu_1 s) + 2\hat{c}_2/\lambda_3 \\ a_3 \cos(\mu_2 s) + a_4 \sin(\mu_2 s) - 2\hat{c}_1/\lambda_3 \end{pmatrix},$$

$$\bar{\boldsymbol{\eta}} = \begin{pmatrix} b_1 \cos(\mu_3 s) + b_2 \sin(\mu_3 s) + 2\hat{d}_2/\lambda_3 \\ b_3 \cos(\mu_4 s) + b_4 \sin(\mu_4 s) - 2\hat{d}_1/\lambda_3 \end{pmatrix},$$

where

$$\mu_1 = \sqrt{\lambda_3/B_1}, \quad \mu_2 = \sqrt{\lambda_3/B_2}, \quad \mu_3 = \sqrt{\lambda_3/C_1}, \quad \mu_4 = \sqrt{\lambda_3/C_2}.$$

We use parameter continuation to find solutions to algebraic problem

$$|\mathcal{A}|\,(B_1, B_2, C_1, C_2, \lambda_3) = 0,$$

to find critical values of λ_3 as another parameter is varied. Figure 4.1 shows critical λ_3 values (which we call λ_c) against C_1, where $B_2 = C_2 = 1$, $L = 2$, $L_1 = 1$, and $B_1 = 0.5$, 1, and 2. Note that the values of B_3 and C_3 do not affect pure compression buckling. In each subfigure, there is a critical value of $\lambda_3 = \pi^2$ representing the rod buckling into the $(\boldsymbol{e}_1, \boldsymbol{e}_3)$ plane. The other buckling point λ_c is the branch point connecting to solutions in the $(\boldsymbol{e}_2, \boldsymbol{e}_3)$ plane, which varies as we vary C_1. If the value $\lambda_c < \pi^2$, it buckles into a stable branch of solutions (at least locally), indicated by the red line. If $\lambda_c > \pi^2$, then it buckles into an unstable branch, indicated by the green line. Subfigure (a) shows that for $B_1 = 0.5$, if $C_1 < 4.172$, then the branch of solutions in the $(\boldsymbol{e}_2, \boldsymbol{e}_3)$ plane begin stable. Subfigure (b) shows that for $B_1 = 1$, if $C_1 < 1$, then the branch of solutions in the $(\boldsymbol{e}_2, \boldsymbol{e}_3)$ plane begin stable. Subfigure (c) shows that for $B_1 = 2$, if $C_1 < 0.688$, then the branch of solutions in the $(\boldsymbol{e}_2, \boldsymbol{e}_3)$ plane begin stable. Subfigure (d) illustrates, for the case of $B_1 = 2$, the limit of the critical value λ_c as C_1 is increased further. We see that the limit is $8\pi^2$, which is equal to the critical buckling value for a continuous rod of length 1 and bending stiffness 2.

In general, the limiting critical λ_c value, as one stiffness parameter is increased towards infinity, is described as follows: Let $\lambda_c^{(1)}$ be the first critical value of λ_3 for the rod buckling into the $(\boldsymbol{e}_2, \boldsymbol{e}_3)$ plane, and let $\lambda_c^{(2)}$ be the first critical value of λ_3 for the rod buckling into the $(\boldsymbol{e}_1, \boldsymbol{e}_3)$ plane. Through numerical observations, we find the limits of

the buckling values $\lambda_c^{(1)}$ and $\lambda_c^{(2)}$ to be

$$\lim_{C_k \to \infty} \lambda_c^{(k)} = \frac{4B_k \pi^2}{L_1^2} \quad k = 1, 2,$$

$$\lim_{B_k \to \infty} \lambda_c^{(k)} = \frac{4C_k \pi^2}{L_2^2} \quad k = 1, 2,$$

where $L_2 := L - L_1$. This result is physically intuitive since, as the bending stiffness on one side of the rod becomes very large, it acts like a clamped boundary condition imposed on the other side of the rod (in the relevant plane).
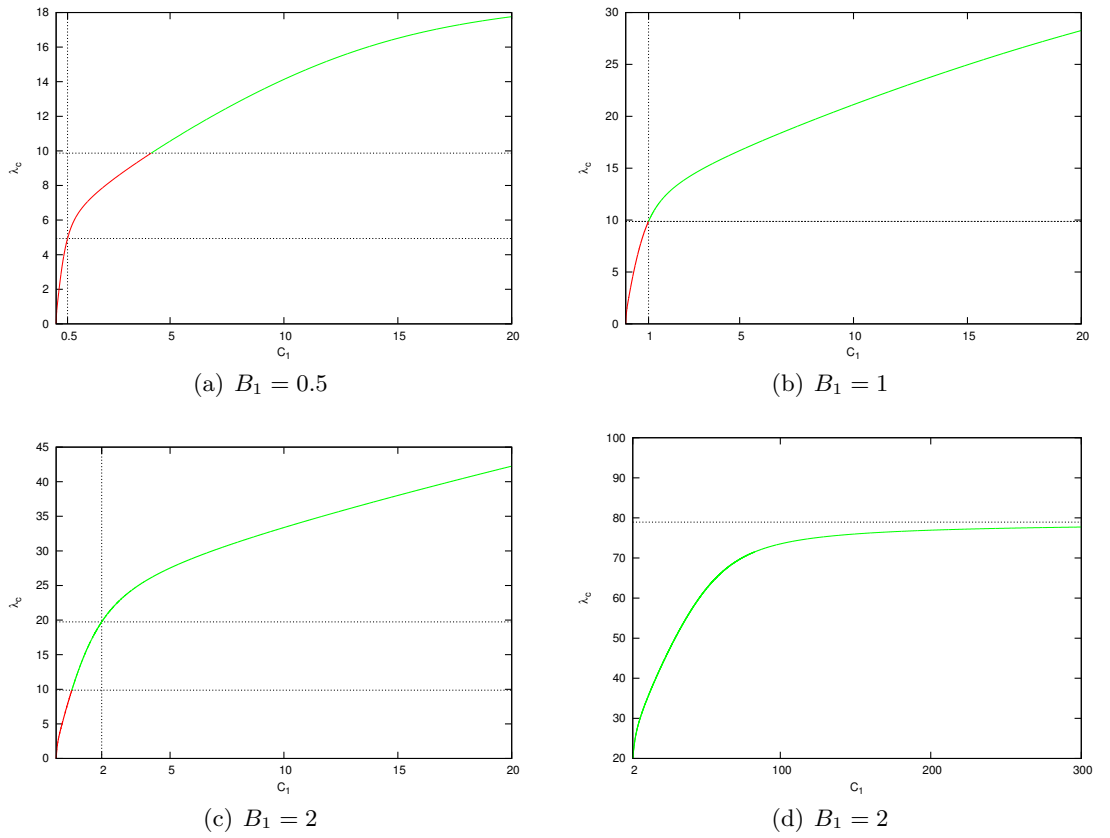

(a) $B_1 = 0.5$

(b) $B_1 = 1$

(c) $B_1 = 2$

(d) $B_1 = 2$

Figure 4.1: First critical buckling values of λ_3 against C_1, for various values of B_1. In each case $B_2 = C_2 = 1$, $L = 2$, and $L_1 = 1$.

4.4   Post-Buckling Stability

To find the index for post-buckled clamped rod configurations with $x(0) = x(L) = 0$, $y(0) = y(L) = 0$, we solve the initial value problem

$$\bar{\mathcal{S}}_1 \boldsymbol{\varphi}_j = 0, \qquad j = 1, 2, 3,$$

$$\bar{\mathcal{S}}_1 \hat{\boldsymbol{\varphi}}_i = \mathbf{T}_{i1}, \qquad i = 1, 2,$$

$$\bar{\mathcal{S}}_2 \boldsymbol{\eta}_j = 0, \qquad j = 1, 2, 3,$$

$$\bar{\mathcal{S}}_2 \hat{\boldsymbol{\eta}}_i = \mathbf{T}_{i2}, \qquad i = 1, 2,$$

$$f'_{ij} = \boldsymbol{\varphi}_j \cdot \mathbf{T}_{i1}, \quad i = 1, 2, \ j = 1, 2, 3,$$

$$\hat{f}'_{ik} = \hat{\boldsymbol{\varphi}}_k \cdot \mathbf{T}_{i1}, \quad i = 1, 2, \ k = 1, 2,$$

$$g'_{ij} = \boldsymbol{\eta}_j \cdot \mathbf{T}_{i2}, \quad i = 1, 2, \ j = 1, 2, 3,$$

$$\hat{g}'_{ik} = \hat{\boldsymbol{\eta}}_k \cdot \mathbf{T}_{i2}, \quad i = 1, 2, \ k = 1, 2,$$

with initial conditions

$$\boldsymbol{\varphi}_j(0) = \mathbf{0}, \quad \boldsymbol{\varphi}'_j(0) = \boldsymbol{e}_j, \quad j = 1, 2, 3,$$

$$\hat{\boldsymbol{\varphi}}_i(0) = \mathbf{0}, \quad \hat{\boldsymbol{\varphi}}'_i(0) = \mathbf{0}, \quad i = 1, 2,$$

$$f_{ij}(0) = 0, \quad i = 1, 2, \ j = 1, 2, 3,$$

$$\hat{f}_{ik}(0) = 0, \quad i = 1, 2, \ k = 1, 2,$$

and matching conditions

$$\boldsymbol{\eta}_j(L_1) = \boldsymbol{\varphi}_j(L_1), \quad \mathbf{P}_1 \boldsymbol{\eta}'_j(L_1) = \mathbf{P}_2 \boldsymbol{\varphi}'_j(L_1), \quad j = 1, 2, 3,$$

$$\hat{\boldsymbol{\eta}}_i(L_1) = \hat{\boldsymbol{\varphi}}_i(L_1), \quad \mathbf{P}_1 \hat{\boldsymbol{\eta}}'_i(L_1) = \mathbf{P}_2 \hat{\boldsymbol{\varphi}}'_i(L_1), \quad i = 1, 2,$$

$$g_{ij}(L_1) = f_{ij}(L_1), \quad i = 1, 2, \ j = 1, 2, 3,$$

$$\hat{g}_{ik}(L_1) = \hat{f}_{ik}(L_1), \quad i = 1, 2, \ k = 1, 2.$$

Let

$$\mathcal{A} = \begin{pmatrix} \boldsymbol{\varphi}_1(\sigma) & \boldsymbol{\varphi}_2(\sigma) & \boldsymbol{\varphi}_3(\sigma) & \hat{\boldsymbol{\varphi}}_1(\sigma) & \hat{\boldsymbol{\varphi}}_2(\sigma) \\ f_{11}(\sigma) & f_{12}(\sigma) & f_{13}(\sigma) & \hat{f}_{11}(\sigma) & \hat{f}_{12}(\sigma) \\ f_{21}(\sigma) & f_{22}(\sigma) & f_{23}(\sigma) & \hat{f}_{21}(\sigma) & \hat{f}_{22}(\sigma) \end{pmatrix}, \tag{4.10}$$

and

$$\mathcal{B} = \begin{pmatrix} \boldsymbol{\eta}_1(\sigma) & \boldsymbol{\eta}_2(\sigma) & \boldsymbol{\eta}_3(\sigma) & \hat{\boldsymbol{\eta}}_1(\sigma) & \hat{\boldsymbol{\eta}}_2(\sigma) \\ g_{11} & g_{12}(\sigma) & g_{13}(\sigma) & \hat{g}_{11}(\sigma) & \hat{g}_{12}(\sigma) \\ g_{21} & g_{22}(\sigma) & g_{23}(\sigma) & \hat{g}_{21}(\sigma) & \hat{g}_{22}(\sigma) \end{pmatrix}, \tag{4.11}$$

then the index is the number of times the function

$$\xi(\sigma) = \begin{cases} |\mathcal{A}|(\sigma) & : & 0 \leq \sigma \leq L_1 \\ |\mathcal{B}|(\sigma) & : & L_1 \leq \sigma \leq L \end{cases} \tag{4.12}$$

crosses zero. Solutions for the rod equations were found in AUTO97 [11] using parameter continuation for the boundary value problem. To find the index for each solution, we solved the initial value problem constructed above, first over the region $[0, L_1]$ using the initial data obtained from the rod solutions, then over the region $[L_1, L]$ using the matching conditions as the initial data. The function ξ is then monitored to find the number of conjugate points. Note that we do not need to find the conjugate point values, just the number of conjugate points, which we find by counting the roots of ξ.
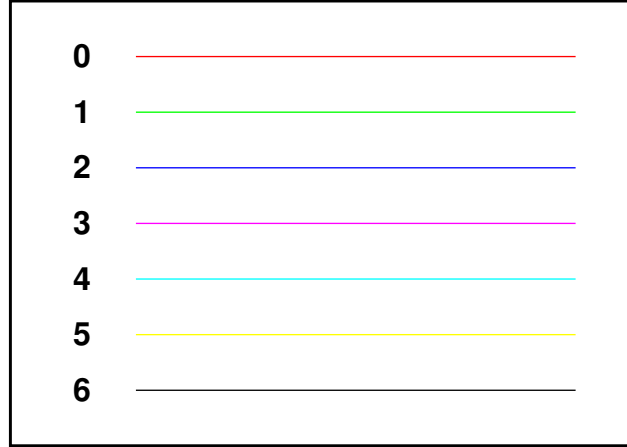
4.5 Numerical Results

Figure 4.2: Colour scheme for solution branches with different stability index.

In this section, we will use the methods described above to perform stability analysis on rods with discontinuous bending stiffness. We will first look at the simplified case

of planar rod solutions, which reduces the variation $\mathbf{h} \in \mathbb{R}^4$ to a function $h \in \mathbb{R}$, and then study three-dimensional rod configurations. Here, and throughout this thesis, all solution branches in bifurcation diagrams will be coloured according to the stability index. Figure 4.2 shows the colour scheme for different values of the index. Note that this colour scheme is for bifurcation diagrams only.

Plots of three-dimensional rod profiles were made using the *tubeplot* function in Maple 13, by plotting a tube with centreline $\boldsymbol{r}(s)$, and radius $\tilde{a}$. We also plot $\boldsymbol{r}(s) + \tilde{a}\boldsymbol{d}_1(s)$ and $\boldsymbol{r}(s) - \tilde{a}\boldsymbol{d}_1(s)$ (in red) along the surface, to illustrate the twist of the tube. Note, the Cosserat rod model deals only with the centreline and directors, therefore the value of $\tilde{a}$ is chosen arbitrarily, purely as a means of visualisation.

4.5.1 Planar Rod Solutions

For the case of planar rod solutions, we add the following restrictions:

$$\boldsymbol{r} \equiv (*, 0, *)^T, \quad \boldsymbol{d}_2 \equiv (0, 1, 0)^T,$$

which reduces the rod equilibrium equations to

$$\theta_1'(s) = u_2, \quad 0 \le s \le L_1,$$
$$\theta_2'(s) = u_2, \quad L_1 \le s \le L,$$
$$x'(s) = \cos\theta_1, \quad z'(s) = \sin\theta_1, \quad 0 \le s \le L_1,$$
$$x'(s) = \cos\theta_2, \quad z'(s) = \sin\theta_2, \quad L_1 \le s \le L,$$
$$B_2\theta_1''(s) = \lambda_3 \sin\theta_1 - \lambda_1 \cos\theta_1, \quad 0 \le s \le L_1,$$
$$C_2\theta_2''(s) = \lambda_3 \sin\theta_2 - \lambda_1 \cos\theta_2, \quad L_1 \le s \le L,$$
$$u_1 = u_3 = \lambda_2 = 0.$$

The Jacobi equation is reduced to

$$-B_2 h_1''(s) - h_1(s)\left[\lambda_1 \sin\theta_1 + \lambda_3 \cos\theta_1\right] = c_1 \cos\theta_1, \quad 0 \le s \le L_1,$$
$$-C_2 h_2''(s) - h_2(s)\left[\lambda_1 \sin\theta_2 + \lambda_3 \cos\theta_2\right] = c_2 \cos\theta_2, \quad L_1 \le s \le L,$$

where $h_i(s) \in \mathbb{R}$ is the variation of $\theta_i(s)$, for $i = 1, 2$.

Introduce the dimensionless parameters

$$\beta := \frac{C_2}{B_2}, \quad \gamma := \frac{L_1}{L}, \quad D := 1 - \frac{z(L)}{L},$$

and let $\lambda := \lambda_3$. Therefore, $D = 0$ represents straight rod solutions and $D = 1$ represents closed rod solutions.

Figure 4.3 shows bifurcation diagrams of λ against the end shortening D. For $\beta = 1$ there is a branch of closed rods at $D = 1$, connecting the first and second branches buckling from the trivial branch at $D = 0$. As β is increased from 1, this connecting branch splits into two distinct solution branches. As β is increased further, a stable branch of solutions appears between two limit points on one of the branches which had split from the $D = 1$ branch. If we perform two-parameter fold-continuation on these limit points, we can find the critical value of β for which this stable solution branch occurs. Numerical continuation of folds is performed using the software AUTO97. Figure 4.5 illustrates the stable solution branch in question, and shows the limit point values for the parameter space (λ, β). We find that when $\gamma = 0.5$, there exists an extra stable branch for values of $\beta > 2.23$. The extra stable region represents rod configurations of the first buckling mode, where the endpoint $z(L)$ has passed through the point $z(0)$. Corresponding configurations in the case where there is no bending discontinuity ($\beta = 1$) have an index value of 1, and are therefore unstable. This is an example of how the discontinuity can have a stabilising affect for certain rod shapes.

Figure 4.4 shows rod configurations from the three different stable solution branches for $\beta = 8$ and $\gamma = 0.5$. Profiles (1) and (3) represent first-mode solutions, and profile (2) represents the second-mode solution. The difference in bending energy between the two sides of the rod is clearly visible in each case.

Figure 4.6 shows bifurcation diagrams of λ against D where $\beta = 3$, for various values of γ. We find that the extra stable region found when $\gamma = 0.5$, gets smaller as γ decreases from 0.5, and an unstable region of index 2 is found, which increases in range as γ decreases. As γ increases from 0.5, the range of the stable region also increases. However, the stable branch is not shown in subfigures 4.6(e) and 4.6(f), since the values
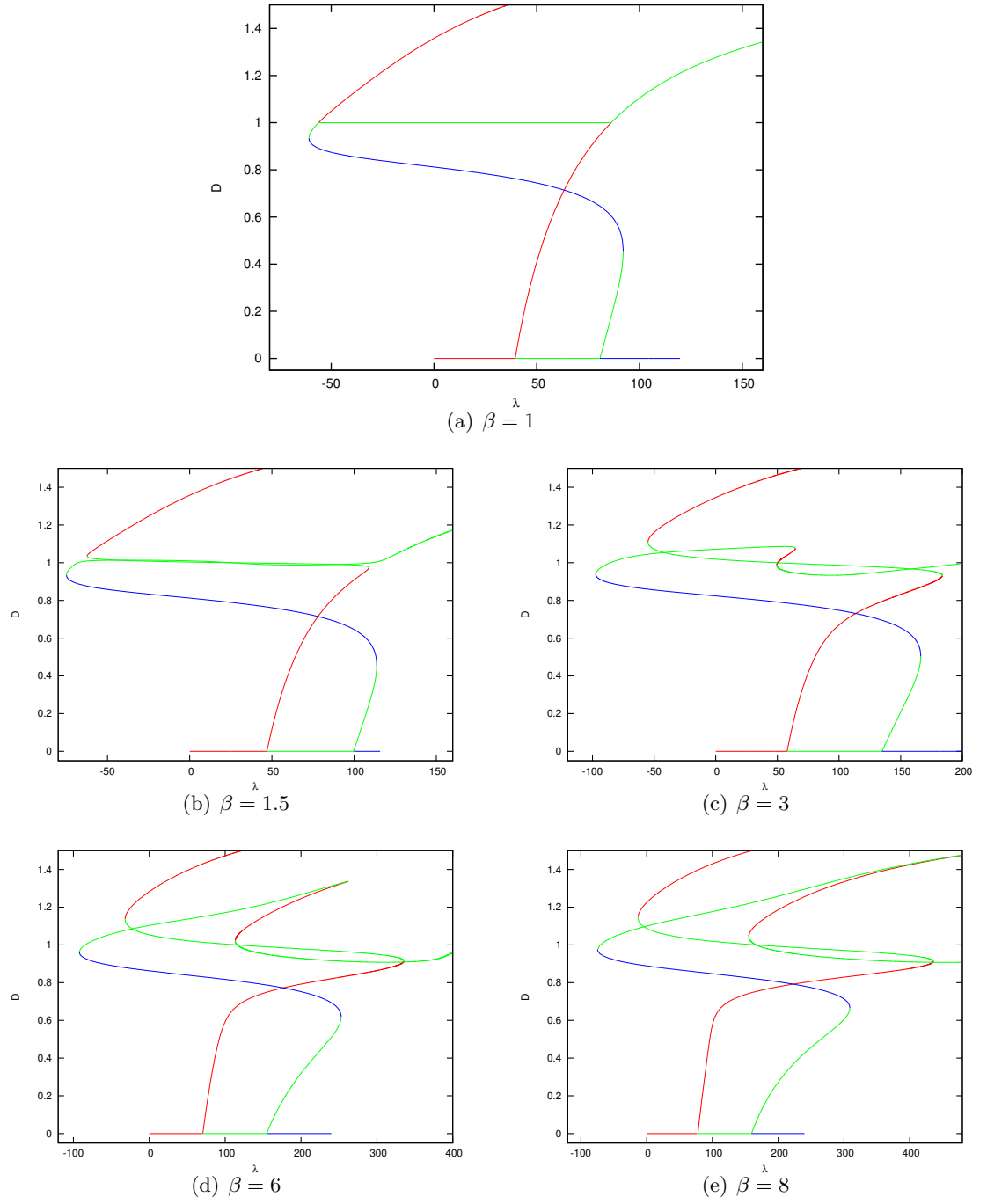
51

(a) $\beta = 1$

(b) $\beta = 1.5$

(c) $\beta = 3$

(d) $\beta = 6$

(e) $\beta = 8$

Figure 4.3: λ against D with $\gamma = 0.5$ and various values of β.
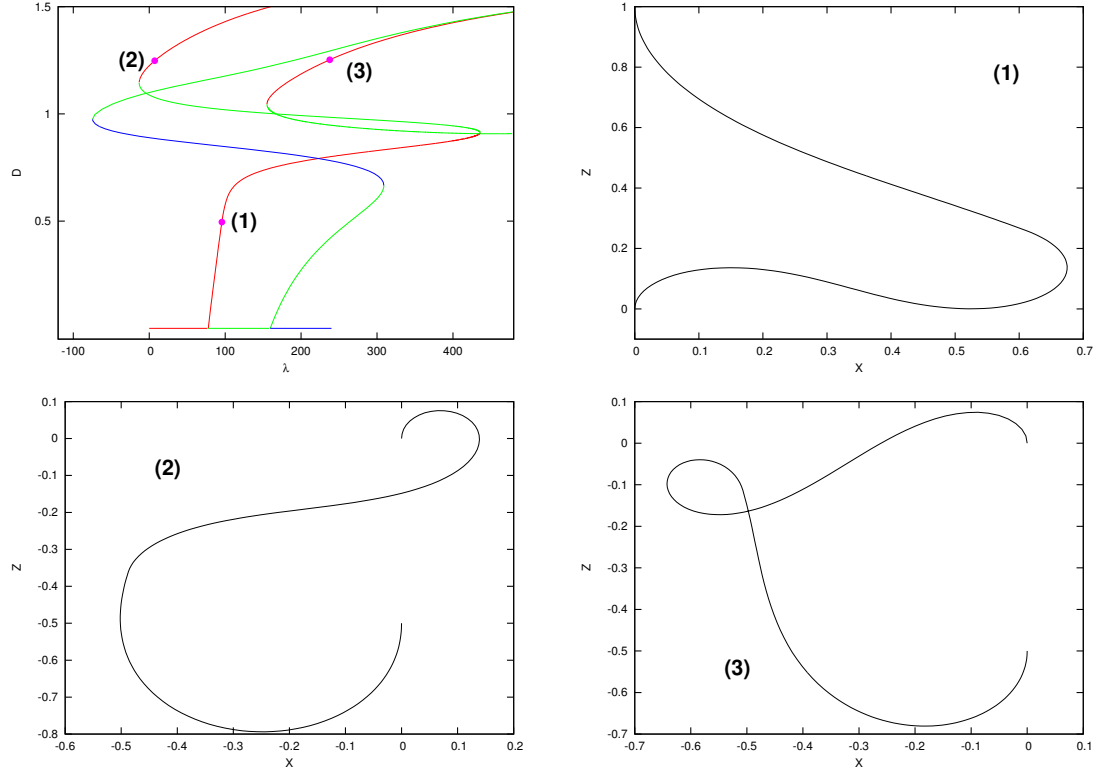
Figure 4.4: Rod profiles for $\gamma = 0.5$ and $\beta = 8$ at the three points indicated in the bifurcation diagram.
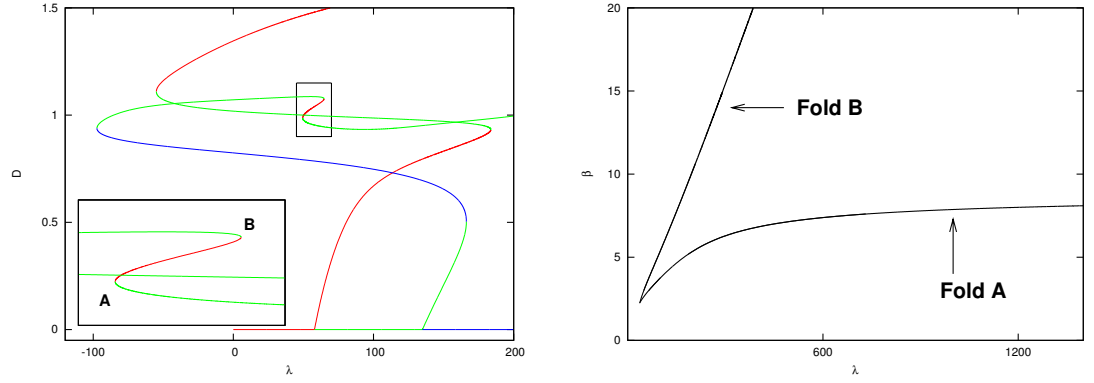

Figure 4.5: Two parameter continuation of the folds indicated in the bifurcation diagram on the left. The values of λ in which the folds **A** and **B** occur with respect to β. Here, $\gamma = 0.5$.

of λ are too large. Figure 4.7 shows the values of the limit points of the stable region in the parameter space (λ, γ), for various values of β.
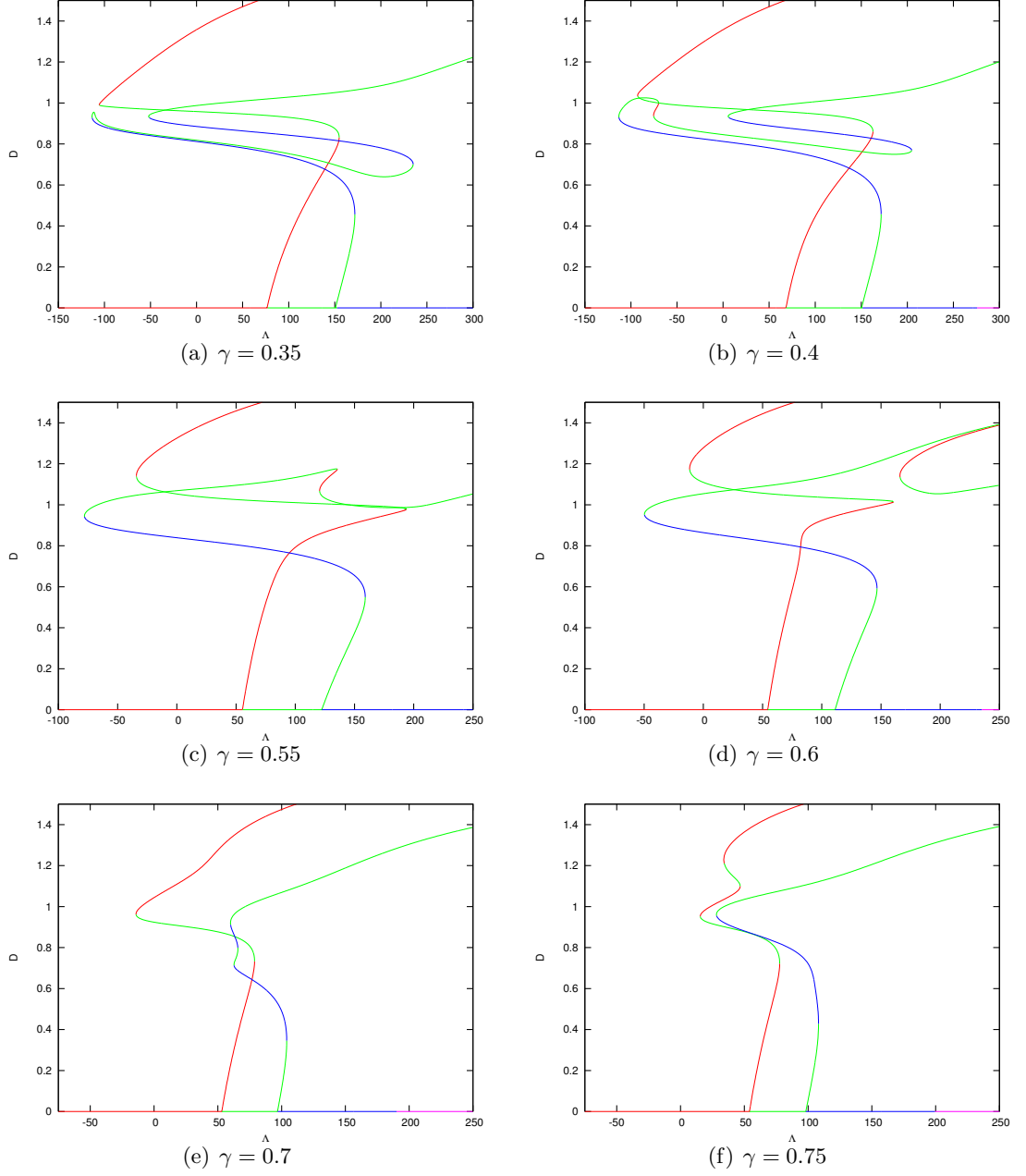

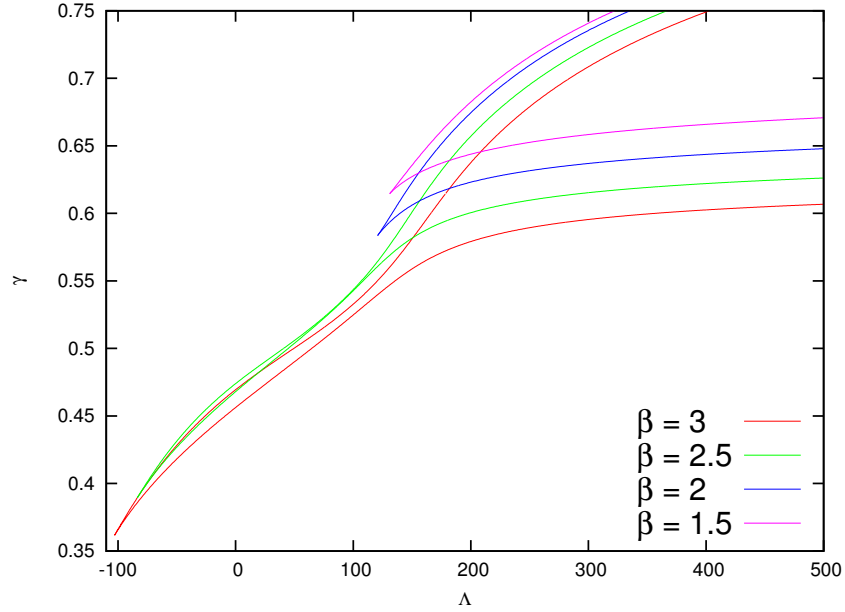**Figure 4.6:** λ against D with $\beta = 3$ and various values of γ.

Figure 4.7: Fold continuation of the limit points **A** and **B** given in figure 4.5. Values of the folds are found in the parameter space (λ, γ), for $\beta = 1.5$, 2, 2.5, and 3.

4.5.2 Three-dimensional Rod Solutions

Figure 4.8 shows bifurcation diagrams of λ against D, for various values of C_1, where $B_1 = B_2 = C_2 = 1$, $B_3 = C_3 = 0.8$, $L = 2$ and $L_1 = 1$. All subfigures show the first two branches buckling form the straight rod solution branch $D = 0$. In subfigure (a), for $C_1 = 0.1$, the first two branches represent the first and second buckling modes in the $(\boldsymbol{e}_1, \boldsymbol{e}_3)$ plane. In subfigure (b), for $C_1 = 0.25$, the first two branches also represent the first and second buckling modes in the $(\boldsymbol{e}_1, \boldsymbol{e}_3)$ plane, but the second branch bifurcates into a branch of non-planar first-mode solutions, and a branch of planar second-mode solutions. In subfigures (c), (e), and (f), the first two branches represent the first-modes in the $(\boldsymbol{e}_1, \boldsymbol{e}_3)$ and $(\boldsymbol{e}_2, \boldsymbol{e}_3)$ planes. Out-of-plane branches are shown bifurcating from both planar branches. As C_1 is increased, the out-of-plane branch points become more frequent on the second branch. Figure 4.9 shows three-dimensional rod profiles from (a) at $D = 0.25$. Figure 4.10 shows three-dimensional rod profiles from (b) at $D = 0.5$, of the first and second planar buckling modes in the $(\boldsymbol{e}_1, \boldsymbol{e}_3)$ plane, and of the out-of-plane
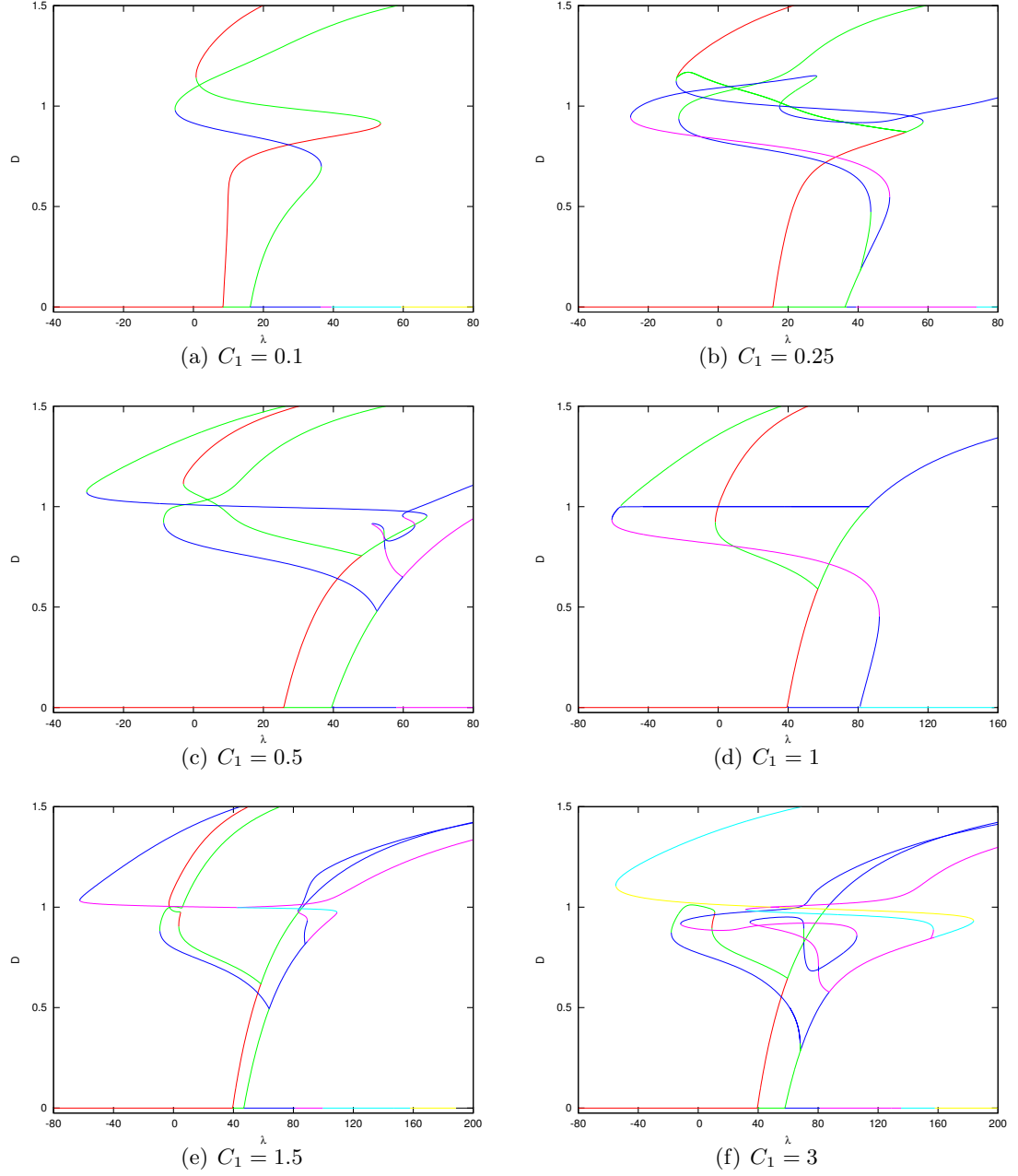
55

branch.

Figure 4.8: Bifurcation diagrams of λ against D. All subfigures show the first two branches buckling from the straight rod solutions ($D = 0$). In each case $B_1 = B_2 = C_2 = 1$, $B_3 = C_3 = 0.8$, $L = 2$, and $L_1 = 1$.
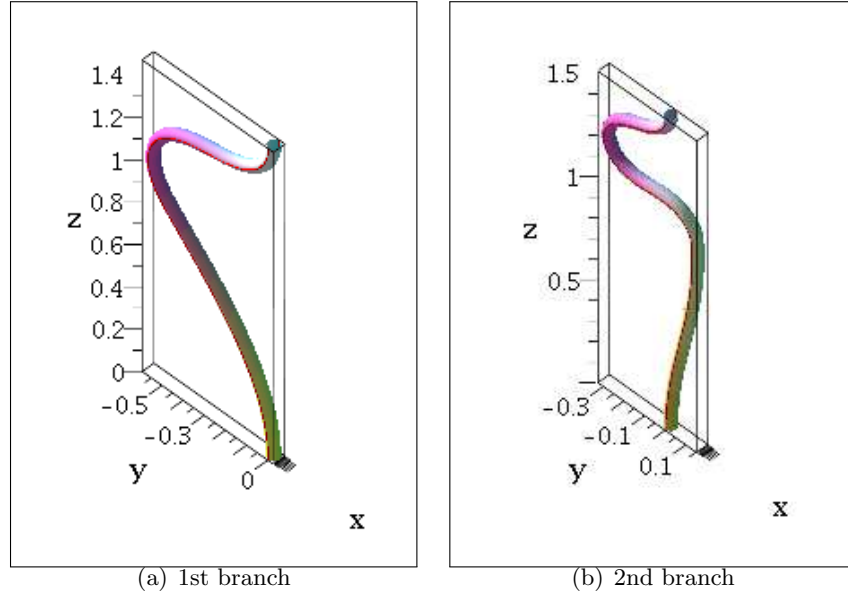
(a) 1st branch   (b) 2nd branch

Figure 4.9: Rod profiles at $D = 0.25$, for $B_1 = B_2 = C_2 = 1$, $B_3 = C_3 = 0.8$, and $C_1 = 0.1$. Both the first and second branches from the trivial branch buckle into the $(\boldsymbol{e}_1, \boldsymbol{e}_3)$ plane.

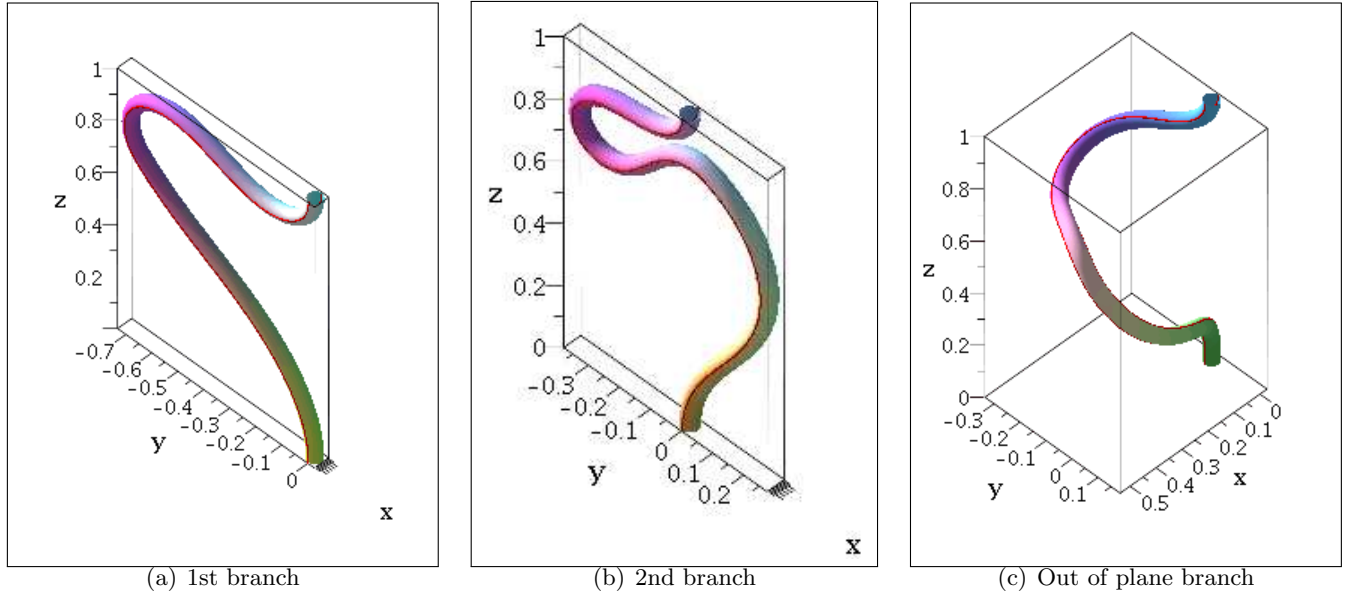(a) 1st branch   (b) 2nd branch   (c) Out of plane branch

Figure 4.10: Rod profiles at $D = 0.5$, for $B_1 = B_2 = C_2 = 1$, $B_3 = C_3 = 0.8$, and $C_1 = 0.25$. The first and second branches from the trivial branch buckle into the $(\boldsymbol{e}_1, \boldsymbol{e}_3)$ plane.

4.6 Nanotube Junction

Carbon nanotubes can potentially be used as intramolecular junctions by axially compressing part of the tube, creating a metal to semi-conductor transition [23]. The tubes can be permanently deformed by applying a radial strain, which distorts the circular cross-section into an elliptic cross-section [15], and it has also been shown that nanotube cross-sections can deform into ellipses from the effects of van der Waals forces [17].

In this section, we study the buckling and post-buckling stability of a specific class of rods with a single discontinuity in the bending stiffness, such that for each partition of the rod, the pair of bending stiffnesses (B_1, B_2) are in the set

$$\left\{ (B_1, B_2) \quad : \quad \tilde{C}(B_1, B_2) = 2\pi \right\},$$

where $\tilde{C}(B_1, B_2) = 4a\tilde{E}(k)$, and $\tilde{E}(k)$ is the complete elliptic integral of the second kind, given by the infinite sum

$$\tilde{E}(k) = \frac{\pi}{2} \sum_{n=0}^{\infty} \left[\frac{(2n)!}{2^{2n}(n!)^2} \right]^2 \frac{k^{2n}}{1 - 2n},$$

where

$$k = \sqrt{1 - \left(\frac{b}{a} \right)^2}, \quad a = \max\{B_1, B_2\}, \quad \text{and} \quad b = \min\{B_1, B_2\}.$$

In other words, each cross-section of the rod is an ellipse with circumference 2π.

Given that $B_1 = YI_1$ and $B_2 = YI_2$, and $B_3 = GI_3$, for an elliptic cross section we have (see, e.g. [41])

$$I_3 = \frac{4I_1 I_2}{I_1^2 + I_2^2}.$$

Therefore, using (3.16) we get

$$B_3 = \frac{2B_2}{(1 + \rho)(1 + \nu)},$$

where

$$\rho = \frac{B_2}{B_1},$$

and ν is Poisson's ratio. Throughout this section, we will choose $\nu = 0.25$ for both parts of the rod. Therefore, for each partition of the rod, values of all three stiffness parameters will be implied by imposing the bending stiffness in just one direction. Figure 4.11 plots values of B_2 and B_3 against values of B_1.
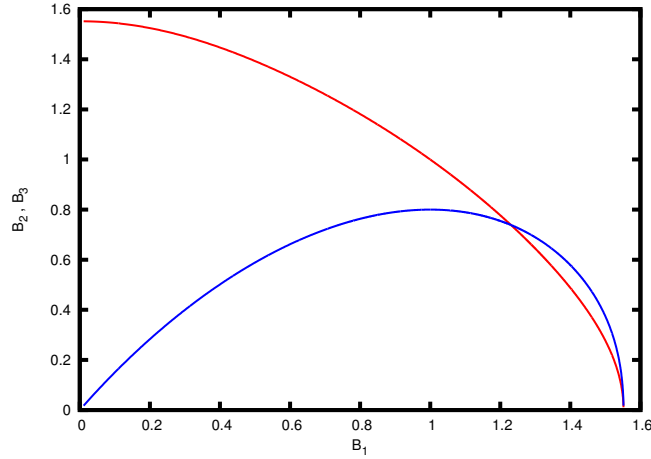

Figure 4.11: B_1 against B_2 (red) and B_3 (blue), for a circumference of 2π, and Poisson's ratio $\nu = 0.25$.

4.6.1 Dead Loading

Dead loading of an elastic strut refers to specifying the value of the end force λ_3. Figure 4.12 shows critical buckling values of λ_3 against B_1 for different values of C_1. We see that for all values of (C_1, C_2), $\lambda_c \to 0$ as $(B_1, B_2) \to (\frac{\pi}{2}, 0)$. Figure 4.13 shows the first buckling branches from the trivial solution branch, for various values of B_1, all with $(C_1, C_2) = (1, 1)$. Branches bifurcate from the trivial branch at $D = 0$. Buckling λ values tend to zero as (B_1, B_2) tends to $(\pi/2, 0)$. Each branch represents solutions that have buckled into the $(\boldsymbol{e}_1, \boldsymbol{e}_3)$ plane. The change in stability index from 0 to 1 (red to green) represents a branch point connecting the branch of planar solutions to a branch of out-of-plane solutions. In the two leftmost branches (representing the highest values of B_1) we see that the planar solutions become unstable at a limit point (a local maximum), and then stable again at a second limit point (a local minimum). Under a
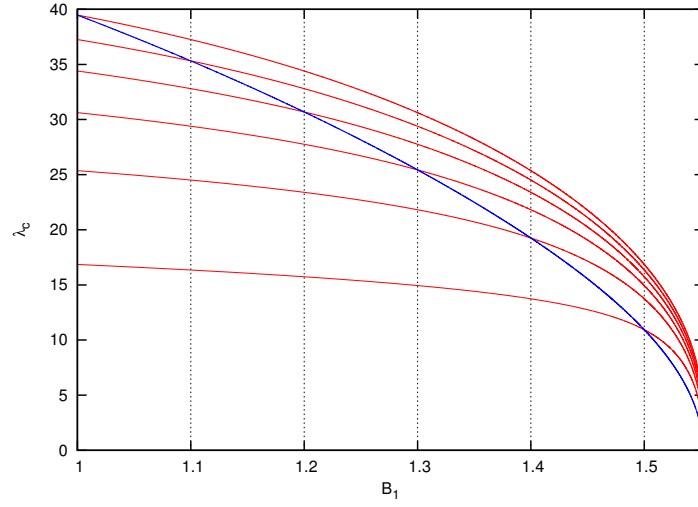
Figure 4.12: First critical buckling values of λ_3 as B_1 is varied. Red: $C_1 = 1$, 1.1, 1.2, 1.3, 1.4, 1.5. Blue: $C_1 = B_1$ (no jump in bending stiffness). Length $L = 1$, and $\gamma = 0.5$.

controlled increase of the load parameter λ, these solutions would become unstable at the first limit point and then jump to a remote stable solution (see, e.g. [13] and [40]). This process is called snap buckling. A rod profile at the first limit point is given in figure 4.14(a). Figure 4.14(b) shows a rod profile from the second point indicated by a solid black dot in figure 4.13, which is a likely stable rod configuration that the solution at the first limit point would jump to. Note that during this jump, a plastic deformation could occur, resulting in a permanently damaged *kinked* nanotube [13]. We will look into the stability of these kinked deformations further in chapter 6. Figure 4.15 shows bifurcation diagrams of the first two branches bifurcating from the trivial branch as λ is increased, as well as the out-of-plane solution branches bifurcating from the first two planar solution branches. Three-dimensional rod profiles for points on the out-of-plane branches are shown in figures 4.16 and 4.17.
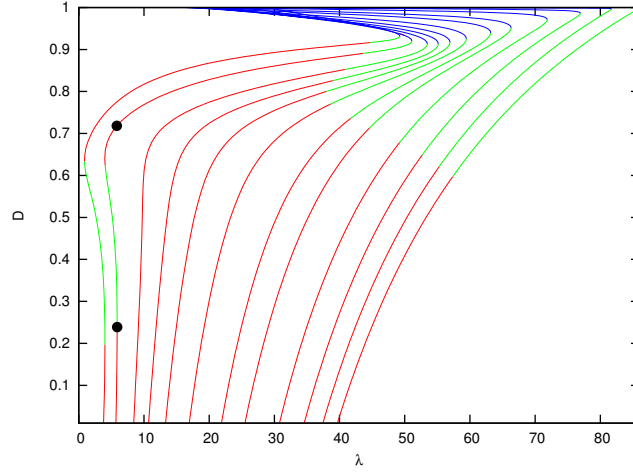
Figure 4.13: First buckling branches from the trivial solution branch, for various values of B_1, with $C_1 = 1$. $B_1 = 1$, 1.1, 1.2, 1.3, 1.4, 1.45, 1.5, 1.525, 1.535, 1.545, 1.55, and 1.55125. Rod profiles are plotted in figure 4.14 at the points indicated by the solid black dots.
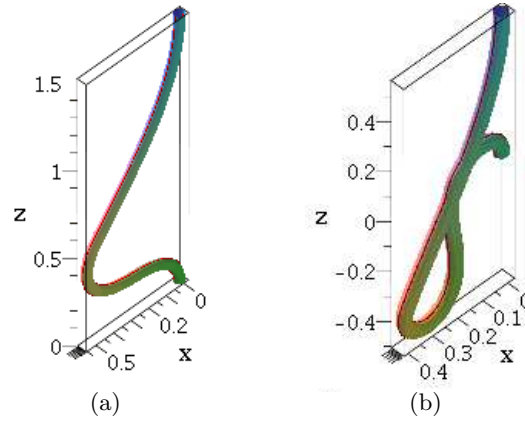

(a)   (b)

Figure 4.14: Rod profiles at the points indicated in figure 4.13. Subfigure (a) is from the limit point and subfigure (b) is of the point shown above the limit point on the stable solution branch. Here, $L = 2$ and $L_1 = 1$.

4.6.2   Hard Loading

If we wish to specify the end position of the rod, instead of specifying a force at the end, then there is a third isoperimetric constraint

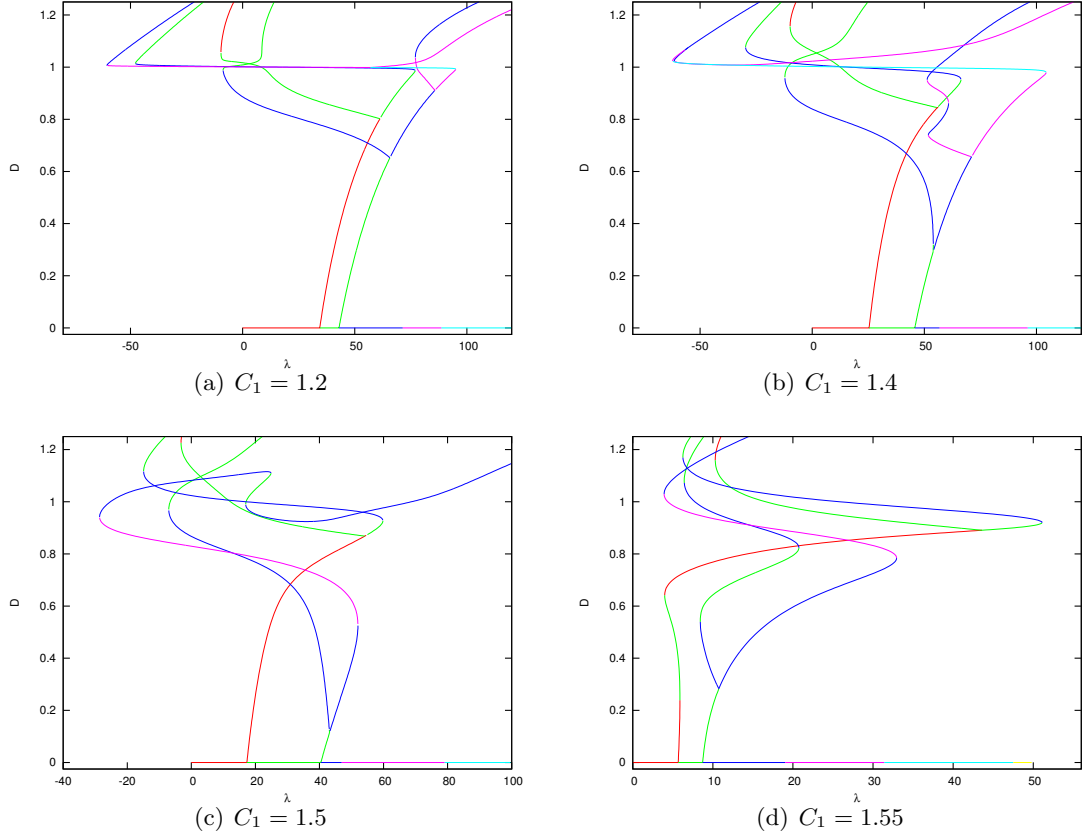$$\int_0^L d_{3z}(\mathbf{q}(s)) \ \mathrm{d}s = d, \tag{4.13}$$

Figure 4.15: Bifurcation diagrams of λ against D for $B_1 = 1$.

where $d = z(L)$, the imposed distance between the end points. The third projected, linearised constraint

$$\mathbf{T}_3 = \mathbf{\Pi}^T \left(d_{3z}\right)_{\mathbf{q}},\tag{4.14}$$

must now be added to the constrained Jacobi equation (4.3). The constant λ_3, now becomes a Lagrange multiplier in the variational problem, and the constrained stability matrices (4.10) and (4.11) become 6×6 matrices, incorporating the extra constraint.

We will now consider clamped-sleeved boundary conditions with fixed end points:

$$\boldsymbol{r}(0) = \mathbf{0}, \quad \boldsymbol{r}(L) = (0, 0, d), \quad \mathbf{q}(0) = (0, 0, 0, 1), \quad \mathbf{q}(L) = \left(0, 0, \sin\left(\frac{\phi}{2}\right), \cos\left(\frac{\phi}{2}\right)\right).$$

Figure 4.18 shows bifurcation diagrams of end rotation R against end moment M,
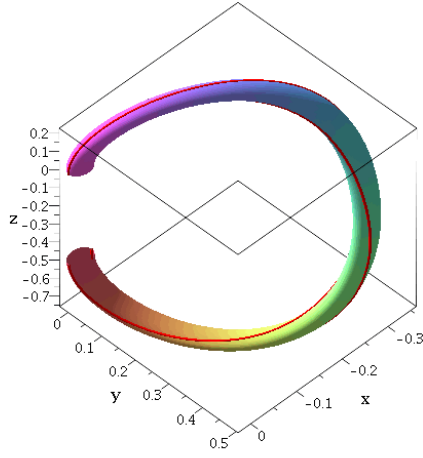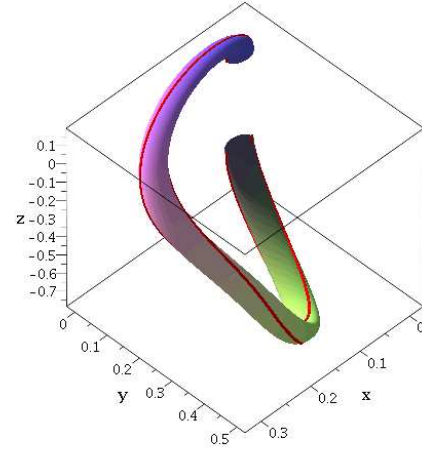
(a) $C_1 = 1.2$

(b) $C_1 = 1.4$

Figure 4.16: Stable rod profiles from the out-of-plane solution branch in figures 4.15(a) and 4.15(b). $D = 1.25$, $B_1 = 1$.
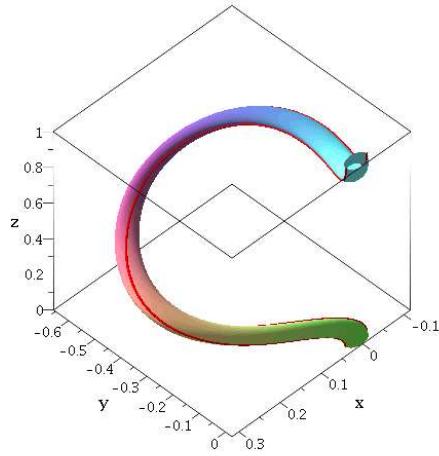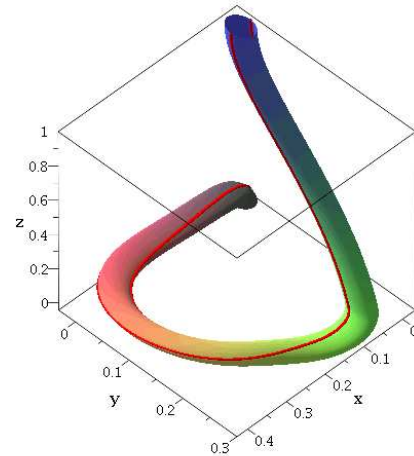

(a) $C_1 = 1.4$

(b) $C_1 = 1.55$

Figure 4.17: Unstable rod profiles from the out-of-plane solution branch in figures 4.15(b) and 4.15(d). $D = 0.5$, $B_1 = 1$.

for various fixed values of D. Parameters M and R are given by

$$M := m_3(L), \quad R := \frac{\phi}{2\pi}.$$

The point $(R, M) = (1, 0)$ corresponds to self-intersecting planar looped solutions (see figure 4.19). This point is unstable for $D =$0.25, 0.375, and 0.5 (see figure 4.18(a)), and is stable for $D =$0.625, 0.75, and 0.875 (see figure 4.18(b)). In the case of anisotropic rods with no discontinuities ($B_1 = C_1$), the stable solution branches found are consistent with those found in van der Heijden, Neukirch and Thompson [40], in which stability properties of the solution branches were predicted using the rule of stability exchange at a fold in a distinguished bifurcation diagram (see, e.g. [26]). Figures 4.20, 4.21 and 4.22 show rod profiles at the points indicated on the bifurcation diagrams in figure 4.18.

(a) $D = 0.25, 0.375, 0.5$.

(b) $D = 0.625, 0.75, 0.875$.
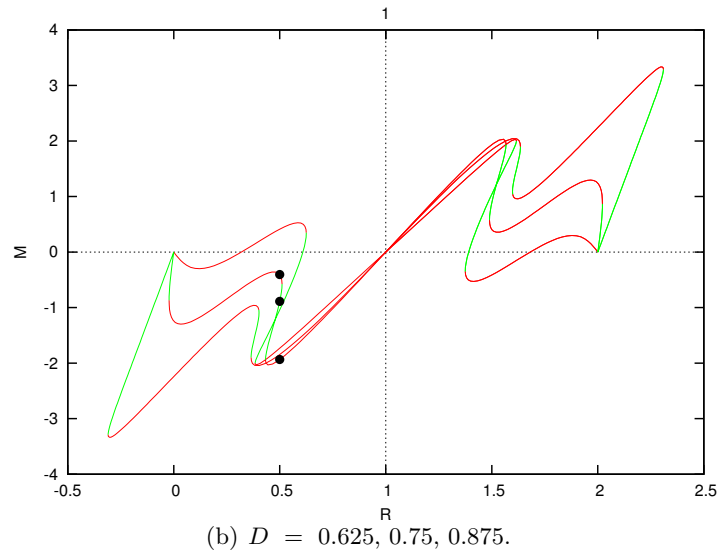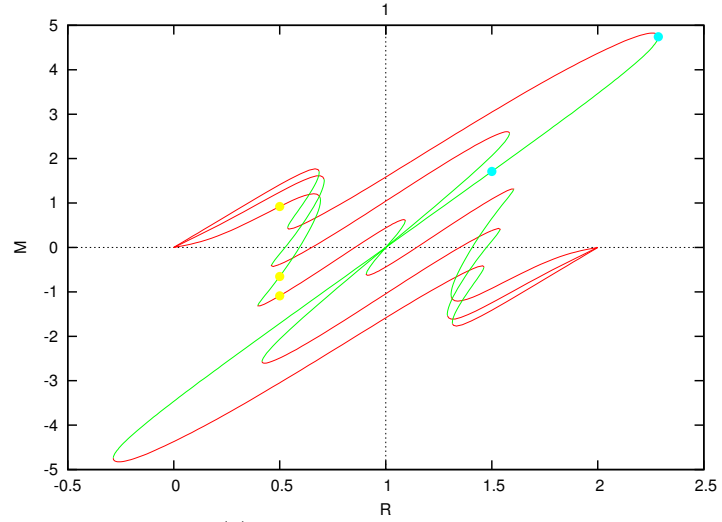
Figure 4.18: Bifurcation diagrams of R against M, where $B_1 = 1.4$, and $C_1 = 1$.
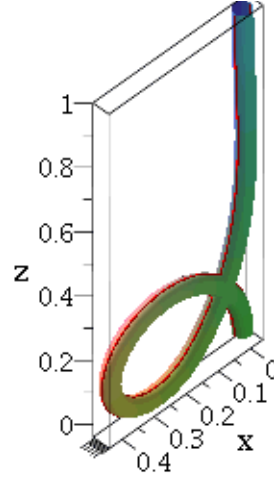
Figure 4.19: Self intersecting planar rod solution at $(R, M) = (1, 0)$, for $D = 0.5$, $B_1 = 1.4$, and $C_1 = 1.0$.

(a) $M = -0.4$ (b) $M = -0.89$ (c) $M = -1.93$
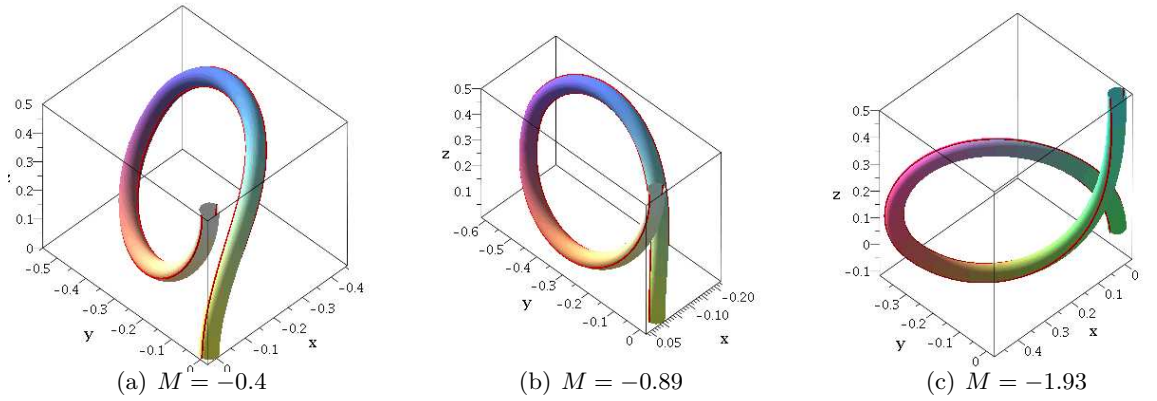
Figure 4.20: Rod profiles for hard loaded rods with $D = 0.75$, corresponding to the black solid circles in figure 4.18(b). In each case, $R = 0.5$, $B_1 = 1.4$, and $C_1 = 1$. Subfigures (a) and (c) are stable configurations, and subfigure (b) is a critical point of index $I = 1$.

(a) $M = 0.92$ (b) $M = -0.65$ (c) $M = -1.09$
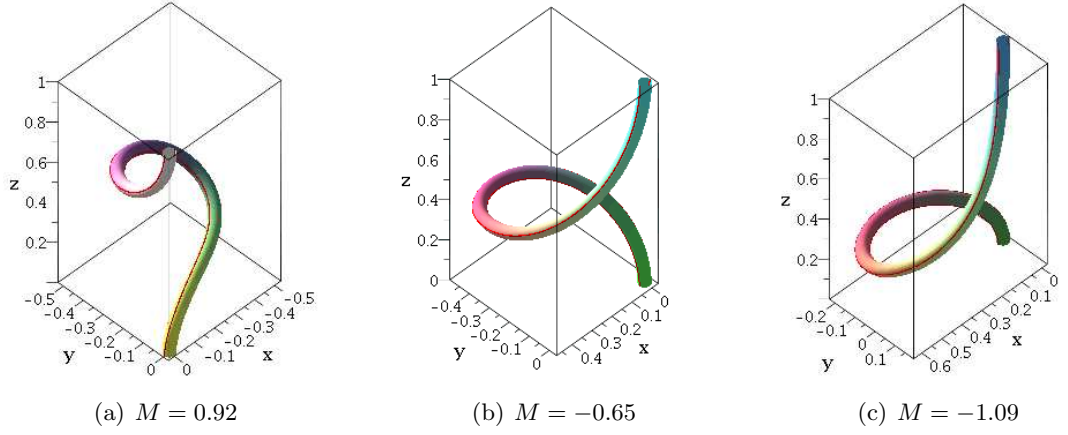
Figure 4.21: Rod profiles for hard loaded rods with $D = 0.5$, corresponding to the yellow solid circles in figure 4.18(a). In each case, $R = 0.5$, $B_1 = 1.4$, and $C_1 = 1$. Subfigures (a) and (c) are stable configurations, and subfigure (b) is a critical point of index $I = 1$.

(a) $M = 4.74$ (b) $M = 1.71$
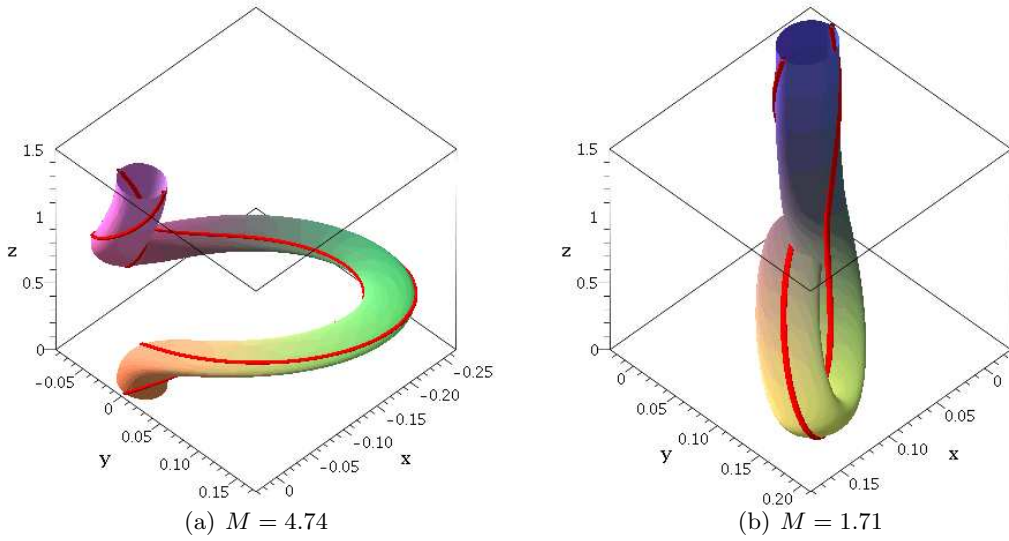
Figure 4.22: Rod profiles for hard loaded rods with $D = 0.25$, corresponding to the light blue solid circles in figure 4.18(a). In each case, $B_1 = 1.4$, and $C_1 = 1$. In subfigure (a), $R = 2.25$ (fold). In (b), $R = 1.5$ (index=1).

Chapter 5

Pinned Boundary Conditions

Here, we study the effects of changing the boundary conditions on $\mathbf{q}$ from the standard Dirichlet conditions to Neumann conditions. The homogeneous Neumann conditions

$$\mathbf{q}'(0) = \mathbf{0}, \quad \mathbf{q}'(L) = \mathbf{0},$$

are equivalent to homogeneous conditions on the strains

$$\boldsymbol{u}(0) = \mathbf{0}, \quad \boldsymbol{u}(L) = \mathbf{0}.$$

These are equivalent to the boundary conditions discussed in section (3.5.2), and represent a rod with zero moment at the end points. The revised conjugate point theory discussed in section (2.2), gives a new definition for the index:

$$I = N_i + N_n - N_p,$$

where

$$
\begin{aligned}
N_i &= \text{the number of negative inborn eigenvalues;} \\
N_n &= \text{the number of zero eigenvalues with negative velocity;} \\
N_p &= \text{the number of zero eigenvalues with positive velocity.}
\end{aligned}
$$

The linearised and projected boundary conditions are

$$\mathbf{\Pi}\boldsymbol{\zeta}'(0) + \mathbf{\Pi}'\boldsymbol{\zeta}(0) = \mathbf{0}, \quad \mathbf{\Pi}\boldsymbol{\zeta}'(L) + \mathbf{\Pi}'\boldsymbol{\zeta}(L) = \mathbf{0}.$$

Using $(D_1\mathbf{q}, D_2\mathbf{q}, D_3\mathbf{q})$ as our choice for $\mathbf{\Pi}$, we obtain the homogeneous Neumann boundary conditions for the projected variation $\boldsymbol{\zeta}$,

$$\boldsymbol{\zeta}'(0) = \mathbf{0}, \quad \boldsymbol{\zeta}'(L) = \mathbf{0}.$$

5.1 Inborn Eigenvalues of the Jacobi Operator

We now attempt to find the eigenvalues of the projected Jacobi operator $\bar{\mathcal{S}}$ (defined in (4.2)), for σ close to zero, which we call the inborn eigenvalues of $\bar{\mathcal{S}}$.

$$\bar{\mathcal{S}}\boldsymbol{\zeta} = \rho\boldsymbol{\zeta}, \quad \boldsymbol{\zeta}'(0) = \mathbf{0}, \quad \boldsymbol{\zeta}'(\sigma) = \mathbf{0}. \tag{5.1}$$

Expanding $\bar{\mathbf{P}}(\sigma), \bar{\mathbf{C}}(\sigma)$ and $\bar{\mathbf{Q}}(\sigma)$ about $s = 0$ gives

$$\bar{\mathbf{P}}(\sigma) = \bar{\mathbf{P}}(0) + \sigma\bar{\mathbf{P}}'(0) + \mathcal{O}(\sigma^2), \tag{5.2}$$

$$\bar{\mathbf{Q}}(\sigma) = \bar{\mathbf{Q}}(0) + \sigma\bar{\mathbf{Q}}'(0) + \mathcal{O}(\sigma^2), \tag{5.3}$$

$$\bar{\mathbf{C}}(\sigma) = \bar{\mathbf{C}}(0) + \sigma\bar{\mathbf{C}}'(0) + \mathcal{O}(\sigma^2). \tag{5.4}$$

For our choice of $\mathbf{\Pi}$, we have

$$\bar{\mathbf{P}} = 4\begin{pmatrix} B_1 & 0 & 0 \\ 0 & B_2 & 0 \\ 0 & 0 & B_3 \end{pmatrix} + \mathcal{O}(\sigma)^2, \quad \bar{\mathbf{C}} = \begin{pmatrix} 0 & 0 & 0 \\ 0 & 0 & 0 \\ 0 & 0 & 0 \end{pmatrix} + \mathcal{O}(\sigma)^2,$$

and

$$\bar{\mathbf{Q}} = \begin{pmatrix} Q_3 & 0 & Q_1 \\ 0 & Q_3 & Q_2 \\ Q_1 & Q_2 & 0 \end{pmatrix} + \mathcal{O}(\sigma)^2,$$

where

$$Q_1 = 2\left[\lambda_1 d_{11}(0) + \lambda_2 d_{12}(0) + \lambda_3 d_{13}(0)\right], \tag{5.5}$$

$$Q_2 = 2\left[\lambda_1 d_{21}(0) + \lambda_2 d_{22}(0) + \lambda_3 d_{23}(0)\right], \tag{5.6}$$

$$Q_3 = -4\left[\lambda_1 d_{31}(0) + \lambda_2 d_{32}(0) + \lambda_3 d_{33}(0)\right]. \tag{5.7}$$

This simplifies the eigenvalue problem (5.1) to

$$-\bar{\mathbf{P}}\boldsymbol{\zeta}'' + \bar{\mathbf{Q}}\boldsymbol{\zeta} = \rho\boldsymbol{\zeta}, \tag{5.8}$$

which we will write as the following system:

$$\boldsymbol{\zeta}' \;=\; -\bar{\mathbf{P}}^{-1}\boldsymbol{v}, \tag{5.9}$$

$$\boldsymbol{v}' \;=\; \left(\rho I - \bar{\mathbf{Q}}_1\right)\boldsymbol{\zeta}. \tag{5.10}$$

If we express the solution $\boldsymbol{v}(s)$ as

$$\boldsymbol{v} = \sum_{i=1}^{6} c_i \boldsymbol{v}_i, \tag{5.11}$$

and let

$$\mathcal{A} = \left(\begin{array}{cccccc} \boldsymbol{v}_1(0) & \boldsymbol{v}_2(0) & \boldsymbol{v}_3(0) & \boldsymbol{v}_4(0) & \boldsymbol{v}_5(0) & \boldsymbol{v}_6(0) \\ \boldsymbol{v}_1(\sigma) & \boldsymbol{v}_2(\sigma) & \boldsymbol{v}_3(\sigma) & \boldsymbol{v}_4(\sigma) & \boldsymbol{v}_5(\sigma) & \boldsymbol{v}_6(\sigma) \end{array}\right),$$

then the inborn eigenvalues ρ can be found by finding

$$\left\{\lim_{\sigma\to 0}\rho(\sigma) \quad : \quad |\mathcal{A}(\rho)| = 0\right\}. \tag{5.12}$$

Now let us look individually at the special cases of a straight rod, and a planar rod.

5.1.1   Straight Anisotropic Rod

Constrained

For the special case of a constrained straight anisotropic rod, (5.8) becomes

$$-4\left(\begin{array}{ccc} B_1 & 0 & 0 \\ 0 & B_2 & 0 \\ 0 & 0 & B_3 \end{array}\right)\boldsymbol{\zeta}'' - 4\lambda_3\left(\begin{array}{ccc} 1 & 0 & 0 \\ 0 & 1 & 0 \\ 0 & 0 & 0 \end{array}\right)\boldsymbol{\zeta} + \hat{c}_1\left(\begin{array}{c} 0 \\ 2 \\ 0 \end{array}\right) + \hat{c}_2\left(\begin{array}{c} -2 \\ 0 \\ 0 \end{array}\right) = \rho\boldsymbol{\zeta}.$$

Let $\boldsymbol{\zeta} = (\zeta_1, \zeta_2, \zeta_3)^T$. We are interested in finding the number of negative eigenvalues ρ. If $\rho \leq 0$ then ζ_3 has no non-trivial solution satisfying the boundary conditions. If $4\lambda_3 + \rho \leq 0$ then ζ_1 and ζ_2 have no non-trivial solutions satisfying the boundary conditions and integral constraints. Therefore, we will look at the case of $4\lambda_3 + \rho > 0$. The solution to the above equation is

$$\boldsymbol{\zeta} = c_1\left(\begin{array}{c} \cos\omega_1 s \\ 0 \\ 0 \end{array}\right) + c_2\left(\begin{array}{c} \sin\omega_1 s \\ 0 \\ 0 \end{array}\right) + c_3\left(\begin{array}{c} 0 \\ \cos\omega_2 s \\ 0 \end{array}\right) + c_4\left(\begin{array}{c} 0 \\ \sin\omega_2 s \\ 0 \end{array}\right)$$
$$+ c_5\left(\begin{array}{c} 0 \\ 0 \\ \cos\omega_3 s \end{array}\right) + c_6\left(\begin{array}{c} 0 \\ 0 \\ \sin\omega_3 s \end{array}\right) + \hat{c}_1\left(\begin{array}{c} 0 \\ 1/2\omega_2^2 B_2 \\ 0 \end{array}\right) + \hat{c}_2\left(\begin{array}{c} -1/2\omega_1^2 B_1 \\ 0 \\ 0 \end{array}\right),$$

where $\omega_i = \sqrt{\frac{4\lambda_3+\rho}{4B_i}}$ for $i = 1, 2$, and $\omega_3 = \sqrt{\frac{\rho}{4B_3}}$.

The eigenvalues ρ are found by solving

$$|\mathcal{A}| = -\omega_1^2\omega_2^2\omega_3^2 \sin(\omega_1\sigma) \sin(\omega_2\sigma) \sin(\omega_3\sigma) = 0. \tag{5.13}$$

Since $\omega_1 \neq 0$, $\omega_2 \neq 0$, and $\omega_3 \neq 0$, we find that $|\mathcal{A}| = 0$ when

$$\sin(\omega_1\sigma) = 0 \implies \rho_n = -4\lambda_3 + 4B_1 n^2\pi^2/\sigma^2, \quad n = 1, 2, ...$$
$$\sin(\omega_2\sigma) = 0 \implies \rho_n = -4\lambda_3 + 4B_2 n^2\pi^2/\sigma^2, \quad n = 1, 2, ...$$
$$\sin(\omega_3\sigma) = 0 \implies \rho_n = 4B_3 n^2\pi^2/\sigma^2, \quad n = 1, 2, ...$$

Therefore, for small σ, there are no negative inborn eigenvalues for the constrained, straight, anisotropic rod.

Unconstrained

In the case of an unconstrained straight anisotropic rod, non-trivial solutions of ζ_1 and ζ_2 exist for the case of $4\lambda_3 + \rho = 0$. Therefore there is an inborn eigenvalue (of multiplicity 2) that is negative for positive λ_3. If $4\lambda_3 + \rho < 0$ then there are no non-trivial solutions. If $4\lambda_3 + \rho > 0$, eigenvalues are found by solving

$$|\mathcal{A}| = -\omega_1^2\omega_2^2\omega_3^2 \sin(\omega_1\sigma) \sin(\omega_2\sigma) \sin(\omega_3\sigma) = 0. \tag{5.14}$$

Therefore, as in the constrained case, all other inborn eigenvalues are positive.

This jump by two in the index is due to the unconstrained pinned boundary conditions allowing families of solutions rotating about the $\boldsymbol{e}_1$ and $\boldsymbol{e}_2$ axes when $\lambda_3 = 0$. As a result, the straight rod is only stable ($I = 0$) when $\lambda_3 < 0$, i.e. the rod is being 'pulled'. The constrained case however, does not allow these families of rotations at $\lambda_3 = 0$, and all inborn eigenvalues remain positive as λ_3 passes through zero.

5.1.2   Planar Anisotropic Rod

We shall look at solutions which are restricted to the plane $\boldsymbol{d}_2 = (0, 1, 0)^T$.
Equation (5.8) becomes

$$-4 \begin{pmatrix} B_1 & 0 & 0 \\ 0 & B_2 & 0 \\ 0 & 0 & B_3 \end{pmatrix} \boldsymbol{\zeta}'' + \begin{pmatrix} Q_3 & 0 & Q_1 \\ 0 & Q_3 & 0 \\ Q_1 & 0 & 0 \end{pmatrix} \boldsymbol{\zeta} = \rho \boldsymbol{\zeta}.$$

First look at solutions for $\zeta_2(\sigma)$.

If $\rho < Q_3$, then there is no non-trivial solution of $\zeta_2(\sigma)$ satisfying the boundary conditions. If $\rho = Q_3$, then the solution $\zeta_2 = C$, where C is a constant, satisfies the boundary conditions (but would not satisfy the linearised isoperimetric constraints). If $\rho > Q_3$ then $\zeta_2(\sigma)$ satisfies the boundary conditions (and isoperimetric constraints) only if

$$\rho = Q_3 + 4B_2 n^2 \pi^2 / \sigma^2, \quad n = 1, 2, \ldots$$

Now look at solutions for $\zeta_1(\sigma)$ and $\zeta_3(\sigma)$. Let

$$\omega_{1,2} = \sqrt{\frac{Q_3 B_3 - \rho(B_1 + B_3) \pm R}{8 B_1 B_3}}.$$

If ω_1 and ω_2 are real then

$$\hat{\boldsymbol{\zeta}} := \begin{pmatrix} \zeta_1 \\ \zeta_3 \end{pmatrix} = c_1 \begin{pmatrix} \Omega_1 e^{\omega_1 s} \\ e^{\omega_1 s} \end{pmatrix} + c_2 \begin{pmatrix} \Omega_1 e^{-\omega_1 s} \\ e^{-\omega_1 s} \end{pmatrix} + c_3 \begin{pmatrix} \Omega_2 e^{\omega_2 s} \\ e^{\omega_2 s} \end{pmatrix} + c_4 \begin{pmatrix} \Omega_2 e^{-\omega_2 s} \\ e^{-\omega_2 s} \end{pmatrix},$$

where

$$\Omega_{1,2} = \frac{Q_3 B_3 + \rho(B_1 - B_3) \pm R}{2 Q_1 B_1}, \quad \text{and}$$

$$R = \sqrt{[\rho(B_1 - B_3) + Q_3 B_3]^2 + 4 B_1 Q_1^2}.$$

Eigenvalues are found by solving

$$\left| \begin{array}{c} \hat{\boldsymbol{\zeta}}(0) \\ \hat{\boldsymbol{\zeta}}(\sigma) \end{array} \right| = -4\omega_1^2 \omega_2^2 \sinh(\omega_1 \sigma) \sinh(\omega_2 \sigma) = 0. \tag{5.15}$$

Therefore there are no non-trivial solutions satisfying the boundary conditions.

If ω_1 and ω_2 are imaginary then

$$\begin{pmatrix} \zeta_1 \\ \zeta_3 \end{pmatrix} = c_1 \begin{pmatrix} \Omega_1 \cos(\mu_1 s) \\ \cos(\mu_1 s) \end{pmatrix} + c_2 \begin{pmatrix} \Omega_1 \sin(\mu_1 s) \\ \sin(\mu_1 s) \end{pmatrix} + c_3 \begin{pmatrix} \Omega_2 \cos(\mu_2 s) \\ \cos(\mu_2 s) \end{pmatrix} + c_4 \begin{pmatrix} \Omega_2 \sin(\mu_2 s) \\ \sin(\mu_2 s) \end{pmatrix},$$

where

$$\mu_{1,2} = \sqrt{-\frac{Q_3 B_3 - \rho(B_1 + B_3) \pm R}{8 B_1 B_3}}.$$

If

$$\left| \begin{matrix} \hat{\zeta}(0) \\ \hat{\zeta}(\sigma) \end{matrix} \right| = -\omega_1^2 \omega_2^2 \sin(\omega_1 \sigma) \sin(\omega_2 \sigma) = 0, \tag{5.16}$$

then

$$\sin(\omega_1 \sigma) = 0 \quad \Longrightarrow \quad \rho_n = Q_3 + 4 B_1 n^2 \pi^2 / \sigma^2, \quad n = 1, 2, ...$$

$$\sin(\omega_2 \sigma) = 0 \quad \Longrightarrow \quad \rho_n = Q_3 + 4 B_2 n^2 \pi^2 / \sigma^2, \quad n = 1, 2, ...$$

Therefore $\rho_n > 0$, for small σ.

If $\omega_1 = \omega_2 = 0$ then

$$\begin{pmatrix} \zeta_1 \\ \zeta_3 \end{pmatrix} = c_1 \begin{pmatrix} \rho/Q_1 \\ 1 \end{pmatrix} + c_2 \begin{pmatrix} \rho s/Q_1 \\ s \end{pmatrix} + c_3 \begin{pmatrix} -B_3 Q_1 \cos(\nu s)/B_1 \rho \\ \cos(\nu s) \end{pmatrix} + c_4 \begin{pmatrix} -B_3 Q_1 \sin(\nu s)/B_1 \rho \\ \sin(\nu s) \end{pmatrix},$$

where

$$\nu = \sqrt{\frac{B_1 \rho^2 + B_3 Q_1^2}{4 B_1 B_3 \rho}} > 0.$$

Applying the boundary conditions gives

$$\rho = 4 B_1 B_3 (n\pi)^2 \pm \sqrt{[4 B_1 B_3 (n\pi)^2]^2 - 4 B_1 B_3 Q_1^2 \sigma^4}.$$

Therefore

$$\rho > 0 \quad \text{for} \quad \sigma > 0.$$

In the unconstrained planar problem, if $Q_2 = 0$ there is one negative inborn eigenvalue when $Q_3 < 0$. It can easily be shown that the same is true for the case $Q_1 = 0$ (when the rod lies in the (e_2, e_3) plane). If $Q_1 = Q_2 = 0$ (when the rod is straight) then there is an inborn eigenvalue of multiplicity 2 when $Q_3 < 0$.

5.2   Velocity of the Zero Eigenvalue

To determine whether the zero eigenvalue $\rho(\sigma)$ is becoming negative or becoming positive with respect to σ we need to determine the sign of $\rho(\sigma - \epsilon)$. To do this we construct the function

$$\boldsymbol{\xi}(\sigma) \equiv \boldsymbol{\zeta}(\sigma) + \boldsymbol{A}s^2,$$

where $\boldsymbol{A}$ is chosen, such that $\boldsymbol{\xi}$ belongs to the space

$$\mathcal{H}_n(0, \sigma - \epsilon) \equiv \left\{ \mathbf{h} \in H^2(0, \sigma - \epsilon) : \mathbf{h}'(0) = \mathbf{h}'(\sigma - \epsilon) = \mathbf{0} \right\}.$$

It can be shown (e.g. in [27] and [19]) that $\left\langle \boldsymbol{\xi}, \bar{\mathcal{S}}\boldsymbol{\xi} \right\rangle$ has the same sign as $\rho(\sigma - \epsilon)$, for sufficiently small ϵ. Therefore, we aim to find the leading order term of $\left\langle \boldsymbol{\xi}, \bar{\mathcal{S}}\boldsymbol{\xi} \right\rangle$. Let $\boldsymbol{\xi} = (\xi_1, \xi_2, \xi_3)^T$ and $\boldsymbol{A} = (A_1, A_2, A_3)^T$. The function $\boldsymbol{\xi}$ satisfies the boundary conditions

$$\boldsymbol{\xi}'(0) \quad = \quad \mathbf{0},$$

$$\boldsymbol{\xi}'(\sigma - \epsilon) \quad = \quad \mathbf{0}.$$

The value of $\boldsymbol{A}$ is determined so that boundary conditions at $s = \sigma - \epsilon$ are satisfied, therefore

$$\boldsymbol{\zeta}'(\sigma - \epsilon) + 2\boldsymbol{A}(\sigma - \epsilon) = 0.$$

Taylor expanding about $s = \sigma$ and using the boundary conditions for $\boldsymbol{\zeta}$ at $s = \sigma$ gives

$$\boldsymbol{A} = \epsilon \frac{\boldsymbol{\zeta}''(\sigma)}{2(\sigma - \epsilon)}.$$

Since removing the ϵ terms from the denominators would change $\boldsymbol{A}$ by only $\mathcal{O}(\epsilon^2)$, we write

$$\boldsymbol{A} = \epsilon \frac{\boldsymbol{\zeta}''(\sigma)}{2\sigma}.$$

Now,

$$\bar{\mathcal{S}}\boldsymbol{\xi} = \bar{\mathcal{S}}\boldsymbol{\zeta} + \bar{\mathcal{S}}(s^2 \boldsymbol{A}),$$

so given that $\bar{\mathbf{P}}$ is constant, we have

$$\bar{\mathcal{S}}\boldsymbol{\xi} = \left[-2\bar{\mathbf{P}} + 2(\bar{\mathbf{C}} - \bar{\mathbf{C}}^T)s + (\bar{\mathbf{Q}} - \bar{\mathbf{C}}'^T)s^2 \right] \boldsymbol{A},$$

and

$$\langle \bar{\mathcal{S}}\boldsymbol{\xi}, \boldsymbol{\xi} \rangle = \int_0^{\sigma-\epsilon} \left\{ \left[-2\bar{\mathbf{P}} + 2(\bar{\mathbf{C}} - \bar{\mathbf{C}}^T)s + (\bar{\mathbf{Q}} - \bar{\mathbf{C}}'^T)s^2 \right] \boldsymbol{A} \cdot \boldsymbol{\zeta} \right.$$
$$\left. + s^2 \left[-2\bar{\mathbf{P}} + 2(\bar{\mathbf{C}} - \bar{\mathbf{C}}^T)s + (\bar{\mathbf{Q}} - \bar{\mathbf{C}}'^T)s^2 \right] \boldsymbol{A} \cdot \boldsymbol{A} \right\} \quad ds.$$

Changing the upper limit of the integral to σ changes the integral by $\mathcal{O}(\epsilon)$, and since $\boldsymbol{A} \cdot \boldsymbol{A} = \mathcal{O}(\epsilon^2)$, we write

$$\langle \mathcal{S}\boldsymbol{\xi}, \boldsymbol{\xi} \rangle = \int_0^{\sigma} \left[-2\bar{\mathbf{P}} + 2(\bar{\mathbf{C}} - \bar{\mathbf{C}}^T)s + (\bar{\mathbf{Q}} - \bar{\mathbf{C}}'^T)s^2 \right] \boldsymbol{A} \cdot \boldsymbol{\zeta} \, ds + \mathcal{O}(\epsilon^2).$$

Using the boundary condition for $\boldsymbol{\zeta}$ at $s = \sigma$, and since $\bar{\mathcal{S}}\boldsymbol{\zeta} = 0$, $\boldsymbol{A}$ becomes

$$\boldsymbol{A} = \epsilon \frac{\bar{\mathbf{P}}^{-1}(\bar{\mathbf{Q}} - \bar{\mathbf{C}}'^T)\boldsymbol{\zeta}(\sigma)}{2\sigma}.$$

For the special case of a straight rod, we have

$$\boldsymbol{A} = -\frac{\epsilon\lambda_3}{2\sigma} \begin{pmatrix} \zeta_1(\sigma)/B_1 \\ \zeta_2(\sigma)/B_2 \\ 0 \end{pmatrix},$$

where

$$\boldsymbol{\zeta} = \begin{pmatrix} c_1 \cos(\omega_1 s) \\ c_2 \cos(\omega_2 s) \\ c_3 \end{pmatrix}, \quad \omega_{1,2} = \sqrt{\frac{\rho}{4B_{1,2}}}.$$

Therefore

$$\langle \bar{\mathcal{S}}\boldsymbol{\xi}, \boldsymbol{\xi} \rangle = \int_0^{\sigma} \left[A_1\zeta_1(2B_1 + \lambda_3 s^2) + A_2\zeta_2(2B_2 + \lambda_3 s^2) \right] \, ds + \mathcal{O}(\epsilon^2).$$

If the eigenvalue ρ is zero, then

$$|\mathcal{A}| = \begin{vmatrix} -\omega_1 \sin(\omega_1\sigma) & 0 \\ 0 & -\omega_2 \sin(\omega_2\sigma) \end{vmatrix} = 0.$$

Zero eigenvalues occur when $\omega_1\sigma = n\pi$, or $\omega_2\sigma = n\pi$, for $n = 1, 2, ...$

If $\omega_1\sigma = n\pi$ then the kernel of $\mathcal{A}$ is $\{(c_1, 0, 0)\}$ and $\boldsymbol{\zeta} = c_1\zeta_1$, thus

$$\langle \bar{\mathcal{S}}\boldsymbol{\xi}, \boldsymbol{\xi} \rangle = -\epsilon\lambda_3 c_1^2.$$

If $\omega_2\sigma = n\pi$ then the kernel of $\mathcal{A}$ is $\{(0, c_2, 0)\}$ and $\boldsymbol{\zeta} = c_2\zeta_2$, thus

$$\langle \bar{\mathcal{S}}\boldsymbol{\xi}, \boldsymbol{\xi} \rangle = -\epsilon\lambda_3 c_2^2.$$

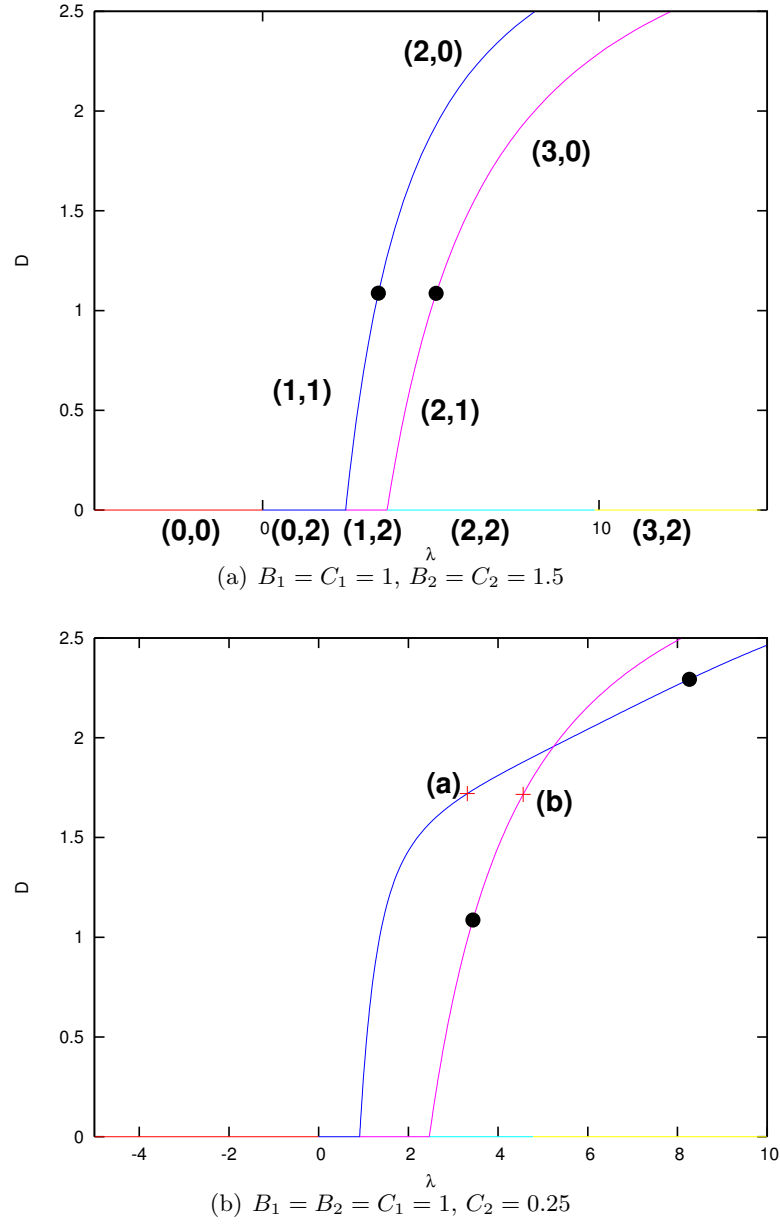Therefore, for the straight rod, if $\lambda_3 > 0$, all zero eigenvalues have negative velocity, with respect to σ.

(a) $B_1 = C_1 = 1$, $B_2 = C_2 = 1.5$

(b) $B_1 = B_2 = C_1 = 1$, $C_2 = 0.25$

Figure 5.1: Bifurcation diagrams of λ against D, for unconstrained rods with pinned boundary conditions. The solid circles indicate the points where $Q_3 = 0$ and the number of negative inborn eigenvalues change from 1 to 0 (for increasing λ). The index doesn't change at these points however, since the number of conjugate points decreases by 1 at the same points at which Q_3 changes sign. Subfigure (a) shows the values of the pairs (N_n, N_i) for each segment of the diagram. In both diagrams, $N_p = 0$ for all solutions calculated. In subfigure (b), the red crosses correspond to the rod profiles in figure 5.2.
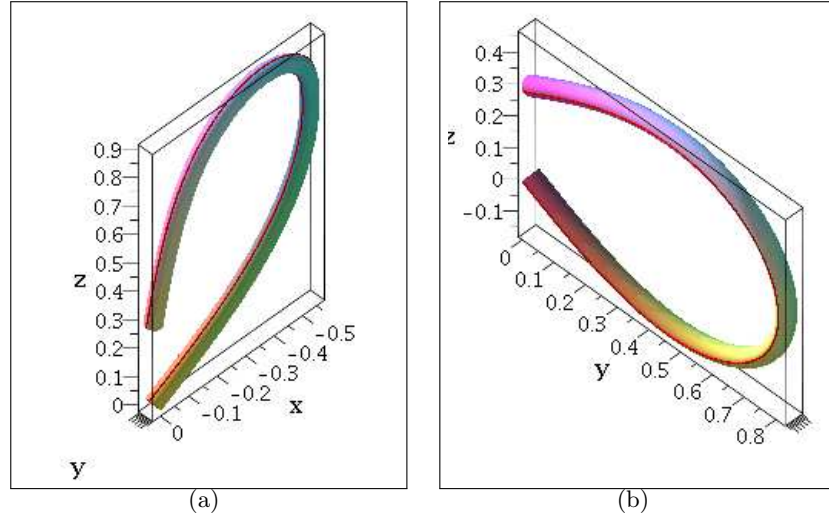
Figure 5.2: Profiles of a rod with pinned ends, corresponding to points (a) and (b) in figure 5.1(b). In the left subfigure, the influence of the discontinuity in bending stiffness is clearly visible as the rod buckles into the (e_1, e_3) plane. In the right subfigure, the buckling into the (e_2, e_3) plane is symmetrical, since $B_1 = C_1$.

Remark. Given that we can find the unconstrained stability index for straight and planar rod configurations, the constrained index could be found by using a correction method (used in [29]), which makes use of the following formula of Maddocks [25]:

$$I = I_u + d(\mathcal{W}),$$

where I_u is the unconstrained index, and $d(\mathcal{W})$ is the number of non-positive eigenvalues of the matrix $\mathcal{W}$, defined by

$$\mathcal{W} := \begin{pmatrix} \left\langle \hat{\zeta}_1, \mathbf{T}_1 \right\rangle & \left\langle \hat{\zeta}_1, \mathbf{T}_2 \right\rangle \\ \left\langle \hat{\zeta}_2, \mathbf{T}_1 \right\rangle & \left\langle \hat{\zeta}_2, \mathbf{T}_2 \right\rangle \end{pmatrix},$$

where

$$\bar{\mathcal{S}}\hat{\zeta}_i = \mathbf{T}_i, \quad \hat{\zeta}_i'(0) = \hat{\zeta}_i'(L) = \mathbf{0}, \quad i = 1, 2.$$

77

Chapter 6

Rods with Kinks

In this chapter we model a planar elastic rod that has a single kink at some point along the arclength $s \in [0, L]$.

The production of carbon nanotubes and carbon nanotube intramolecular junctions can cause the tube to form topological defects [5], [8], [45]. Figure 6.2, parts (a) and (b) show images from an atomic force microscope of nanotubes with kinks. Part (c) illustrates how the bonding of two carbon nanotubes of different diameters and chiralities can cause a kink in the topography of the resulting tube. Assuming the nanotubes to have a high aspect ratio, we model the kinked carbon nanotube by a rod with a piecewise smooth centreline.

Here, we will look at planar rod configurations in the (x, y) plane, with the rod centreline described by

$$
\begin{aligned}
x'(s) &= \sin\theta(s), \\
y'(s) &= \cos\theta(s),
\end{aligned}
$$

where $\theta(s)$ is the angle from the y-axis to the rod's tangent vector. The kink will be described by a discontinuity in $\theta(s)$ at the point $s = L_1$. The kink angle α, will therefore be given by

$$
\alpha \equiv \Big[\theta(s) \Big]_{s=L_1-}^{s=L_1+}, \tag{6.1}
$$

as illustrated in figure 6.1.

78

An alternative way to model a kink would be to express the intrinsic curvature as an approximation to the Dirac delta function, e.g. for an intrinsic curvature $\hat{\theta}'(s)$, let $\hat{\theta}'(s) = \frac{1}{a}e^{-(s-L_1)^2/a^2}$, for a small valued parameter a. However, we find the kink angle α to be a more measurable and numerically stable parameter.
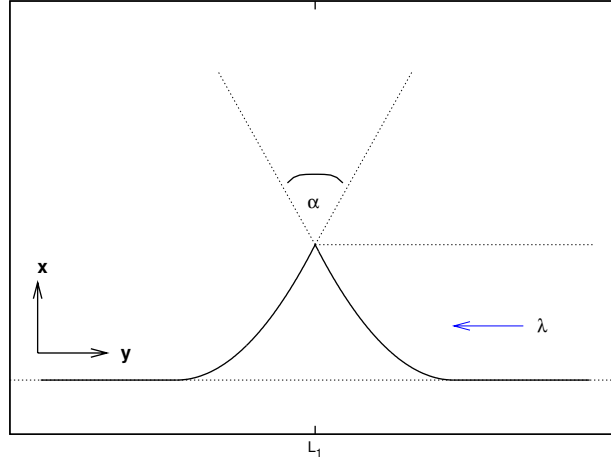

Figure 6.1: Discontinuity in θ at the point $s = L_1$. $\alpha = \theta(L_1+) - \theta(L_1-)$.

Classical calculus of variations theory consists of finding critical points $\mathbf{q}^{(0)}(s)$ such that a functional $E[\mathbf{q}]$ is stationary relative to all weak variations of $\mathbf{q}(s)$. In the standard theory, the function $\mathbf{q}(s)$ is continuous, and $\mathbf{q}'(s)$ is continuous except at a finite number of points, where the well known Weierstrass-Erdmann corner conditions must be satisfied [12]. Such extremals in which $\mathbf{q}'(s)$ has a finite number of discontinuities are called broken extremals.

In chapter 4, we looked at rods with discontinuities in the bending stiffness, which corresponded to discontinuous $\mathbf{q}'(s)$. In this chapter we look for extremals of a functional $E[\theta]$, which allows discontinuities in both $\theta(s)$ and $\theta'(s)$. The discontinuous variational problem discussed in chapter 2 allows for discontinuous $\theta(s)$, so in this chapter we will use the continuity conditions formulated previously, which are the continuity of $W_{\mathbf{q}'}$ and the continuity of $W_{\mathbf{q}'\mathbf{q}'}\mathbf{h}'$. Figure 6.3 gives an example of a discontinuous extremal and a weak variation.
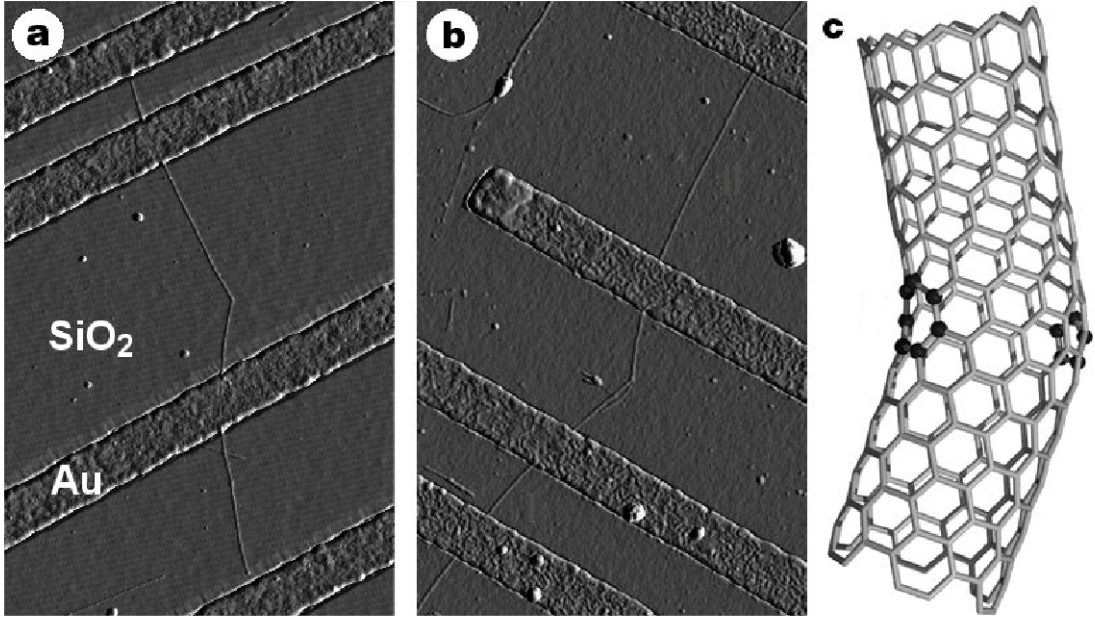
Figure 6.2: Parts **a** and **b** are images from an atomic force microscope of nanotubes which contain kinks of 36° and 41° respectively. Part **c** illustrates how the bonding of two carbon nanotubes of different diameters and chiralities can cause a kink in the topography of the resulting tube. Image taken from [45].

6.1 Variational Formulation

The total energy of the system is described by

$$E = \int_0^{L_1} \frac{1}{2} B_1 \left[\theta'(s) \right]^2 + \lambda \cos \theta(s) \; \mathrm{d}s \; + \; \int_{L_1}^{L} \frac{1}{2} B_2 \left[\theta'(s) \right]^2 + \lambda \cos \theta(s) \; \mathrm{d}s,$$

where λ is the force exerted on the rod at the end ($s = L$), and B_1, B_2 are the constant bending stiffnesses for each section of the rod.

If we add a constraint to the rod, which fixes the end at $s = L$ to lie on the vertical y-axis, then $x(L) = x(0) = 0$, which can be written in isoperimetric form:

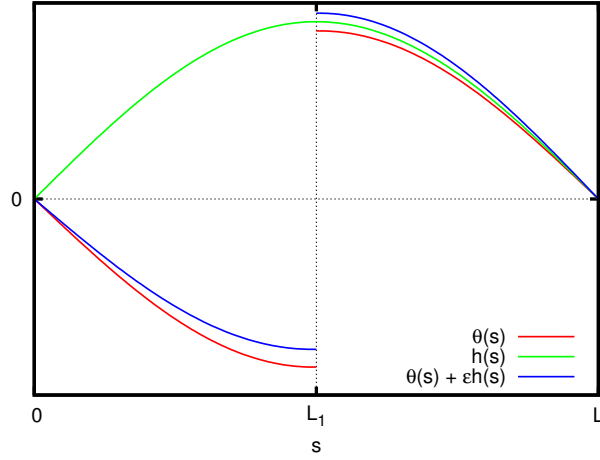$$\int_0^L \sin \theta(s) \; \mathrm{d}s = 0.$$

Figure 6.3: Variation of a discontinuous extremal. In this example, the second order matching condition is $h'(L_1-) = h'(L_1+)$.

Adding the isoperimetric constraint to the energy functional, the first variation is

$$
\begin{aligned}
\delta E &= \int_0^{L_1} h \left[B_1 \theta'' - \lambda \sin\theta + \mu \cos\theta \right] \, \mathrm{d}s \\
&+ \int_{L_1}^{L} h \left[B_2 \theta'' - \lambda \sin\theta + \mu \cos\theta \right] \, \mathrm{d}s \\
&+ B_1 h \theta'(L_1-) - B_2 h \theta'(L_1+),
\end{aligned}
\tag{6.2}
$$

where μ is a Lagrange multiplier.

For continuous h, equation (6.2) is zero for any h, only if

$$
\begin{aligned}
B_1 \theta'' &= \lambda \sin\theta - \mu \cos\theta, \quad 0 \le s < L_1, \\
B_2 \theta'' &= \lambda \sin\theta - \mu \cos\theta, \quad L_1 < s \le L, \\
B_1 \theta'(L_1-) &= B_2 \theta'(L_1+).
\end{aligned}
$$

Let

$$
\begin{aligned}
h_1(s) &= h(s), \quad 0 \le s < L_1, \\
h_1(L_1) &= \lim_{\epsilon \to 0} h(L_1 - \epsilon), \\
h_2(s) &= h(s), \quad L_1 < s \le L, \\
h_2(L_1) &= \lim_{\epsilon \to 0} h(L_1 + \epsilon),
\end{aligned}
$$

and

$$\theta_1(s) = \theta(s), \quad 0 \le s < L_1,$$

$$\theta_1(L_1) = \lim_{\epsilon \to 0} \theta(L_1 - \epsilon),$$

$$\theta_2(s) = \theta(s), \quad L_1 < s \le L,$$

$$\theta_2(L_1) = \lim_{\epsilon \to 0} \theta(L_1 + \epsilon).$$

Conjugate points can be found by solving the initial value problems

$$\mathcal{S}_1 h_1 = \hat{c}_1 T_1, \quad 0 \le s \le L_1,$$

$$f_1'(s) = h_1 T_1, \quad 0 \le s \le L_1,$$

$$\mathcal{S}_2 h_2 = \hat{c}_2 T_2, \quad L_1 \le s \le L,$$

$$f_2'(s) = h_2 T_2, \quad L_1 \le s \le L,$$

with initial conditions

$$h_1(0) = 0, \quad h_1'(0) = 1, \quad f_1(0) = 0,$$

$$h_2(L_1) = h_1(L_1), \quad B_2 h_2'(L_1) = B_1 h_1'(L_1), \quad f_2(L_1) = f_1(L_1)$$

where the operators $\mathcal{S}_i$ are defined by

$$\mathcal{S}_i h \equiv -B_i h'' - h(\lambda \cos \theta_i + \mu \sin \theta_i), \quad i = 1, 2,$$

and

$$T_i = \cos \theta_i, \quad i = 1, 2.$$

If we write h_i and f_i in the form

$$h_i = c_i h_i^{(h)} + \hat{c}_i h_i^{(p)}, \quad i = 1, 2,$$

$$f_i = c_i f_i^{(h)} + \hat{c}_i f_i^{(p)}, \quad i = 1, 2,$$

then Jacobi's condition for a minimum extremal is that

$$|\mathcal{A}| = \begin{cases} \left|\mathcal{A}^{(1)}\right| & : \quad 0 \le s \le L_1 \\ \left|\mathcal{A}^{(2)}\right| & : \quad L_1 \le s \le L \end{cases} \neq 0 \quad \forall s \in (0, L),$$

where

$$\left| \mathcal{A}^{(i)} \right| (s) = \left| \begin{matrix} h_i^{(h)}(s) & h_i^{(p)}(s) \\ f_i^{(h)}(s) & f_i^{(p)}(s) \end{matrix} \right|, \quad i = 1, 2.$$

Note that if $h(s)$ is a solution to $\mathcal{S}_1 h_1 = \hat{c}_1 T_1$, $\mathcal{S}_2 h_2 = \hat{c}_1 T_1$, $h_1(0) = 0$, $h_2(\sigma) = 0$, then $Ch(s)$ is also a solution, and we can choose C such that $h_1'(0) = 1$.

6.2   Numerical Results

Using the dimensionless parameters

$$\beta = \frac{B_2}{B_1}, \quad \gamma = \frac{L_1}{L},$$

we will use parameter continuation to create bifurcation diagrams, and investigate the stability of kinked planar rod solutions. Using AUTO, we vary the kink parameter α from zero to a desired value, then increase λ from zero to compute a solution branch of kinked rods. Since the rod is no longer straight for any non-zero value of α, there is no trivial branch at $D = 0$. As λ is increased, solution branches follow the path of either the first-mode solutions (for rods with no kink) or the second-mode solutions, depending on whether the rod is constrained or unconstrained. We will now look at the results of both cases separately.

6.2.1   Unconstrained

Figure 6.4 shows bifurcation diagrams of λ against D. Each subfigure shows solution curves for $\alpha = 0, 0.2, 0.4, ..., 2.2$. In (a), $\gamma = 0.5$ and $\beta = 1$. We see that for $\alpha > 0$, as λ is increased the stable branches become unstable (with index 1) at a (supercritical) pitchfork bifurcation point, then increasing λ further, become stable again at a second (subcritical) pitchfork bifurcation point. The unstable region between these branch points becomes smaller as the branch points get closer together with increasing α. For $\alpha = 2.2$, we see that the stable branch no longer contains any bifurcation points. Subfigures (b), (c) and (d) show that a break in symmetry of the kink position, or a jump in the bending stiffness, causes the solution curves from $\lambda = 0$ to follow the branch representing

the first-mode of buckling. There are no longer any pitchfork bifurcation points on the stable solution curves. When symmetry is broken, the first-mode solution branches split into two distinct sets of branches. Solutions that bend in the same direction as the kink follow the path of the first buckling mode and remain stable. Solutions that bend in the opposite direction to the kink connect to the unstable branch of second-mode solutions via a limit point.

Figure 6.5 shows bifurcation diagrams of λ against $x(L)$ for $\beta = 1$ and $\gamma = 0.5$. The three branches from the pitchfork bifurcations are all distinctly visible in the $(\lambda, x(L))$ diagram. Rod profiles at the points indicated are given in figure 6.7

Figure 6.6 shows fold continuation in the (λ, α) parameter space of the limit points indicated in figure 6.5. From the curve of limit points in figure 6.6, we find critical values of α, called α_1 and α_2, which dictate the type of bifurcation that occurs locally. We find $\alpha_1 \approx 1.89$ and $\alpha_2 \approx 2.07$. This is summarised by table 6.1.

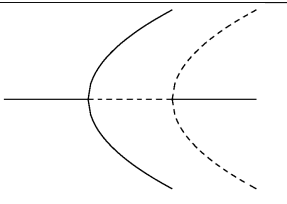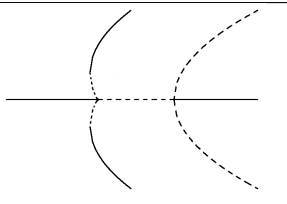Figures 6.8 and 6.9 show λ against $x(L)$ for various values of γ.
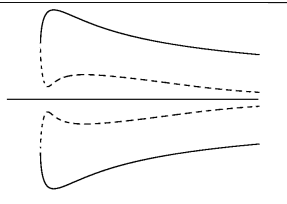
$\alpha < \alpha_1$	$\alpha_1 \leq \alpha \leq \alpha_2$	$\alpha_2 < \alpha$
A supercritical bp followed by a subcritical bp.	First bp splits into 3 unstable branches (locally), followed by a subcritical bp.	No bifurcation points along the stable branch.

Table 6.1: Types of bifurcation from the stable solution branch.

6.2.2 Constrained

Figure 6.10 plots λ against D for $\gamma = 0.5$, $\beta = 1$, and $\alpha = 0, 0.2, 0.4, ..., 2$. As α is increased from zero, the branch of first buckling modes splits into two distinct branches. The branches to the left represent rod configurations buckling in the negative x direction

Figure 6.4: Bifurcation diagrams of λ against D, for $\alpha = 0, 0.2, 0.4, ..., 2.2$.
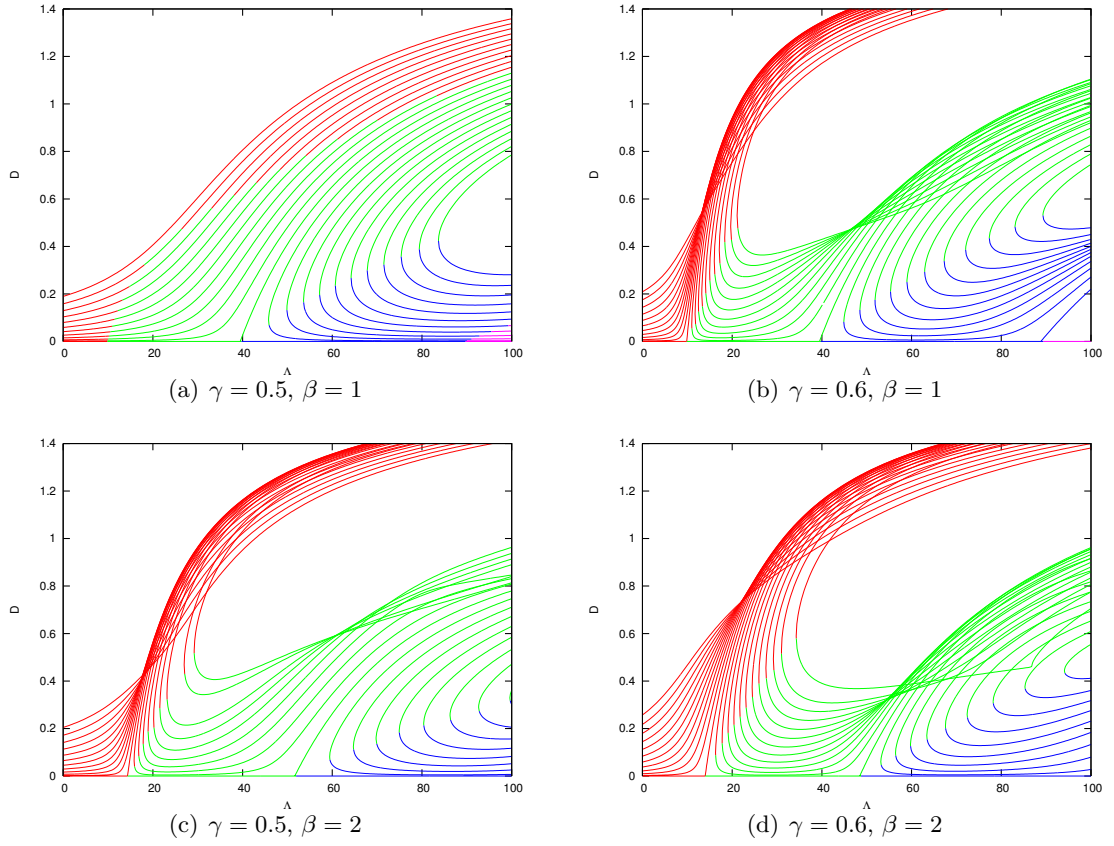
(in the same direction as the kink), and the branches to the right represent rods buckling in the positive x direction (in the opposite direction of the kink). These stable branches connect to unstable branches corresponding to the third-mode of buckling via a limit point. There is a subcritical bifurcation point connecting the third-mode branch to the second-mode branch for certain values of α, which vanishes as α is increased beyond a critical value.

Figure 6.11 shows the bifurcation diagram for $\alpha = 1.2$, with rod profiles plotted at $D = 0.2$ for solutions representing the first-, second-, and third-modes. The presence of a kink causes odd-mode buckling branches to split and connect to the next odd branch, i.e. the second of the $(2n-1)$-th pair of branches connects with the first of the $(2n+1)$-th
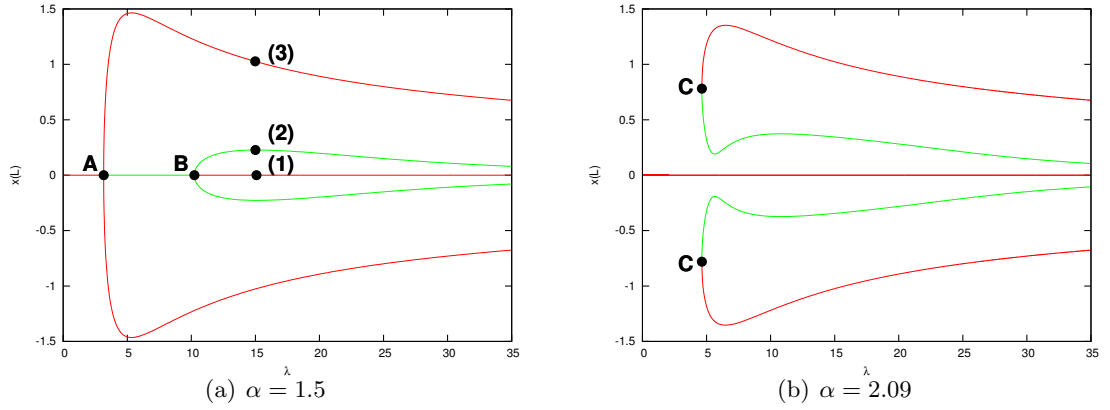
(a) $\alpha = 1.5$ (b) $\alpha = 2.09$

Figure 6.5: Bifurcation diagrams of λ against $x(L)$, where $\beta = 1$ and $\gamma = 0.5$. Points A and B are pitchfork bifurcation points, which are followed in two parameters in figure 6.6. Rod profiles at the points (1), (2) and (3) are given in figure 6.7.

(a)   (b)
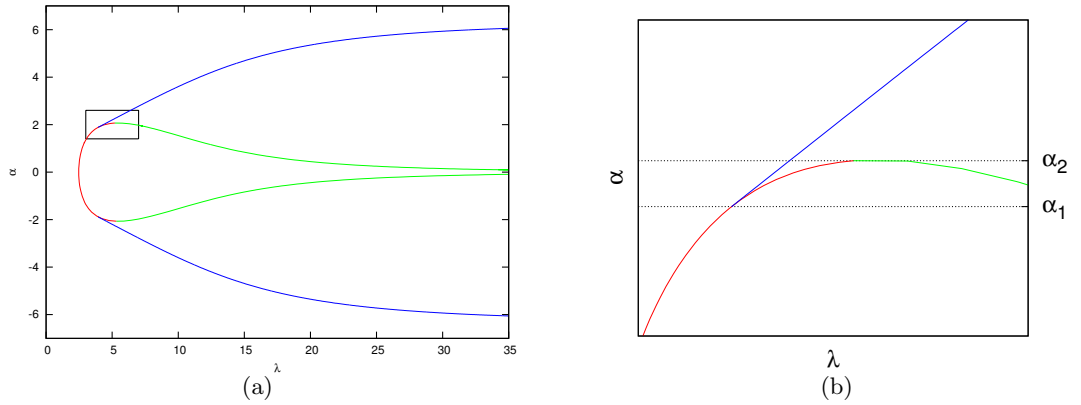
Figure 6.6: Fold continuation of the points given in figure 6.5. Values of the folds A (red), B (green) and C (blue) are plotted in the parameter space (λ, α).

pair of branches, for $n = 1, 2, ...$

If we break symmetry further by having $\beta \neq 1$ or $\gamma \neq 0.5$, then the second-mode branch will split into two distinct solution branches. Figure 6.12 shows for $\alpha = 0.8$ and $\gamma = 0.6$, the second-mode branch splits, with one (closed) branch connecting to the stable first-mode solutions, and the other (open) branch connecting to the unstable third-mode solutions.
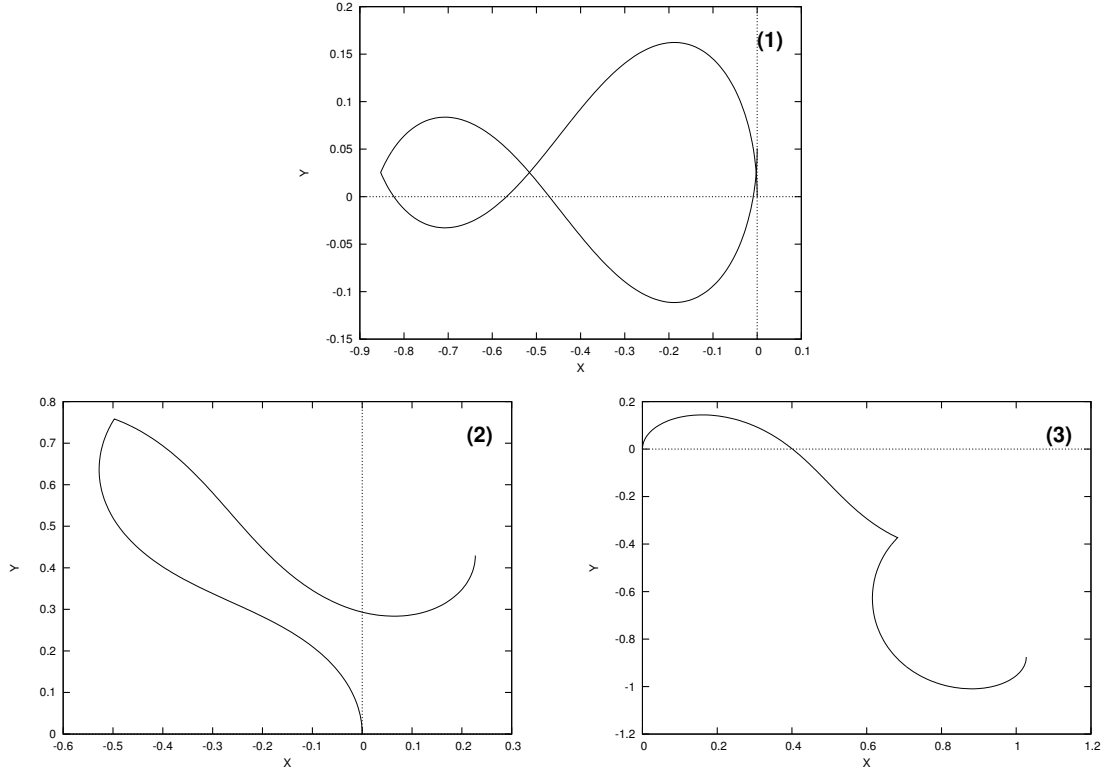
Figure 6.7: Rod profiles from the points (1), (2), and (3), from figure 6.5.

(a) $\gamma = 0.5$

(b) $\gamma = 0.05, 0.1, 0.15, 0.2, 0.25, 0.3, 0.35, 0.4, 0.45,$ 0.55, 0.6, 0.65, 0.7, 0.75, 0.8, 0.85, 0.9, and 0.95.

Figure 6.8: λ against $x(L)$, for $\alpha = 0.5$.

(a) $\gamma = 0.5$

(b) $\gamma = 0.05, 0.1, 0.15, 0.2, 0.25, 0.3, 0.35, 0.4, 0.45,$ $0.55, 0.6, 0.65, 0.7, 0.75, 0.8, 0.85, 0.9,$ and $0.95.$
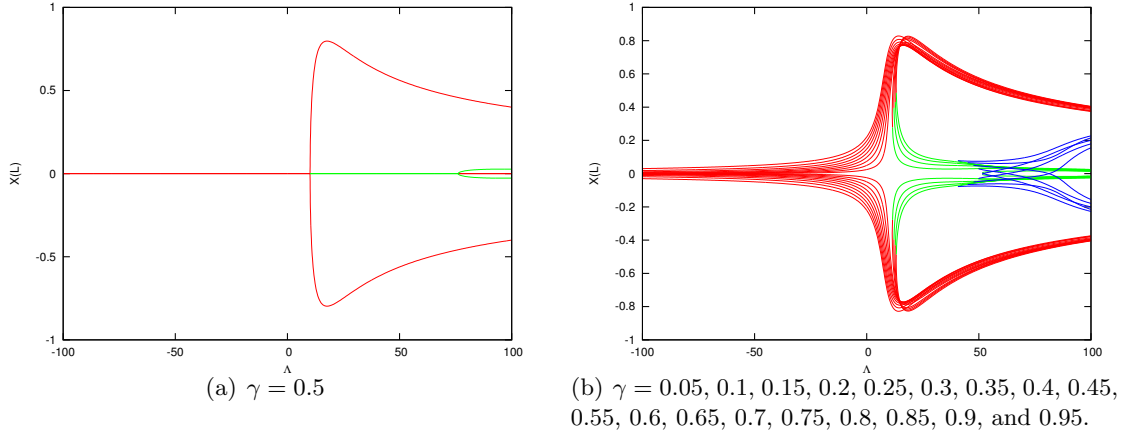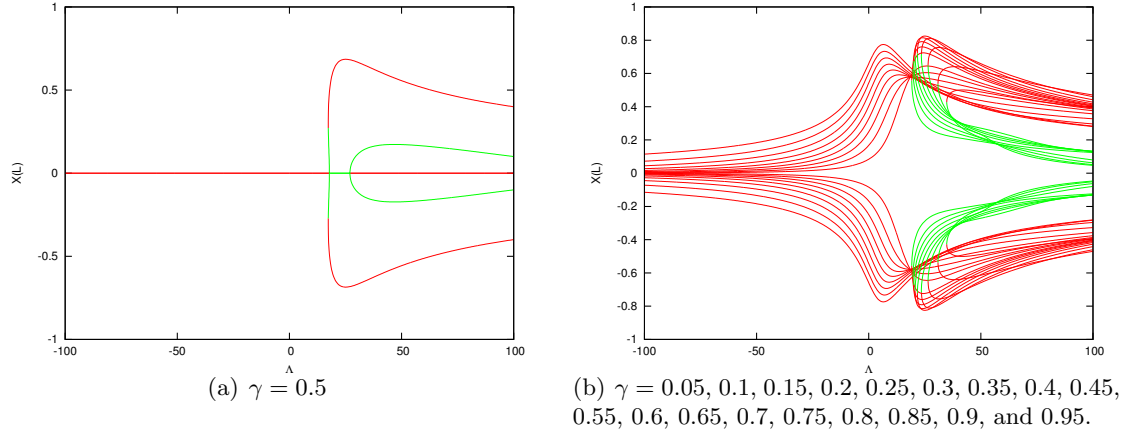
Figure 6.9: λ against $x(L)$ for $\alpha = 2.$
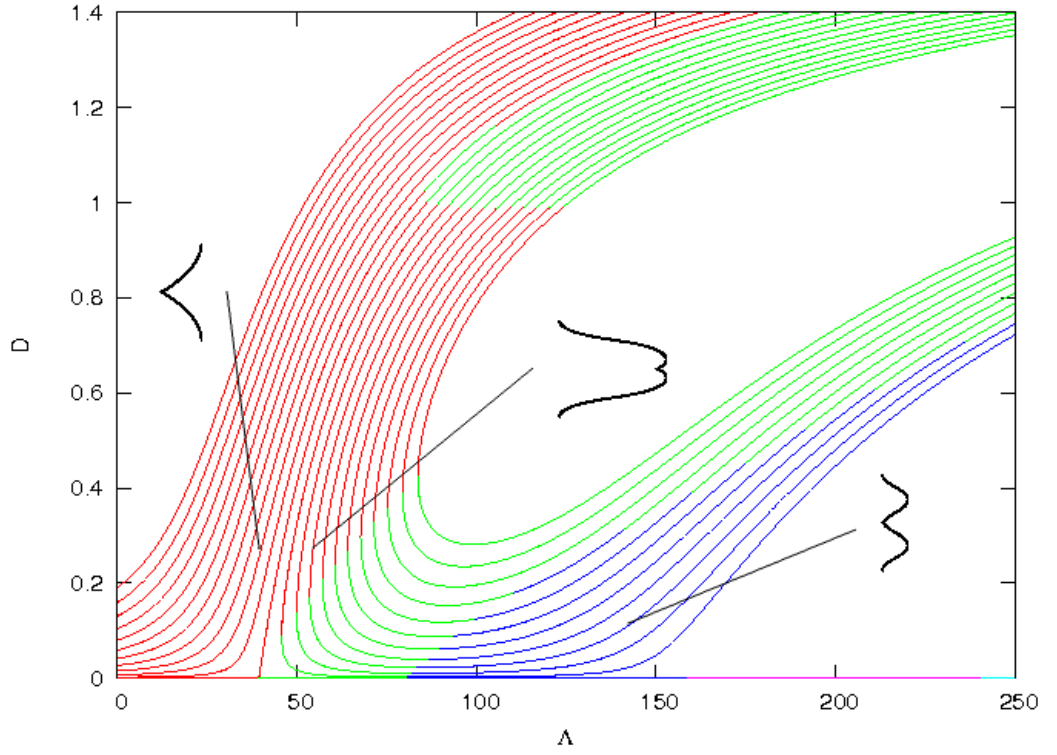
Figure 6.10: Bifurcation diagrams of λ against D for $\alpha = 0, 0.2, 0.4, ..., 2.$ $\beta = 1,$ and $\gamma = 0.5.$

(a) $\alpha = 1.2$, $\beta = 1$, $\gamma = 0.5$

(b) **1(a)** = red, **1(b)** = green

(c) **2** = red & green

(d) **3(a)** = red, **3(b)** = green

Figure 6.11: Bifurcation diagram of λ against D for $\alpha = 1.2$, $\gamma = 0.5$, $\beta = 1$, and rod profiles at the points indicated at $D = 0.2$. The dashed lines in the bifurcation diagram indicate the first, second and third buckling branches of a rod without a kink ($\alpha = 0$).

(a) $\alpha = 0.8$, $\beta = 1$, $\gamma = 0.6$

(b) Point **1**

(c) Point **2(a)** = red. Point **2(b)** = green

(d) Point **3**

Figure 6.12: Bifurcation diagram of λ against D for $\alpha = 0.8$, $\gamma = 0.6$, $\beta = 1$, and rod profiles at the points indicated at $D = 0.2$. The dashed lines in the bifurcation diagram indicate the first, second and third buckling branches of a rod without a kink ($\alpha = 0$).

Chapter 7

Interactions Between a Rod and a Surface

In the previous chapters we have studied the buckling and post-buckling behaviour of a rod in free space, i.e. the rod was not influenced by any external forces (other than end compression or end rotation). However, sin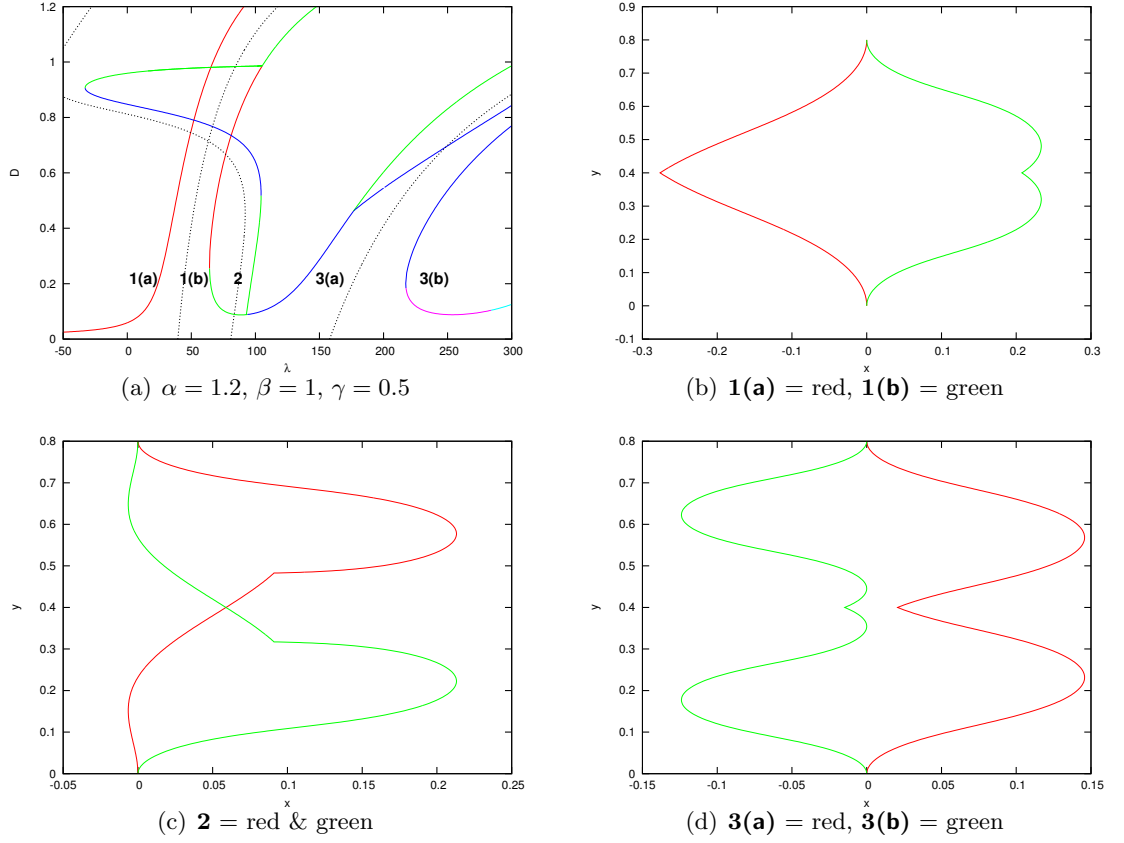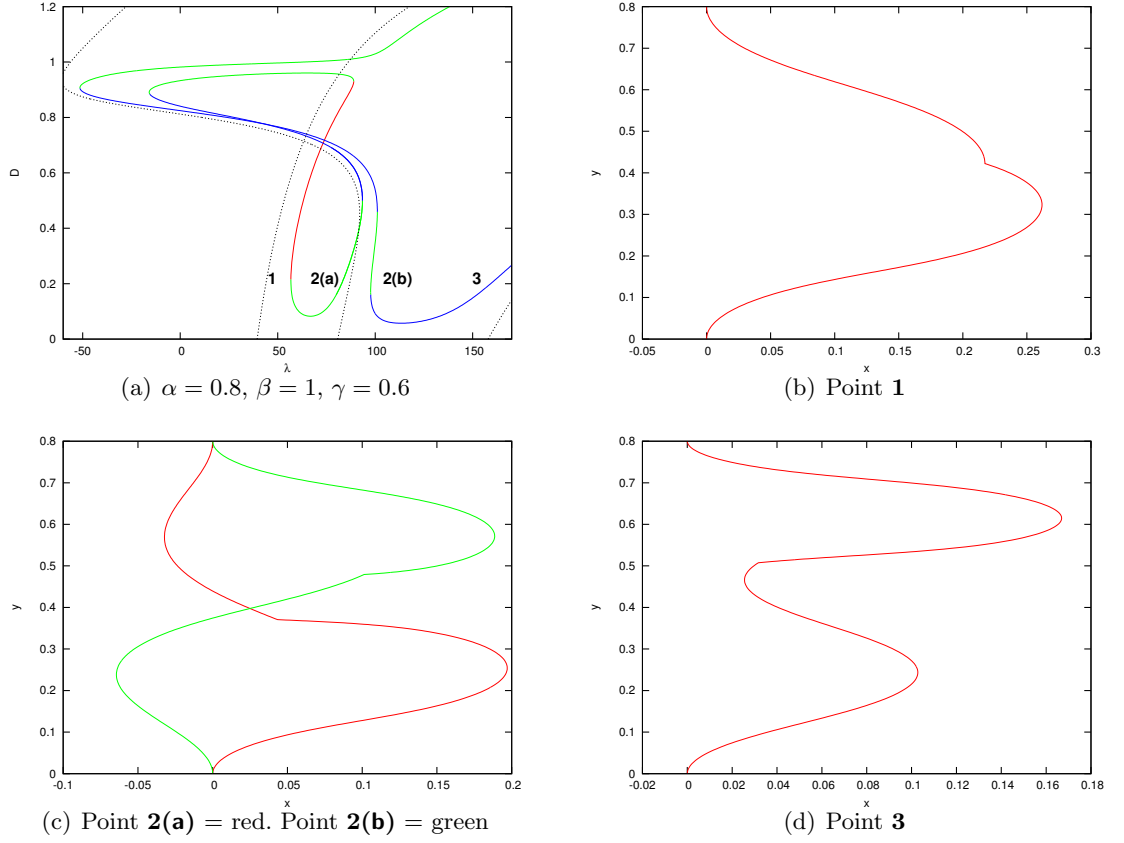ce many potential applications of carbon nanotubes involve the tube resting on a substrate, (usually a hydrogenerated silicon surface [16]), the effect of this substrate should be taken into account. In this chapter, we introduce a potential to the total energy occurring from van der Waals forces between the silicon surface and the carbon nanotube.

Hertel *et al.* [17] study the effects of surface van der Waals forces on the cross-section shape of nanotubes. Sear and Batra [38] look at axial compressive buckling of rod and shell models using molecular mechanics simulations. Buehler *et al.* [4] study the compressive loading of nanotubes as shells and rods using molecular dynamics simulations, and showed that a nanotube buckles like a rod (Euler buckling) when the tube has an appropriately high aspect ratio. However, we are unaware of any work that studies the buckling of a nanotube using a continuum model, which takes into account the effects of surface van der Waals forces.

In [28] and [39] a repulsive potential is used to model an elastic rod buckling into a soft wall. Here, we use an attractive-repulsive Morse potential. We are interested in the post-buckling solutions in which the rod breaks away from the surface, therefore we

will use a planar rod model with a compressive force λ exerted in the y direction and an interactive surface force in the x direction, as illustrated by figure 7.1.
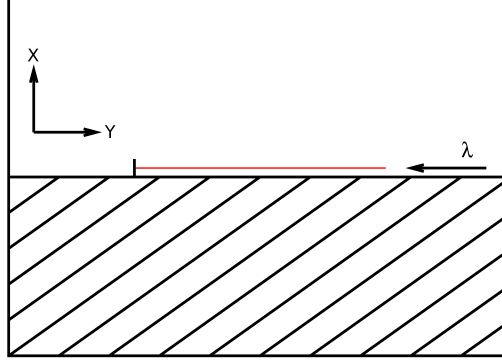
Figure 7.1: A rod, fixed at one end, lying on a surface with a compressive force λ in the y direction.

7.1 Variational Formulation

As in the previous chapter, we use assume the total energy of the rod depends quadratically on the curvature $\theta'(s)$, and we add the force term as well as a potential energy term $V(x)$, describing the surface interaction with respect to $x(s)$, the distance from the surface at s.

$$E = \int_0^L \frac{1}{2} B \left[\theta'(s)\right]^2 + \lambda \cos\theta(s) + V\left(x(s)\right) \ \mathrm{d}s.$$

Equilibrium Equations

The first variation is given by

$$\delta E \;\; = \;\; \int_0^L \left[h(s)\left(-B\theta''(s) - \lambda\sin\theta(s)\right) + \delta x V_x(s)\right] \ \mathrm{d}s, \tag{7.1}$$

where

$$x(s) = \int_0^s \sin\theta(\tau) \ \mathrm{d}\tau,$$

and

$$\delta x = \int_0^s \cos\theta(\tau) h(\tau) \ \mathrm{d}\tau.$$

Substituting these expressions into (7.1), we get

$$\delta E = \int_0^L h(s) \left(-B\theta''(s) - \lambda \sin\theta(s) \right) \, ds + \int_0^L \int_0^s \cos\theta(\tau) h(\tau) V_x(s) \, d\tau \, ds.$$

Using the identity

$$\int_a^b \int_a^s H(\tau) G(s) \, d\tau \, ds = \int_a^b \int_s^b H(s) G(\tau) \, d\tau \, ds, \tag{7.2}$$

which can be verified directly using integration by parts, it can be easily shown that

$$\delta E = \int_0^L h(s) \left(-B\theta''(s) - \lambda \sin\theta(s) + \cos\theta(s) \int_s^L V_x(\tau) \, d\tau \right) \, ds.$$

The condition $x(0) = x(L) = 0$, gives us the isoperimetric constraint

$$\int_0^L \sin\theta(s) \, ds = 0.$$

The linearised isoperimetric constraint is

$$\int_0^L \cos\theta(s) h(s) \, ds = 0.$$

If $\delta E = 0$ for all h then, adding the Lagrange multiplier term, we must have

$$-B\theta''(s) - \lambda \sin\theta(s) - \mu \cos\theta(s) + \cos\theta(s) \int_s^L V_x(\tau) \, d\tau = 0.$$

If we define

$$\boldsymbol{n} := \begin{pmatrix} n_1 \\ n_2 \end{pmatrix} = \begin{pmatrix} \int_s^L V_x(\tau) \, d\tau \\ 0 \end{pmatrix} + \begin{pmatrix} -\mu \\ \lambda \end{pmatrix}, \tag{7.3}$$

then the equilibrium equations become

$$B\theta''(s) = n_1 \cos\theta(s) - n_2 \sin\theta(s).$$

Stability Equations

The second variation is given by

$$\delta^2 E = \frac{1}{2} \int_0^L \left[h(s) \left(-B_1 h''(s) - \lambda \cos\theta(s) h(s) + \mu \sin\theta(s) h(s) \right) + \delta^2 x V_x(s) + (\delta x)^2 V_{xx}(s) \right] \, ds,$$

which we will write as

$$\delta^2 E = \frac{1}{2} \int_0^L h(s) \left(-B h''(s) - \lambda \cos\theta 1(s) h(s) + \mu \sin\theta(s) h(s) \right) \, ds + R_1[h] + R_2[h]$$

93

where

$$R_1[h] = \frac{1}{2} \int_0^L \int_0^s -h(\tau)^2 \sin\theta(\tau) V_x(s) \, \mathrm{d}\tau \, \mathrm{d}s,$$

and

$$R_2[h] = \frac{1}{2} \int_0^L \int_0^s \int_0^s h(\kappa) \cos\theta(\kappa) h(\tau) \cos\theta(\tau) V_{xx}(s) \, \mathrm{d}\kappa \, \mathrm{d}\tau \, \mathrm{d}s.$$

Using (7.2), it can be easily shown that

$$R_1[h] = \frac{1}{2} \int_0^L \int_s^L -h(s)^2 \sin\theta(s) V_x(\tau) \, \mathrm{d}\tau \, \mathrm{d}s,$$

and

$$R_2[h] = \frac{1}{2} \int_0^L h(s) \left[\cos\theta(s) \int_s^L F(\kappa) \, \mathrm{d}\kappa \right] \mathrm{d}s,$$

where

$$F(\kappa) = V_{xx}(\kappa) \int_0^\kappa h(\tau) \cos\theta(\tau) \, \mathrm{d}\tau = V_{xx}(\kappa) z,$$

and

$$z'(s) = h \cos\theta(s), \quad z(0) = 0.$$

We can now write the second variation as

$$\delta^2 E = \frac{1}{2} \int_0^L h(s) \left[-B_1 h''(s) - h(s) \sin\theta(s) \left(\int_s^L V_x(\tau) \, \mathrm{d}\tau - \mu \right) - \lambda h(s) \cos\theta(s) + \cos\theta(s)\psi(s) \right] \mathrm{d}s,$$

where

$$\psi'(s) = -F(s) = -V_{xx}(s)z(s), \quad \psi(L) = 0.$$

From the definition of $\boldsymbol{n}$ in (7.3) we get

$$\delta^2 E = \frac{1}{2} \int_0^L h \left[-Bh'' - h \left(n_1 \sin\theta + n_2 \cos\theta \right) + \psi \cos\theta \right] \mathrm{d}s.$$

Finally, second variation can be expressed as

$$\delta^2 E = \frac{1}{2} \langle \mathcal{S}h, h \rangle,$$

where the operator $\mathcal{S}$ is defined by

$$\mathcal{S}h \equiv -Bh'' - h \left(n_1 \sin\theta + n_2 \cos\theta \right) + \psi \cos\theta,$$

and $\langle \cdot, \cdot \rangle$ denotes the standard L^2 inner product over $[0, L]$.

Bullman and Manning [28] show that the operator $\mathcal{S}$, with the extra integrodiffer-ential term, is self-adjoint and has the properties **1**, **2** and **3** from section 2.1, and as such, the constrained stability index can be defined by the number of conjugate points $\sigma \in (0, L)$, such that

$$\mathcal{S}h + \hat{c}T = 0, \quad h(0) = h(\sigma) = 0,$$

has a non-trivial solution, where $T = \cos\theta$.

The full system of equations for the rod equilibrium and the stability index is

$$x'(s) \quad = \quad \sin\theta \tag{7.4}$$

$$y'(s) \quad = \quad \cos\theta \tag{7.5}$$

$$B\theta''(s) \quad = \quad n_1 \cos\theta - n_2 \sin\theta \tag{7.6}$$

$$n_1'(s) \quad = \quad -V_x \tag{7.7}$$

$$n_2'(s) \quad = \quad 0 \tag{7.8}$$

$$Bh''(s) \quad = \quad -h\left(n_1 \sin\theta + n_2 \cos\theta\right) + \psi\cos\theta - T \tag{7.9}$$

$$z'(s) \quad = \quad y'h \tag{7.10}$$

$$\psi'(s) \quad = \quad -V_{xx}z \tag{7.11}$$

with boundary conditions

$$x(0) = 0, \quad y(0) = 0, \quad \theta(0) = 0, \quad h(0) = 0, \quad z(0) = 0,$$

$$x(L) = 0, \quad n_2(L) = \lambda, \quad \theta(L) = 0, \quad h(L) = 0, \quad \psi(L) = 0.$$

To model the interactive force between the substrate and the rod, we will use the Morse potential given by

$$V_x(x) = \frac{-12a}{\omega}\left[e^{-12x/\omega} - e^{-6x/\omega}\right], \quad V_{xx}(x) = \frac{12a}{\omega^2}\left[12e^{-12x/\omega} - 6e^{-6x/\omega}\right], \tag{7.12}$$

where a is the depth of the potential well, and ω is the distance at which the inter-particle potential is zero. Figure 7.2 plots the Morse energy potential against x. For negative x values, $V_x(x)$ is highly negative, representing a repulsive force away from the surface. For positive x, the function $V_x(x)$ is positive, becoming smaller with increasing x (as the

rod gets further from the surface). For $x = 0$, $V_x(x) = 0$ and there is no force between the rod and the surface.
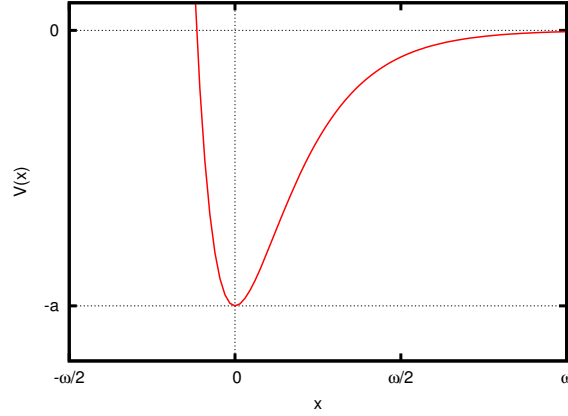

Figure 7.2: The Morse potential $V(x)$ against x.

Since we are concerned with the centreline $(x(s), y(s))$, the parameter ω will be proportional to the equilibrium distance between tube surface and the substrate surface, plus the radius of the nanotube.

Experimental results and molecular mechanics simulations (e.g. [16] and [17]) show that the binding force a is related to the diameter, thus, a is related to the parameters ω and B. We will take into account these relationships, but treat a, ω, and B as independent parameters. Hertel *et al.* [17] gives $a = 1.6$nN for a tube diameter of 6nm, and gives $a = 4$nN for a tube diameter of 10nm.

7.2 Numerical Results

Using parameter continuation, we vary a from zero to a desired value, then increase λ to find branch points along the trivial branch of straight solutions. Due to the effects of the potential, the force component of the buckled solution branches vary rapidly with respect to λ for small values of the solution measure D. Therefore, we will define the branches of buckled solutions in two regions: inner, for small D, and outer, for $D = \mathcal{O}(1)$. This rapid variation of the solution causes standard numerical methods to be numerically

unstable, i.e., the problem is *stiff*.

We find the index of the solution branches in the same way as before, using parameter continuation to find the rod solutions and initial values for the stability equations, then solving the stability equations as an initial value problem. However, we must now use a stiff IVP solver. Here, we use the stiff IVP solver DLSODE [18].

For the following numerical results we will use the dimensionless variables defined by making the following transformations:

$$\lambda \to \frac{\lambda L^2}{B}, \quad a \to \frac{aL^2}{B}, \quad \text{and} \quad \omega \to \frac{\omega}{L}. \tag{7.13}$$

If the tube-surface binding force is 4nN, then for a nanotube of length 100nm, radius 6nm, and Young's modulus 1000 nN/nm^2, we get $a = 0.031$ and $\omega = 0.06$. These values of a and ω are used to generate the results given in figure 7.6(a), and represent typical realistic parameter values for the nanotube and the surface interaction. Increasing a is equivalent to increasing the tube length or decreasing the Young's modulus. Increasing ω is equivalent to decreasing the tube length.

Figure 7.3 shows the bifurcating branches from the straight rod for $a = 0.5$ and $a = 1$. When $a = 0.5$, the first branch bifurcating from the trivial branch actually represents the second buckling mode. However, due to the effects of the surface interaction, this configuration doesn't last long as D is increased, and the branch connects to the branch of the first-mode solutions. The second branch bifurcating from the trivial branch represents the first and third buckling modes. This branch is split into two curves: the left branch of solutions buckling away from the surface, and the right branch of solutions buckling towards the surface. When $a = 1$, the order in which the two branch points appear (with respect to λ) has changed. The first branch now represents the first- and third-mode solutions, and the second branch represents the second-mode solutions.

Figure 7.4 shows the first and second outer region solution branches for $a = 0.5$ and $\omega = 0.1$. The first solution branch is unaffected by the surface interactions in the outer region. However, the second branch is significantly affected by the surface interactions, and we see that three separate stable branches occur for values of D greater than 1.
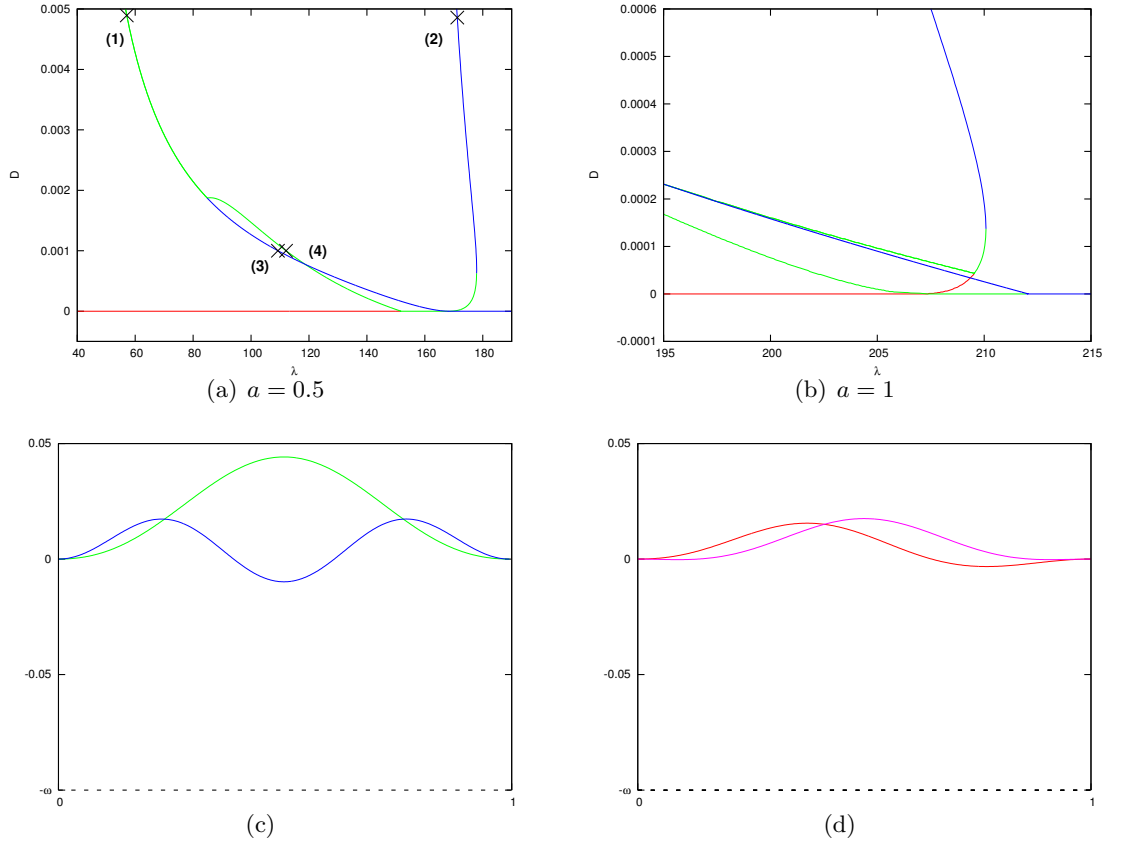
Figure 7.3: Bifurcation diagrams of λ against D for small values of D, where $\omega = 0.1$. Rod profiles at the crosses in subfigure (a) are given in subfigures (c) and (d). The dashed line indicates the surface.

Figure 7.5 shows rod shapes at points along these three stable regions, which represent third-mode rod solutions.

Figure 7.6 shows inner region solution branches for various values of a, when $\omega = 0.06$. We see that as a tends to zero, the first buckling point gets closer to $4\pi^2$, and the stable region on the branches (representing third-mode solutions) get bigger.

7.3 Buckling Loads of Rods on an Interactive Surface

In this section, we obtain expressions for the critical buckling values of λ with respect to the Morse potential parameters a and ω. To find critical buckling values of λ, we

(a) First branch, outer region. (b) Second branch, outer region.
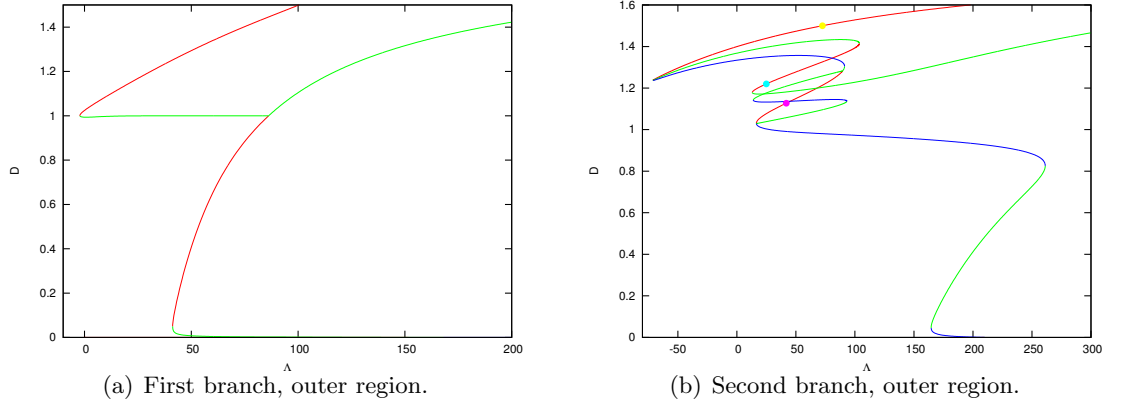
Figure 7.4: Bifurcation diagrams of λ against D, where $a = 0.5$ and $\omega = 0.1$.

(a) (b) (c)
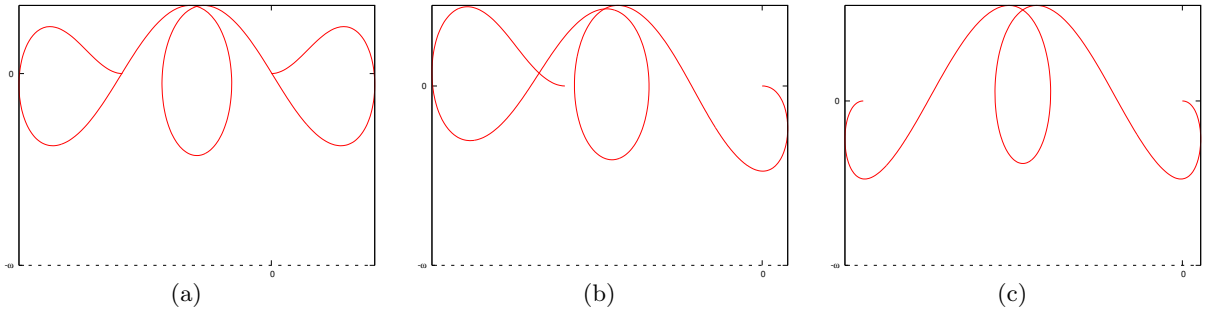
Figure 7.5: Rod shapes from stable solution branches at the points indicated in figure 7.4. Subfigure (a) corresponds to the purple solid circle, subfigure (b) corresponds to the light blue solid circle, and subfigure (c) corresponds to the yellow solid circle.

linearise about the straight rod solution,

$$
\begin{aligned}
x(s) &= x^0(s) + \epsilon \hat{x}(s) + \mathcal{O}\left(\epsilon^2\right) = 0 + \epsilon \hat{x}(s) + \mathcal{O}\left(\epsilon^2\right), \\
y(s) &= y^0(s) + \epsilon \hat{y}(s) + \mathcal{O}\left(\epsilon^2\right) = s + \epsilon \hat{y}(s) + \mathcal{O}\left(\epsilon^2\right), \\
\theta(s) &= \theta^0(s) + \epsilon \varphi(s) + \mathcal{O}\left(\epsilon^2\right) = 0 + \epsilon \varphi(s) + \mathcal{O}\left(\epsilon^2\right).
\end{aligned}
$$

99

(a) $a = 0.031$.   (b) $a = 0.0005, 0.001, \ldots, 0.004$.

Figure 7.6: Bifurcation diagrams of λ against D, where $\omega = 0.06$.

Substituting these into (7.4), (7.5) and (7.6), we obtain

$$\epsilon \hat{x}'(s) = \epsilon \varphi(s) + \mathcal{O}\left(\epsilon^2\right), \tag{7.14}$$

$$\epsilon \hat{y}'(s) = 0 + \mathcal{O}\left(\epsilon^2\right), \tag{7.15}$$

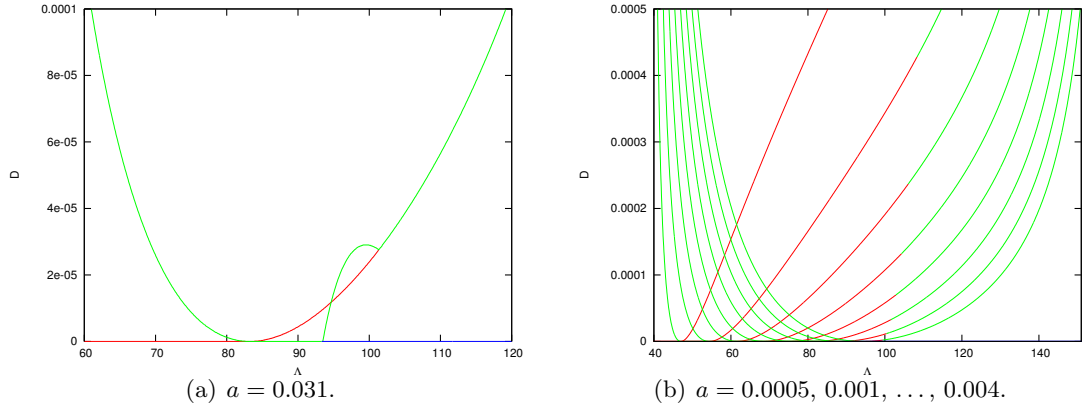$$\epsilon B \varphi''(s) = n_1(s) - \epsilon n_2(s)\varphi(s) + \mathcal{O}\left(\epsilon^2\right). \tag{7.16}$$

Differentiating (7.16), and using (7.14), we get the fourth order differential equation

$$\epsilon B \hat{x}''''(s) + V_x\left(\epsilon \hat{x}(s)\right) + \epsilon \lambda \hat{x}''(s) = 0. \tag{7.17}$$

Now,

$$V_x(\epsilon \hat{x}) = \frac{-12a}{\omega}\left(e^{-12\epsilon \hat{x}/\omega} - e^{-6\epsilon \hat{x}/\omega}\right) = \frac{72\epsilon a \hat{x}}{\omega^2} + \mathcal{O}(\epsilon^2),$$

therefore (7.17) becomes

$$B\hat{x}''''(s) + \lambda \hat{x}''(s) + \frac{72a\hat{x}}{\omega^2} = 0. \tag{7.18}$$

7.3.1   Constrained Buckling of a Clamped-Clamped Rod

We wish to solve (7.18) with clamped boundary conditions, and the constraint of $x(0) = x(L) = 0$, which is equivalent to the conditions

$$\hat{x}(0) = \hat{x}(1) = \hat{x}'(0) = \hat{x}'(1) = 0. \tag{7.19}$$

If $\hat{x}(s)$ has the general solution

$$\hat{x}(s) = \sum_{i=1}^{4} c_i \hat{x}_i(s),$$

then we require

$$\mathcal{A} \begin{pmatrix} c_1 \\ \vdots \\ c_4 \end{pmatrix} := \begin{pmatrix} \hat{x}_1(0) & \cdots & \hat{x}_4(0) \\ \hat{x}_1(L) & \cdots & \hat{x}_4(L) \\ \hat{x}_1'(0) & \cdots & \hat{x}_4'(0) \\ \hat{x}_1'(L) & \cdots & \hat{x}_4'(L) \end{pmatrix} \begin{pmatrix} c_1 \\ \vdots \\ c_4 \end{pmatrix} = 0,$$

which can only be true if $|\mathcal{A}| = 0$.

Let

$$\mu_{1,2}^2 = \frac{-\lambda \pm \sqrt{\lambda^2 - 288aB/\omega^2}}{2B},$$

then depending on the sign of μ_i^2, the expression for determinant of $\mathcal{A}$ takes the following forms:

Case 1: μ_1 and μ_2 are real

Then

$$\mathcal{A} = \begin{pmatrix} 1 & 1 & 1 & 1 \\ e^{\mu_1} & e^{-\mu_1} & e^{\mu_2} & e^{-\mu_2} \\ \mu_1 & -\mu_1 & \mu_2 & -\mu_2 \\ \mu_1 e^{\mu_1} & -\mu_1 e^{-\mu_1} & \mu_2 e^{\mu_2} & -\mu_2 e^{-\mu_2} \end{pmatrix},$$

and

$$|\mathcal{A}| = 8\mu_1\mu_2 \left(\cosh \mu_1 \cosh \mu_2 - 1 \right) - 4 \left(\mu_1^2 + \mu_2^2 \right) \sinh \mu_1 \sinh \mu_2 = 0. \qquad (7.20)$$

Case 2: μ_1 and μ_2 are imaginary

Then

$$\mathcal{A} = \begin{pmatrix} 1 & 0 & 1 & 0 \\ \cos \nu_1 & \sin \nu_1 & \cos \nu_2 & \sin \nu_2 \\ 0 & \nu_1 & 0 & \nu_2 \\ -\nu_1 \sin \nu_1 & \nu_1 \cos \nu_1 & -\nu_2 \sin \nu_2 & \nu_2 \cos \nu_2 \end{pmatrix},$$

and

$$|\mathcal{A}| = \nu_1\nu_2 \left(\cos \nu_1 - \cos \nu_2 \right)^2 + \left(\nu_1 \sin \nu_1 - \nu_2 \sin \nu_2 \right) \left(\nu_2 \sin \nu_1 - \nu_1 \sin \nu_2 \right) = 0, \qquad (7.21)$$

where

$$\nu_{1,2}^2 = \frac{\lambda \mp \sqrt{\lambda^2 - 288aB/\omega^2}}{2B}.$$

Case 3: μ_1 is real and μ_2 is imaginary

Then

$$\mathcal{A} = \begin{pmatrix} 1 & 1 & 1 & 0 \\ e^{\mu_1} & e^{-\mu_1} & \cos\nu_2 & \sin\nu_2 \\ \mu_1 & -\mu_1 & 0 & \nu_2 \\ \mu_1 e^{\mu_1} & -\mu_1 e^{-\mu_1} & -\nu_2\sin\nu_2 & \nu_2\cos\nu_2 \end{pmatrix},$$

and

$$|\mathcal{A}| = 4\mu_1\nu_2\left(1 - \cosh\mu_1\cos\nu_2\right) + 2\left(\mu_1^2 - \nu_2^2\right)\sinh\mu_1\sin\nu_2 = 0. \qquad (7.22)$$

Case 4: $\lambda^2 < 288aB/\omega^2$

Let $\mu_{1,2} = u \pm iv$, then

$$\mathcal{A} = \begin{pmatrix} 0 & 0 & 1 & 1 \\ e^u\sin v & e^{-u}\sin v & e^u\cos v & e^{-u}\cos v \\ v & v & u & -u \\ e^u(u\sin v + v\cos v) & e^{-u}(-u\sin v + v\cos v) & e^u(u\cos v - v\sin v) & e^{-u}(-u\cos v - v\sin v) \end{pmatrix},$$

and

$$|\mathcal{A}| = 2v^2\left(\cosh 2u - 1\right) + 4u^2\left(\cos^2 v - 1\right) = 0. \qquad (7.23)$$
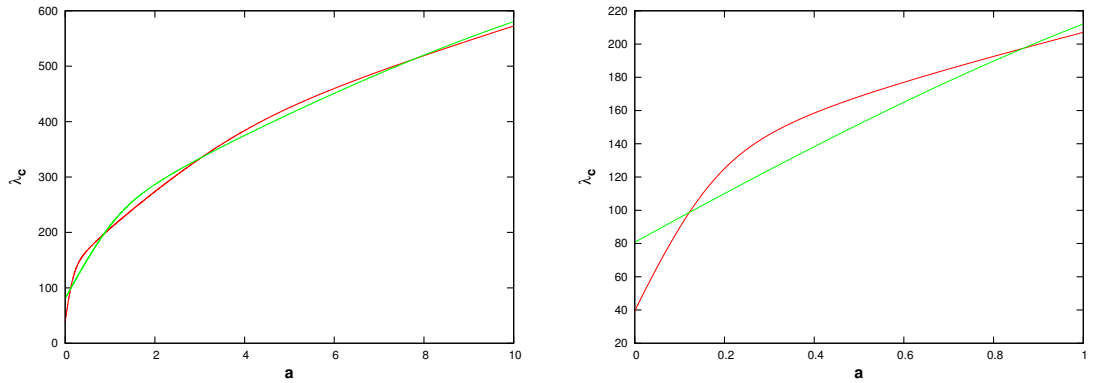
Figure 7.7: First and second buckling points of λ with respect to a, where $\omega = 0.1$ and $B = 1$. The red curve represents values of λ when the straight rod buckles into the first buckling mode. The green curve represents values of λ when the straight rod buckles into the second buckling mode.

Figure 7.7 shows the first two critical buckling values of λ as a is varied and $\omega = 0.1$. As we would expect, the stability of the unbuckled rod is proportional to the strength of

the surface interaction. By that we mean that the two buckling values both increase as a is increased. However, these two curves representing the first two branch points along the trivial solution branch, intersect and cross paths at various values of a, as λ is varied. The left subfigure shows that for $0.122 < a < 0.865$, as λ is increased, the rod buckles first into the branch of second-mode solutions, and secondly into the branch of first-mode solutions. This was observed in the previous section, in figure 7.3. This kind of buckling behaviour is also observed in [20], in which branch points along the trivial branch (for the case of three-dimensional rods) are followed with respect to the parameters λ and the end rotation ϕ.

Using the results from figure 7.7, we find critical buckling values of the end force for various values of the Young's modulus of the nanotube. Table 7.1 shows critical buckling values for a nanotube of length of 30nm and radius of 3nm, and table 7.2 shows critical buckling values for a nanotube of length of 50nm and radius of 5nm. In each table, the values of the binding force between the surface and the nanotube are based on results given in [17], with values of the Young's modulus ranging from 100nN/nm^2 to 1000nN/nm^2.

Young's Modulus	First Critical λ	Second Critical λ
1000 nN/nm^2	4430 nN	7511 nN
500 nN/nm^2	2641 nN	3875 nN
250 nN/nm^2	1714 nN	2055 nN
100 nN/nm^2	1075 nN	965 nN

Table 7.1: Critical buckling values of λ, for a nanotube of length 30nm and radius 3nm. The tube-surface interaction force is 1.6nN. The bending stiffness is given by B=Yr^4, where Y is the Young's modulus and r is the radius, and ω is given by r/L.

7.3.2   Unconstrained Buckling of a Clamped-Clamped Rod

In the unconstrained case, we replace the boundary condition $x(L) = 0$, with the condition $n_1(L) = 0$. To find buckling values for λ, solve (7.18) with the boundary conditions

$$\hat{x}(0) = \hat{x}'(0) = \hat{x}'(L) = \hat{x}'''(L) = 0. \tag{7.24}$$

103

Young's Modulus	First Critical λ	Second Critical λ
1000 nN/nm^2	12048 nN	20788 nN
500 nN/nm^2	7074 nN	10687 nN
250 nN/nm^2	4549 nN	5641 nN
100 nN/nm^2	2410 nN	2607 nN

Table 7.2: Critical buckling values of λ, for a nanotube of length 50nm and radius 5nm. The tube-surface interaction force is 4nN. The bending stiffness is given by B=Yr^4, where Y is the Young's modulus and r is the radius, and ω is given by r/L.

We now find the determinant of the matrix $\mathcal{B}$ to be zero, where

$$
\mathcal{B} \left(\begin{array}{c} c_1 \\ \vdots \\ c_4 \end{array} \right) := \left(\begin{array}{ccc} \hat{x}_1(0) & \cdots & \hat{x}_4(0) \\ \hat{x}'_1(L) & \cdots & \hat{x}'_4(L) \\ \hat{x}'_1(0) & \cdots & \hat{x}'_4(0) \\ \hat{x}'''_1(L) & \cdots & \hat{x}'''_4(L) \end{array} \right) \left(\begin{array}{c} c_1 \\ \vdots \\ c_4 \end{array} \right) = 0. \tag{7.25}
$$

The general solution of $\hat{x}(s)$ has been found in the previous section, so we are able to find the critical buckling values of λ with respect to a, by numerical parameter continuation.

Figure 7.8: First and second buckling points of λ with respect to a, for an unconstrained, clamped-clamped rod, where $\omega = 0.1$ and $B = 1$.

7.3.3 Unconstrained Buckling of a Clamped-Free Rod

In the case of an unconstrained rod, which is clamped at one end and able to move freely at the other end, we replace the condition $\theta(L) = 0$, with the condition $\theta'(L) = 0$.

To find buckling values for λ, solve (7.18) with the boundary conditions

$$\hat{x}(0) = \hat{x}'(0) = \hat{x}''(L) = 0, \quad B\hat{x}'''(L) + \lambda\hat{x}'(L) = 0. \tag{7.26}$$

We now find the determinant of the matrix $\mathcal{C}$ to be zero, where

$$\mathcal{C}\begin{pmatrix} c_1 \\ \vdots \\ c_4 \end{pmatrix} := \begin{pmatrix} \hat{x}_1(0) & \cdots & \hat{x}_4(0) \\ \hat{x}_1''(L) & \cdots & \hat{x}_4''(L) \\ \hat{x}_1'(0) & \cdots & \hat{x}_4'(0) \\ B\hat{x}_1'''(L) + \lambda\hat{x}_1'(L) & \cdots & B\hat{x}_4'''(L) + \lambda\hat{x}_4'(L) \end{pmatrix} \begin{pmatrix} c_1 \\ \vdots \\ c_4 \end{pmatrix} = 0. \tag{7.27}$$

Figures 7.8 and 7.9 show the first and second critical values of λ with respect to a, for
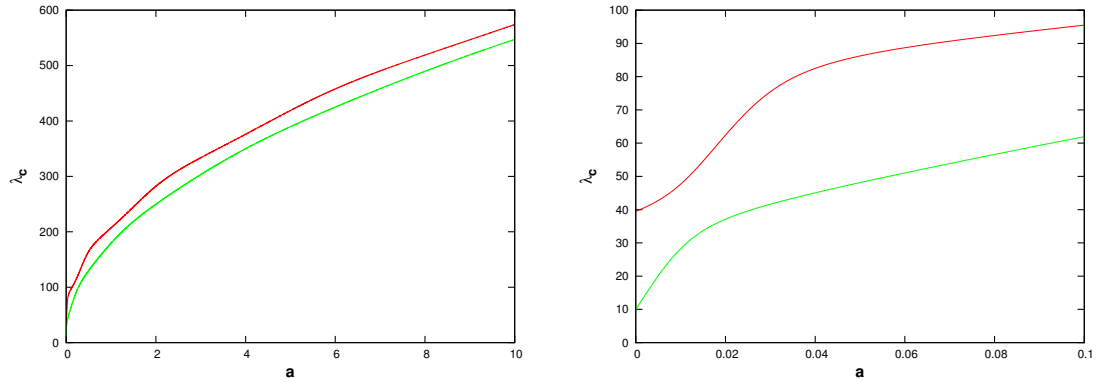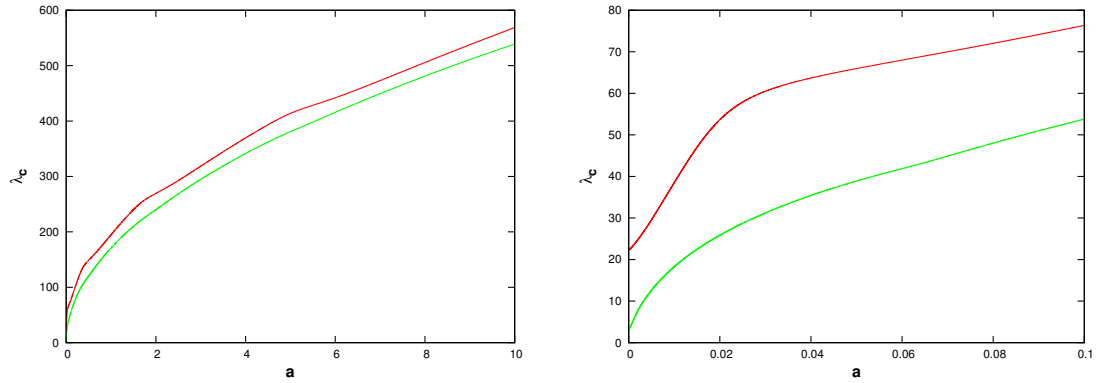

Figure 7.9: First and second buckling points of λ with respect to a, for an unconstrained, clamped-free rod, where $\omega = 0.1$ and $B = 1$.

an unconstrained clamped-clamped rod, and an unconstrained clamped-free rod respectively. In both cases, critical buckling values of λ increase as a is increased. However, unlike in the constrained case, the curves of the first and second branch points along the trivial branch do not intersect and cross paths as a is varied.

7.4   Discontinuous Bending Stiffness

In this section, we extend the model to incorporate a discontinuity in the bending stiffness B. Consider an elastic rod of length L, with a discontinuity in the bending stiffness at $s = L_1$, and let $L = L_1 + L_2$. Let $\theta_1 : [0, L_1] \to \mathbb{R}$ and $\theta_2 : [L_1, L] \to \mathbb{R}$ describe the angle that the tangent to the centreline makes with the vertical y-axis on

each partition of the rod, and let $x_i'(s) = \sin\theta_i$, and $y_i'(s) = \cos\theta_i$, for $i = 1, 2$. We seek solutions of continuous θ, so impose the condition $\theta_1(L_1) = \theta_2(L_1)$.

The total energy is given by

$$
\begin{aligned}
E[\theta_1, \theta_2] &= \int_0^{L_1} \frac{1}{2} B_1 \left(\theta_1'(s)\right)^2 + \lambda\cos\theta_1(s) + V\left(x_1(s)\right) \, \mathrm{d}s \\
&+ \int_{L_1}^{L} \frac{1}{2} B_2 \left(\theta_2'(s)\right)^2 + \lambda\cos\theta_2(s) + V\left(x_2(s)\right) \, \mathrm{d}s
\end{aligned}
$$

Equilibrium Equations

The first variation of $E[\theta_1, \theta_2]$ is given by

$$
\begin{aligned}
\delta E[h_1, h_2] &= \int_0^{L_1} \left[h_1(s)\left(-B_1\theta_1''(s) - \lambda\sin\theta_1(s)\right) + \delta x_1 V_{x_1}(s) \right] \, \mathrm{d}s \\
&+ \int_{L_1}^{L} \left[h_2(s)\left(-B_2\theta_2''(s) - \lambda\sin\theta_2(s)\right) + \delta x_2 V_{x_2}(s) \right] \, \mathrm{d}s \\
&+ B_1 h_1\left(L_1\right)\theta_1'\left(L_1\right) - B_2 h_2\left(L_1\right)\theta_2'\left(L_1\right), \tag{7.28}
\end{aligned}
$$

where

$$
x_1(s) = \int_0^s \sin\theta_1(\tau) \, \mathrm{d}\tau, \quad x_2(s) = \int_L^s \sin\theta_2(\tau) \, \mathrm{d}\tau,
$$

and

$$
\delta x_1 = \int_0^s \cos\theta_1(\tau) h_1(\tau) \, \mathrm{d}\tau, \quad \delta x_2 = \int_L^s \cos\theta_2(\tau) h_2(\tau) \, \mathrm{d}\tau.
$$

Substituting these expressions into (7.28), and using the boundary conditions

$$
h_1(L_1) = h_2(L_1), \quad B_1\theta_1'(L_1) = B_2\theta_2'(L_1),
$$

the first variation becomes

$$
\begin{aligned}
\delta E &= \int_0^{L_1} h_1(s)\left(-B_1\theta_1''(s) - \lambda\sin\theta_1(s)\right) \, \mathrm{d}s + \int_0^{L_1}\int_0^s \cos\theta_1(\tau) h_1(\tau) V_{x_1}(s) \, \mathrm{d}\tau \, \mathrm{d}s \\
&+ \int_{L_1}^{L} h_2(s)\left(-B_2\theta_2''(s) - \lambda\sin\theta_2(s)\right) \, \mathrm{d}s + \int_{L_1}^{L}\int_L^s \cos\theta_2(\tau) h_2(\tau) V_{x_2}(s) \, \mathrm{d}\tau \, \mathrm{d}s
\end{aligned}
$$

Using (7.2), it can be shown that

$$
\begin{aligned}
\delta E &= \int_0^{L_1} h_1(s)\left(-B_1\theta_1''(s) - \lambda\sin\theta_1(s) + \cos\theta_1(s)\int_s^{L_1} V_{x_1}(\tau) \, \mathrm{d}\tau\right) \, \mathrm{d}s \\
&+ \int_{L_1}^{L} h_2(s)\left(-B_2\theta_2''(s) - \lambda\sin\theta_2(s) + \cos\theta_2(s)\int_s^{L_1} V_{x_2}(\tau) \, \mathrm{d}\tau\right) \, \mathrm{d}s.
\end{aligned}
$$

The constraint, $x_1(0) = x_2(L) = 0$, and continuity condition $x_1(L_1) = x_2(L_1)$ implies the isoperimetric constraint

$$\int_0^{L_1} \sin\theta_1(s)\ \mathrm{d}s + \int_{L_1}^{L} \sin\theta_2(s)\ \mathrm{d}s = 0.$$

The linearised isoperimetric constraint is

$$\int_0^{L_1} \cos\theta_1(s)h_1(s)\ \mathrm{d}s + \int_{L_1}^{L} \cos\theta_2(s)h_2(s)\ \mathrm{d}s = 0.$$

If $\delta E = 0$ for all h_1 and h_2 then, adding the Lagrange multiplier term, we get

$$-B_1\theta_1''(s) - \lambda\sin\theta_1(s) - \mu\cos\theta_1(s) + \cos\theta_1(s)\int_s^{L_1} V_x(\tau)\ \mathrm{d}\tau = 0,$$

$$-B_2\theta_2''(s) - \lambda\sin\theta_2(s) - \mu\cos\theta_2(s) + \cos\theta_2(s)\int_s^{L_1} V_x(\tau)\ \mathrm{d}\tau = 0.$$

If we define

$$\boldsymbol{n}_i := \left(\begin{array}{c} n_{1i} \\ n_{2i} \end{array}\right) = \left(\begin{array}{c} \int_s^{L_1} V_{x_i}(\tau)\ \mathrm{d}\tau \\ 0 \end{array}\right) + \left(\begin{array}{c} -\mu \\ \lambda \end{array}\right), \quad i = 1, 2, \tag{7.29}$$

then the equilibrium equations are

$$B_i\theta_i''(s) = n_{1i}\cos\theta_i(s) - n_{2i}\sin\theta_i(s), \quad i = 1, 2.$$

Stability Equations

The second variation is given by

$$
\begin{aligned}
\delta^2 E[h_1, h_2] = \quad & \frac{1}{2}\int_0^{L_1} h_1(s)\left(-B_1 h_1''(s) - \lambda\cos\theta_1(s)h_1(s) + \mu\sin\theta_1(s)h_1(s)\right)\ \mathrm{d}s \\
+ \quad & \frac{1}{2}\int_{L_1}^{L} h_2(s)\left(-B_2 h_2''(s) - \lambda\cos\theta_2(s)h_2(s) + \mu\sin\theta_2(s)h_2(s)\right)\ \mathrm{d}s \\
+ \quad & R_1[h]\ +\ R_2[h],
\end{aligned}
$$

where

$$
\begin{aligned}
R_1[h_1, h_2] = \quad & \frac{1}{2}\int_0^{L_1}\int_0^{s} -h_1(\tau)^2 \sin\theta_1(\tau)V_x(s)\ \mathrm{d}\tau\ \mathrm{d}s \\
+ \quad & \frac{1}{2}\int_{L_1}^{L}\int_L^{s} -h_2(\tau)^2 \sin\theta_2(\tau)V_x(s)\ \mathrm{d}\tau\ \mathrm{d}s,
\end{aligned}
$$

and

$$R_2[h_1, h_2] = \frac{1}{2} \int_0^{L_1} \int_0^s \int_0^s h_1(\kappa) \cos \theta_1(\kappa) h_1(\tau) \cos \theta_1(\tau) V_{xx}(s) \, d\kappa \, d\tau \, ds$$

$$+ \frac{1}{2} \int_{L_1}^L \int_L^s \int_L^s h_2(\kappa) \cos \theta_2(\kappa) h_2(\tau) \cos \theta_2(\tau) V_{xx}(s) \, d\kappa \, d\tau \, ds.$$

Again, using (7.2), we can express R_1 and R_2 as follows:

$$R_1 = \frac{1}{2} \int_0^{L_1} \int_s^{L_1} -h_1(s)^2 \sin \theta_1(s) V_x(\tau) \, d\tau \, ds$$

$$+ \frac{1}{2} \int_{L_1}^L \int_s^{L_1} -h_2(s)^2 \sin \theta_2(s) V_x(\tau) \, d\tau \, ds, \tag{7.30}$$

and

$$R_2 = \frac{1}{2} \int_0^{L_1} h_1(s) \left[\cos \theta_1(s) \int_s^{L_1} F_1(\kappa) \, d\kappa \right] ds$$

$$+ \frac{1}{2} \int_{L_1}^L h_2(s) \left[\cos \theta_2(s) \int_s^{L_1} F_2(\kappa) \, d\kappa \right] ds, \tag{7.31}$$

where

$$F_1(\kappa) = V_{xx}(\kappa) \int_0^\kappa h(\tau) \cos \theta_1(\tau) \, d\tau = V_{xx}(\kappa) z_1(\kappa),$$

$$F_2(\kappa) = V_{xx}(\kappa) \int_L^\kappa h(\tau) \cos \theta_2(\tau) \, d\tau = V_{xx}(\kappa) z_2(\kappa),$$

and where

$$z_1'(s) = h_1(s) \cos \theta_1(s), \quad z_1(0) = 0,$$

$$z_2'(s) = h_2(s) \cos \theta_2(s), \quad z_2(L) = 0.$$

The second variation now becomes

$$\delta^2 E = \frac{1}{2} \int_0^{L_1} h_1 \left[-B_1 h_1'' - h_1 \sin \theta_1 \left(\int_s^{L_1} V_x(\tau) \, d\tau - \mu \right) - \lambda h_1 \cos \theta_1 + \psi_1 \cos \theta_1 \right] ds$$

$$+ \frac{1}{2} \int_{L_1}^L h_2 \left[-B_2 h_2'' - h_2 \sin \theta_2 \left(\int_s^{L_1} V_x(\tau) \, d\tau - \mu \right) - \lambda h_2 \cos \theta_2 + \psi_2 \cos \theta_2 \right] ds,$$

where

$$\psi_1'(s) = -F_1(s) = -V_{xx}(s) z_1(s), \quad \psi_1(L_1) = 0,$$

$$\psi_2'(s) = -F_2(s) = -V_{xx}(s) z_2(s), \quad \psi_2(L_1) = 0.$$

From the definition of $\boldsymbol{n}_1$ and $\boldsymbol{n}_2$ we get

$$
\delta^2 E = \frac{1}{2} \int_0^{L_1} h_1 \left[-B_1 h_1'' - h_1 \left(n_{11} \sin \theta_1 + n_{21} \cos \theta_1 \right) + \psi_1 \cos \theta_1 \right] \, \mathrm{d}s
$$
$$
+ \frac{1}{2} \int_{L_1}^{L} h_2 \left[-B_2 h_2'' - h_2 \left(n_{12} \sin \theta_2 + n_{22} \cos \theta_2 \right) + \psi_2 \cos \theta_2 \right] \, \mathrm{d}s.
$$

The second variation can be written as

$$
\delta^2 E = \frac{1}{2} \left\langle \mathcal{S}_1 h_1, h_1 \right\rangle_1 + \frac{1}{2} \left\langle \mathcal{S}_2 h_2, h_2 \right\rangle_2,
$$

where

$$
\mathcal{S}_i h \equiv -B_i h'' - h \left(n_{1i} \sin \theta_i + n_{2i} \cos \theta_i \right) + \psi_i \cos \theta_i, \quad i = 1 \cdots 2,
$$

and $\langle \cdot, \cdot \rangle_1$ denotes the standard L^2 inner product in the region $[0, L_1]$, and $\langle \cdot, \cdot \rangle_2$ denotes the standard L^2 inner product in the region $[L_1, L]$.

The full system of equations for the rod equilibrium and rod stability is therefore

$$
\begin{aligned}
x_i'(s) &= \sin \theta_i \\
y_i'(s) &= \cos \theta_i \\
B_i \theta_i''(s) &= n_{1i} \cos \theta_i - n_{2i} \sin \theta_i \\
n_{1i}'(s) &= -V_x(x_i) \\
n_{2i}'(s) &= 0 \\
B_i h_i''(s) &= -h_i \left(n_{1i} \sin \theta_i + n_{2i} \cos \theta_i \right) + \psi_i \cos \theta_i - T_i \\
z_i'(s) &= y_i' h_i \\
\psi_i'(s) &= -V_{xx}(x_i) z_i
\end{aligned}
$$

for $i = 1, 2$, where $T_i = \cos \theta_i$, with boundary conditions

$$
x_1(0) = 0, \quad y_1(0) = 0, \quad \theta_1(0) = 0, \quad h_1(0) = 0, \quad z_1(0) = 0,
$$
$$
x_2(L) = 0, \quad n_{22}(L) = \lambda, \quad \theta_2(L) = 0, \quad h_2(L) = 0, \quad z_2(L) = 0,
$$

and matching conditions

$$
x_1(L_1) = x_2(L_1), \quad y_1(L_1) = y_2(L_1), \quad \theta_1(L_1) = \theta_2(L_1), \quad B_1 \theta_1'(L_1) = B_2 \theta_2'(L_1),
$$
$$
n_{11}(L_1) = n_{12}(L_1), \quad n_{21}(L_1) = n_{22}(L_1), \quad h_1(L_1) = h_2(L_1), \quad B_1 h_1'(L_1) = B_2 h_2'(L_1),
$$
$$
\psi_1(L_1) = 0, \quad \psi_2(L_1) = 0.
$$

Recall from chapter 4, the dimensionless parameters

$$\beta = \frac{B_2}{B_1}, \quad \gamma = \frac{L_1}{L},$$

and introduce the dimensionless arclength

$$t = \begin{cases} \frac{s}{L_1} & 0 \le s \le L_1 \\ \frac{s}{L_2} + \left(\frac{1-2\gamma}{1-\gamma}\right) & L_1 \le s \le L \end{cases}.$$

Now, introduce the dimensionless variables

$$X_i = \frac{x_i}{L}, \quad Y_i = \frac{y_i}{L}, \quad Z_i = \frac{z_i}{L}, \quad \Omega = \frac{\omega}{L},$$

$$\Psi_i = \frac{L^2 \psi_i}{B_1}, \quad N_{ij} = \frac{L^2 n_{ij}}{B_1}, \quad A = \frac{L^2 a}{B_1}, \quad \Lambda = \frac{L^2 \lambda}{B_1}.$$

Now we can write down the dimensionless system of rod and stability equations.

For $0 \le t \le 1$:

$$\dot{X}_1(t) = \gamma \sin\theta_1$$

$$\dot{Y}_1(t) = \gamma \cos\theta_1$$

$$\ddot{\theta}_1(t) = \gamma^2 \left[N_{11} \cos\theta_1 - N_{21} \sin\theta_1\right]$$

$$\dot{N}_{11}(t) = \gamma \frac{12A}{\Omega} \left[e^{-12X_1/\Omega} - e^{-6X_1/\Omega}\right]$$

$$\dot{N}_{21}(t) = 0$$

$$\ddot{h}_1(t) = \gamma^2 \left[\Psi_1 \cos\theta_1 - h_1 \left(N_{11} \sin\theta_1 + N_{21} \cos\theta_1\right)\right]$$

$$\dot{Z}_1(t) = \dot{Y}_1 h_1$$

$$\dot{\Psi}_1(t) = -\gamma \frac{12A}{\Omega^2} \left[12 e^{-12X_1/\Omega} - 6 e^{-6X_1/\Omega}\right] Z_1.$$

For $1 \leq t \leq 2$:

$$
\begin{aligned}
\dot{X}_2(t) &= (1 - \gamma) \sin \theta_2 \\
\dot{Y}_2(t) &= (1 - \gamma) \cos \theta_2 \\
\beta \ddot{\theta}_2(t) &= (1 - \gamma)^2 \left[N_{12} \cos \theta_2 - N_{22} \sin \theta_2 \right] \\
\dot{N}_{12}(t) &= (1 - \gamma) \frac{12A}{\Omega} \left[e^{-12X_2/\Omega} - e^{-6X_2/\Omega} \right] \\
\dot{N}_{22}(t) &= 0 \\
\beta \ddot{h}_2(t) &= (1 - \gamma)^2 \left[\Psi_2 \cos \theta_2 - h_2 \left(N_{12} \sin \theta_2 + N_{22} \cos \theta_2 \right) \right] \\
\dot{Z}_2(t) &= \dot{Y}_2 h_2 \\
\dot{\Psi}_2(t) &= -(1 - \gamma) \frac{12A}{\Omega^2} \left[12 e^{-12X_2/\Omega} - 6 e^{-6X_2/\Omega} \right] Z_2,
\end{aligned}
$$

with boundary conditions

$$
X_1(0) = 0, \quad Y_1(0) = 0, \quad \theta_1(0) = 0, \quad h_1(0) = 0, \quad Z_1(0) = 0,
$$

$$
X_2(2) = 0, \quad N_{22}(2) = \Lambda, \quad \theta_2(2) = 0, \quad h_2(2) = 0, \quad Z_2(2) = 0,
$$

and matching conditions

$$
X_1(1) = X_2(1), \quad Y_1(1) = Y_2(1), \quad \theta_1(1) = \theta_2(1), \quad \dot{\theta}_1(1) = \tfrac{\gamma}{1-\gamma} \beta \dot{\theta}_2(1),
$$

$$
N_{11}(1) = N_{12}(1), \quad N_{21}(1) = N_{22}(1), \quad h_1(1) = h_2(1), \quad \dot{h}_1(1) = \tfrac{\gamma}{1-\gamma} \beta \dot{h}_2(1),
$$

$$
\Psi_1(1) = 0, \quad \Psi_2(1) = 0.
$$

Alternative dimensionless variables could occur from scaling s by L instead of L_1 and L_2. This would give a simpler expression for the equations and matching conditions. However, we will solve the rod equilibrium equations as a boundary value problem numerically in AUTO97 [11], which solves over a fixed interval of length 1, therefore the dimensionless variables used here are computationally more convenient.

We find that it is computationally more effective to solve the stability equations as an initial value problem. Therefore we will replace the boundary conditions at $s = L$, with equivalent conditions at $s = L_1$, then to find the conjugate points, solve two IVPs - the first over $[0, L_1]$, and the second over $[L_1, L]$.

Using the isoperimetric constraint

$$\int_0^L h \cos\theta(s) \; \mathrm{d}s \; = \; \int_0^{L_1} h_1 \cos\theta_1(s) \; \mathrm{d}s \; + \; \int_{L_1}^L h_2 \cos\theta_2(s) \; \mathrm{d}s \; = \; 0,$$

we can rewrite equation (7.31) as

$$
\begin{aligned}
R_2[h] \; = \;\; & \frac{1}{2}\int_0^{L_1} h_1(s)\cos\theta_1(s) \left[\int_0^s -F_1(\kappa)\;\mathrm{d}\kappa\right] \mathrm{d}s \\
& + \; \frac{1}{2}\int_{L_1}^L h_2(s)\cos\theta_2(s) \left[\int_0^{L_1} -F_1(\kappa)\;\mathrm{d}\kappa + \int_{L_1}^s -F_2(\kappa)\;\mathrm{d}\kappa\right] \mathrm{d}s,
\end{aligned}
$$

and therefore use initial conditions for $\psi_1(s)$ and $\psi_2(s)$,

$$\psi_1(0) = 0, \quad \psi_2(L_1) = \psi_1(L_1).$$

We can also write an alternative form for $\delta x_2(s)$ as

$$\delta x_2(s) \; = \; \int_0^{L_1} h_1 \cos\theta_1(s) \; \mathrm{d}s \; + \; \int_{L_1}^s h_2 \cos\theta_2(s) \; \mathrm{d}s,$$

which we can use to replace the boundary condition for z_2 at L with the matching condition

$$z_2(L_1) = z_1(L_1).$$

7.5 Numerical Results

The presence of a discontinuity in the bending stiffness causes the branch of second-mode solutions to split into two distinct branches, which connect to the branches of the first- and third-mode solution branches. Subfigure (b) shows that for $\beta = 2$, a stable region of the second-mode solution branch exists, which is not the case when $\beta = 1$, shown in subfigure (a). This stable region is not a solely consequence of increasing β from 1 however. It also is due to the property discussed in section 7.3, that the order of buckling (with respect to Λ) between the first- and second-mode solution branches, continuously interchanges as A is increased.
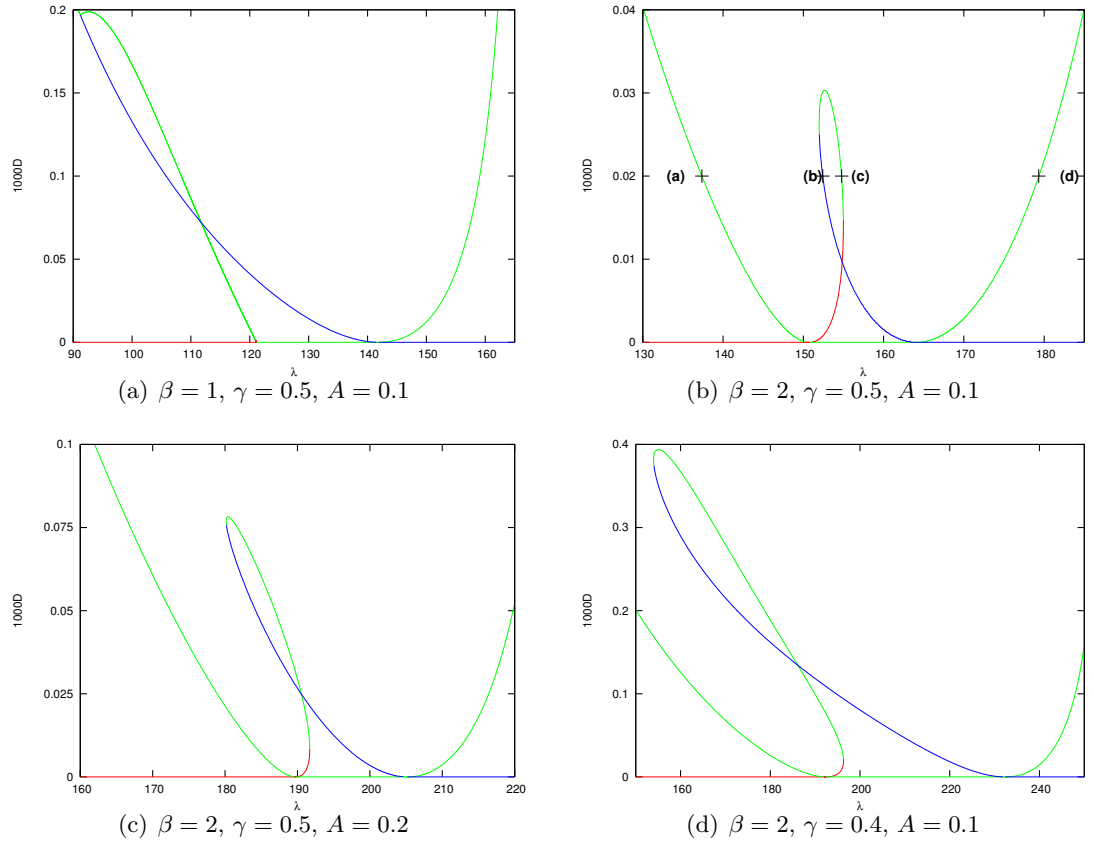
(a) $\beta = 1$, $\gamma = 0.5$, $A = 0.1$

(b) $\beta = 2$, $\gamma = 0.5$, $A = 0.1$

(c) $\beta = 2$, $\gamma = 0.5$, $A = 0.2$

(d) $\beta = 2$, $\gamma = 0.4$, $A = 0.1$

Figure 7.10: Bifurcation diagrams of Λ against D, with $\Omega = 0.06$.

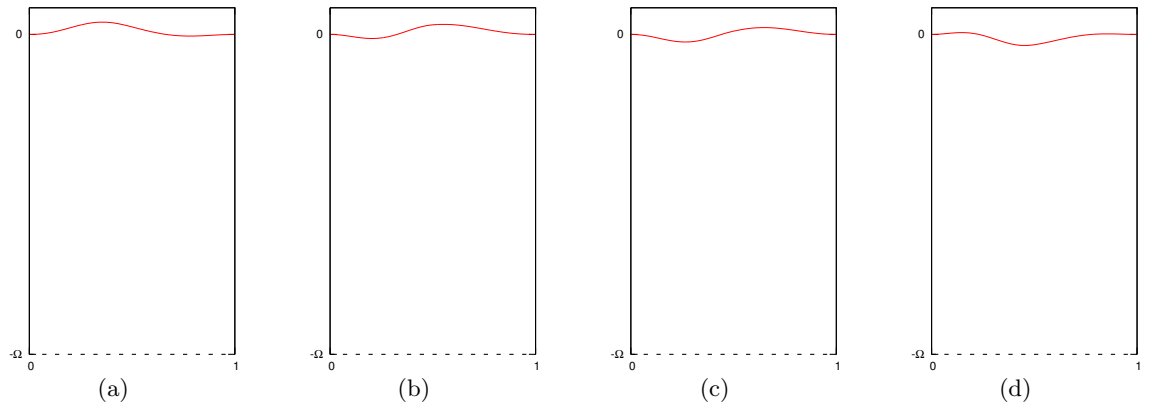(a)   (b)   (c)   (d)

Figure 7.11: Rod shapes at the points indicated in figure 7.10.

Chapter 8

Conclusion

We have used the calculus of variations to analyse the stability of elastic rods. The classic Jacobi condition was extended to account for functionals with discontinuous integrands. It was shown that given the continuity of $W_{\mathbf{q'q'}}\mathbf{h}'(s) + W_{\mathbf{q'q}}\mathbf{h}(s)$, along with the strenthened Legendre condition holding in each interval, the Jacobi condition still holds. This result agrees with Cole [7], who also showed that the stability index for discontinuous systems can be found by counting the conjugate points, as long as this second order continuity condition still holds. We note that since the Jacobi operator for the discontinuous system has the same spectral properties as in the continuous system (e.g. it is regular and self-adjoint), we were able to follow Rogers [36] and extend the definition of an index to cases with isoperimetric constraints.

The extended conjugate point theory was used to analyse the stability of novel rod configurations. Cosserat rod theory has been applied to model carbon nanotubes with three distinct characteristics, those which have a jump in the cross-section shape (modelled by a jump in bending stiffness); those which have a kink (modelled by a jump in curvature), and rods lying on a surface that are influenced by surface van der Waals forces (modelled by adding a potential energy field to the total energy functional).

For the kinked and surface nanotube models, extensions to three-dimensional rod solutions would be relatively straightforward, where the applications to the modelling of kinked DNA helices or kinked submarine cables, would benifit (see, e.g. [44],[10]). Another characteristic of nanotubes not considered in this thesis, is the self-interaction

of the tube caused by van der Waals forces. Hoffman and Manning [19] study the stability of a planar rod with a repulsive self-potential. The stability theory established in [19] could potentially be used with the kinked or surface nanotube models here, to create a more robust nanotube model. A further extension would be to model chiral nanotubes as elastic rods with an intrinsic twist. A nanotube is called chiral if its atoms lie on helices along the tube surface. More specifically, one could model a nanotube junction where two tubes of different chiralities are bound together, by an elastic rod with a discontinuous intrinsic twist.

For rods with discontinuous bending stiffness, expressions for the critical buckling load were found in terms of the load parameter and the bending stiffnesses, for the case of a rod buckling under pure end compression. When the problem was reduced to the case of continuous bending stiffness, our results agreed with critical buckling values found in [39] and [40]. When one stiffness parameter (acting on the partition $[0, L_1] \subset [0, L]$) was increased towards infinity, numerical observations confirmed the intuitive result, that the critical buckling value tends to the critical value for a rod of length $L - L_1$. In other words, the partition $[0, L_1]$ acts like a clamped boundary condition to the partition $[L_1, L]$.

Bifurcation diagrams of post-buckled rod solutions were computed for planar and three-dimensional rod configurations. In the planar case, we found that a jump in the bending stiffness can actually have a stabilising influence on the class of looped $(D > 1)$ first-mode rod solutions, which are otherwise unstable (with index 1) when the bending stiffness is continuous. The critical value of the bending stiffness ratio β, for which this stable region exists, was found by numerically following the limit points (the local maximum and local minimum of λ), for varying values of β (see figure 4.5). For a rod with $\gamma = 0.5$, this critical value was found to be $\beta = 2.23$. Equivalent critical values of γ were also found for various fixed values of β.

The extension of conjugate point theory to incorporate Neumann boundary conditions is a relatively recent one. Manning, in [27] constructs an extended definition of the stability index, and applies the theory to a planar rod with pinned boundary conditions.

In this thesis, we made the extension to three-dimensional rod solutions. Sign properties of the inborn eigenvalues were found analytically, for solutions of unbuckled and buckled pinned end rods. Velocities of the zero eigenvalues were found by extending the method used in [27] for planar rods, giving us all the information necessary to find the index for three-dimensional rods with pinned ends. Post-buckling stability analysis was performed for pinned end rods. However, there still remains room for the study of more complex and realistic rod configurations in this class of Neumann boundary value problems.

Kinked rod solutions were computed for both unconstrained and constrained clamped end problems. In the unconstrained case, the presence of a kink causes a breaking of symmetry of even-mode solutions, so the solution branches split into two distinct branches. The odd-mode solution branches are still double covered, and bifurcate from the even-mode branches at branch points, causing the stability index to decrease by one. If there is a jump in the bending stiffness, or the kink is no longer exactly in the middle of the rod, then the symmetry of all solution branches is broken, and branches of different buckling modes connect at folds, where there is an exchange in the index value. In the constrained case, symmetry is broken in the odd-mode solutions. Even-mode branches bifurcate from the odd-mode branches at branch points. Symmetry of even-mode branches is broken by a jump in bending stiffness, or by altering the kink position. The branch of second-mode solutions split into two branches, one closed branch which is connected to the first-mode solutions by a limit point, and one open branch which is connected to the third-mode solutions by a limit point.

For a rod lying on an interactive surface, stability analysis of unbuckled solutions gives a surprising result in the case of a clamped and constrained rod. As the rod-surface interaction strength a increases, the order of the first and second critical buckling values of the end force λ, continuously changes (see figure 7.7). This kind of buckling behaviour is also seen in [20], where curves representing branch points along the trivial branch are plotted with respect to the twist angle ϕ, and like the case here, these curves are found to intersect and cross paths. In [20], this stability exchange occurs between two branches of the same buckling mode, as an increase in the end rotation effectively transfers the

bending stiffness from one plane to the other. And, at the points of intersection, as one branch is becoming more stable, the other branch is becoming less stable. Here however, the stability exchange occurs between branches of different buckling modes, and both branches are becoming more stable with increasing a. In [20], the index is found on the whole (ϕ, λ) plane of unbuckled equilibria. A nice extension to the stability analysis in chapter 7 would be to find the index on the (a, λ) plane for the unbuckled equilibria. Solutions of first-mode buckling and third-mode buckling bifurcate from the same point, and second-mode solutions bifurcate from either the first- or third-mode solutions, depending on the value of a. The connection between first- and third-mode solutions is not surprising, since as a first-mode solution buckles towards the surface, it naturally deforms into a third-mode solution. As in the kinked model, the second-mode solution branch remains double covered, since the presence of an interactive surface doesn't break the symmetry of the even-mode solutions. Bifurcation diagrams of post-buckled solutions also turn out to have very interesting behaviour. We find stable branches occurring for third-mode rod solutions, in which the end $z(L)$ has passed through $z(0)$ (see figure 7.4(b)).

Bibliography

[1] S. S. Antman, *Nonlinear Problems of Elasticity*, 2nd ed., Applied Mathematical Sciences, no. 107, Springer-Verlag, New York, NY, 1995.

[2] G. A. Bliss and M. Mason, *A problem of the calculus of variations in which the integrand is discontinuous*, Transactions of the American Mathematical Society **9** (1906), 325–336.

[3] O. Bolza, *Lectures of the Calculus of Variations*, Read Books, 2007.

[4] M. J. Buehler, Y. Kong, and H. Gao, *Deformation mechanisms of very long single-wall carbon nanotubes subject to compressive loading*, Journal of Engineering Materials and Technology **126** (2004), 245–300.

[5] J. C. Charlier, *Defects in Carbon Nanotubes*, Accounts of Chemical Research **35** (2002), no. 12, 1063–1069.

[6] N. Chouaieb and J. H. Maddocks, *Kirchhoff's problem of helical equilibria of uniform rods*, Journal of Elasticity **77** (2004), no. 3, 221–247.

[7] N. Cole, *The Index Theorem for a calculus of variations problem in which the integrand is discontinuous*, American Journal of Mathematics (1940), 249–276.

[8] C. Dekker et al., *Carbon nanotubes as molecular quantum wires*, Physics Today **52** (1999), 22–30.

[9] D. J. Dichmann, Y. Li, and J. H. Maddocks, *Hamiltonian formulations and symmetries in rod mechanics*, Mathematical Approaches to Biomolecular Structure and Dynamics **82** (1996), 71–113.

[10] R. E. Dickerson, *Dna bending: the prevalence of kinkiness and the virtues of normality*, Nucleic acids research **26** (1998), no. 8, 1906.

[11] E. J. Doedel, A. R. Champneys, T. F. Fairgrieve, Y. A. Kuznetsov, B. Sandstede, and X. Wang, *AUTO97: Continuation and bifurcation software for ordinary differential equations (with HomCont)*, Computer Science, Concordia University, Montreal, Canada.

[12] I. M. Gelfand and S. V. Fomin, *Calculus of variations*, Prentice Hall, 1963.

[13] V. G. A. Goss, G. H. M. van der Heijden, J. M. T. Thompson, and S. Neukirch, *Experiments on snap buckling, hysteresis and loop formation in twisted rods*, Experimental Mechanics **45** (2005), no. 2, 101–111.

[14] L. M. Graves, *Discontinuous solutions in space problems of the calculus of variations*, American Journal of Mathematics **52** (1930), no. 1, 1–28.

[15] O. Gulseren, T. Yildirim, S. Ciraci, and C. Kılıç, *Reversible band-gap engineering in carbon nanotubes by radial deformation*, Physical Review B **65** (2002), no. 15, 155410.

[16] T. Hertel, R. Martel, and P. Avouris, *Manipulation of individual carbon nanotubes and their interaction with surfaces*, Journal of Physical Chemistry B **102** (1998), no. 6, 910–915.

[17] T. Hertel, R. E. Walkup, and P. Avouris, *Deformation of carbon nanotubes by surface van der Waals forces*, Physical Review B **58** (1998), no. 20, 13870–13873.

[18] A. C. Hindmarsh, *ODEPACK, a systematized collection of ODE solvers*, North-Holland, Amsterdam **1** (1983), 55–64.

[19] K. A. Hoffman and R. S. Manning, *An Extended Conjugate Point Theory with Application to the Stability of Planar Buckling of an Elastic Rod Subject to a Repulsive Self-Potential*, SIAM Journal on Mathematical Analysis **41** (2009), 465–494.

[20] K. A. Hoffman, R. S. Manning, and R. C. Paffenroth, *Calculation of the stability index in parameter dependent calculus of variations problems: buckling of a twisted elastic strut*, SIAM Journal on Applied Dynamical Systems **1** (2002), 115–145.

[21] H. B. Keller, *Numerical solution of bifurcation and non linear eigenvalue problems*, Applications of Bifurcation Theory: Proceedings of an Advanced Seminar, 1997, pp. 359–384.

[22] S. Lijima, *Helical microtubules of graphitic carbon*, Nature **354** (1991), no. 6348, 56–58.

[23] J. Q. Lu, J. Wu, W. Duan, F. Liu, B. F. Zhu, and B. L. Gu, *Metal-to-semiconductor transition in squashed armchair carbon nanotubes*, Physical Review Letters **90** (2003), no. 15, 156601.

[24] J. H. Maddocks, *Stability of nonlinearly elastic rods*, Archive for rational mechanics and analysis **85** (1984), no. 4, 311–354.

[25] J. H. Maddocks, *Restricted quadratic forms and their application to bifurcation and stability in constrained variational principles*, SIAM Journal on Mathematical Analysis **16** (1985), 47–68.

[26] J. H. Maddocks, *Stability and folds*, Archive for Rational Mechanics and Analysis **99** (1987), no. 4, 301–328.

[27] R. S. Manning, *Conjugate points revisited and neumann-neumann problems*, SIAM review **51** (2009), no. 1, 193–212.

[28] R. S. Manning and G. B. Bulman, *Stability of an elastic rod buckling into a soft wall*, Proceedings of the Royal Society A: Mathematical, Physical and Engineering Science **461** (2005), no. 2060, 2423–2450.

[29] R. S. Manning and K. A. Hoffman, *Stability of n-covered circles for elastic rods with constant planar intrinsic curvature*, Journal of Elasticity **62** (2001), no. 1, 1–23.

[30] R. S. Manning and J. H. Maddocks, *Symmetry breaking and the twisted elastic ring*, Computer Methods in Applied Mechanics and Engineering **170** (1999), no. 3-4, 313–330.

[31] R. S. Manning, K. A. Rogers, and J. H. Maddocks, *Isoperimetric conjugate points with application to the stability of DNA minicircles*, Proceedings: Mathematical, Physical and Engineering Sciences **454** (1998), no. 1980, 3047–3074.

[32] M. Morse, *The calculus of variations in the large*, Amer Mathematical Society, 1978.

[33] N. P Osmolovskii, *Quadratic extremality conditions for broken extremals in the general problem of the calculus of variations*, Journal of Mathematical Sciences **123** (2004), no. 3, 3987–4122.

[34] N. P Osmolovskii and F. Lempio, *Jacobi conditions and the Riccati equation for a broken extremal*, Journal of Mathematical Sciences **100** (2000), no. 5, 2572–2592.

[35] N. P. Osmolovskii and F. Lempio, *Transformation of quadratic forms to perfect squares for broken extremals*, Set-Valued Analysis **10** (2002), no. 2, 209–232.

[36] K. A. Rogers, *Stability exchange in parameter-dependent constrained variational principles with applications to elastic rod models of DNA minicircles*, Ph.D. thesis, University of Maryland, College Park, 1997.

[37] H. Sagan, *Introduction to the Calculus of Variations*, Dover Pubns, 1992.

[38] A. Sears and R. C Batra, *Buckling of multiwalled carbon nanotubes under axial compression*, Physical Review B **73** (2006), no. 8, 085410.

[39] G. H. M. van der Heijden, *A robust variational formulation for a rod subject to inequality constraint: a simple model for a drill string*, Complementarity, Duality and Symmetry in Nonlinear Mechanics (Dordrecht) (D. Y. Gao, ed.), Proceedings of the IUTAM Symposium, Kluwer, 2004, pp. 313–325.

[40] G. H. M. van der Heijden, S. Neukirch, V. G. A. Goss, and J. M. T. Thompson, *Instability and self-contact phenomena in the writhing of clamped rods*, Int. J. Mech. Sciences **45** (2003), 161–196.

[41] G. H. M. van der Heijden and J. M. T. Thompson, *Lock-on to tape-like behaviour in the torsional buckling of anisotropic rods*, Phys. D **112** (1998), 201–224.

[42] G. H. M. van der Heijden and J. M. T. Thompson, *Helical and localised buckling in twisted rods: a unified analysis of the symmetric case*, Nonlinear Dynamics **21** (2000), no. 1, 71–99.

[43] G. H. M. van der Heijden and J. Valverde, *Instability of a whirling conducting rod in the presence of a magnetic field*, Proc. of the 5th EUROMECH Nonlinear Dynamics Conference (ENOC 2005), Eindhoven, Netherlands, 7-12 August 2005 (D. H. van Campen, M. D. Lazurko, and W. P. J. M. van den Oever, eds.), (CD), 2005, pp. 2624–2633.

[44] T. Yabuta, N. Yoshizawa, and N. Kojima, *Cable kink analysis: cable loop stability under tension*, Journal of Applied Mechanics **49** (1982), 584.

[45] Z. Yao, H. W. C. Postma, L. Balents, and C. Dekker, *Carbon nanotube intramolecular junctions*, Nature **402** (1999), no. 6759, 273–276.